Terahertz nanoscopy: Advances, challenges, and the road ahead Ⓕ

Xiao Guo Ⓘ ; Karl Bertling Ⓘ ; Bogdan C. Donose Ⓘ ; Michael Brünig Ⓘ ; Adrian Cernescu Ⓘ ;
Alexander A. Govyadinov Ⓘ ; Aleksandar D. Rakić ✉ Ⓘ

Check for updates

View Online   Export Citation

Articles You May Be Interested In

Terahertz near-field nanoscopy based on detectorless laser feedback interferometry under different feedback regimes

APL Photonics (June 2021)

Near-field probes for sensitive detectorless near-field nanoscopy in the 2.0–4.6 THz range

Appl. Phys. Lett. (May 2024)

Terahertz spin currents resolved with nanometer spatial resolution

Appl. Phys. Rev. (December 2023)

AIP Publishing

Special Topics Open for Submissions

Learn More

Applied Physics Reviews

AIP Publishing

Terahertz nanoscopy: Advances, challenges, and the road ahead (F)

View Online   Export Citation   CrossMark

Xiao Guo,[1] (iD) Karl Bertling,[1] (iD) Bogdan C. Donose,[1] (iD) Michael Brünig,[1] (iD) Adrian Cernescu,[2] (iD)
Alexander A. Govyadinov,[2] (iD) and Aleksandar D. Rakić[1,a)] (iD)

AFFILIATIONS

[1]School of Electrical Engineering and Computer Science, The University of Queensland, Brisbane, QLD 4072, Australia
[2]Attocube systems AG (neaspec), Eglfinger Weg 2, 85540 Haar (München), Germany

[a)]Author to whom correspondence should be addressed: a.rakic@uq.edu.au

ABSTRACT

Exploring nanoscale material properties through light-matter interactions is essential to unveil new phenomena and manipulate materials at the atomic level, paving the way for ground-breaking advancements in nanotechnology and materials science. Various elementary excitations and low-energy modes of materials reside in the terahertz (THz) range of the electromagnetic spectrum (0.1–10 THz) and occur over various spatial and temporal scales. However, due to the diffraction limit, a slew of THz studies are restricted to drawing conclusions from the spatially varying THz responses around half of the probing wavelengths, i.e., from tens to a couple of hundred micrometers. To address this fundamental challenge, scanning near-field optical microscopy (SNOM), notably scattering-type SNOM (s-SNOM), combined with THz sources has been employed and is fueling growing interest in this technique across multiple disciplines. This review (1) provides an overview of the system developments of SNOM, (2) evaluates current approaches to understand and quantify light-matter interactions, (3) explores advances in THz SNOM applications, especially studies with THz nano-scale spatial responses employing an s-SNOM, and (4) envisions future challenges and potential development avenues for the practical use of THz s-SNOM.

TABLE OF CONTENTS

I. INTRODUCTION

The physical and chemical characteristics of a material are mainly governed by its structure.[1,2] In this context, the scale at which various phenomena are being probed is of crucial importance since different

levels of assembly are known to have critical repercussions on the macroscopic characteristics.[3,4] Hence, examining materials at the nanoscale becomes critical to unveil the relationship between micro- and macroscopic material responses.[5,6] One of the promising approaches to unravel such relationships is to probe the materials via light-matter interactions at the nanoscale.

Scanning near-field optical microscope (SNOM) is one of the tools used to decipher material properties from the optical responses obtained—beyond the Abbe diffraction limit—over a broad range of wavelengths.[7–16] Since terahertz (THz) photons have energy in the millielectronvolt (meV) range, they interact with energy transitions ranging from zero to tens of meV in condensed matter systems.[17,18] Therefore, THz waves allow us to induce and probe various low-energy modes and collective excitations[19,20] such as charge-carrier scattering, lattice vibrations,[21–24] polaritons,[25,26] molecular vibrations, and inter-molecular non-covalent interactions in molecules.[27–33]

In terms of resolving sub-wavelength features, scattering-type SNOM (s-SNOM) has been demonstrated to achieve nanoscale spatial resolution for long-wavelength radiation, including THz waves.[10–15] Therefore, THz s-SNOM allows the interrogation of optical properties at the nanoscale, which is typically impossible by employing conventional far-field techniques.[34,35] In this article, the fundamental principles of SNOM are briefly reviewed along with recent advances in THz s-SNOM. This review summarizes the seminal works by the THz s-SNOM community and highlights the multi-pronged utility of such a cutting-edge technique in practical use for material characterization.

Structurally, the review comprises of six sections. It begins with a summary of SNOM system developments in Sec. II and then moves the main focus to the studies that are employing scattering-type SNOM (s-SNOM) in the THz regime. In Sec. III, the basic theory underpinning near-field interactions in s-SNOM and the fundamental methodologies to unravel material properties from near-field scattering signals are discussed. In Sec. IV, motivated by abundant responses collected from various materials upon THz excitation, seminal works employing THz s-SNOM for material characterization including solid-state bulk samples, two-dimensional materials, and biological samples are reviewed. In Sec. V, the perspective on several intriguing directions regarding THz s-SNOM applications, including near-field investigations of soft or weak-scattering materials, nanotomography of multilayer structures, near-field interrogations in liquid environments, cryogenic probing of quantum materials, and other emerging topics are provided. Finally, in Sec. VI a summary and conclusions are provided.

II. PRINCIPLES OF OPERATION

Conventional optical interrogation approaches aimed at materials characterization are based on the far-field detection scheme. From a transmitter to detector, the electromagnetic waves with high spatial frequencies (larger than the free-space wavenumber) of electromagnetic waves contribute negligibly to the finally detected signals. This is because a far-field propagation process acts as a low-pass filter in Fourier space. Lacking of such high-spatial-frequency components of a field (also known as evanescent fields), the desirable spatial resolution encompassed by these detection schemes is therefore bounded roughly by half of the incident wavelength, which is known as the diffraction limit.[36,37] Hence, optical interrogation approaches based on conventional far-field schemes preclude the observation of deep subwavelength features. It is essential to collect the high-frequency components of the electromagnetic waves to break such a spatial

resolution limit.[38] For further math details, readers may refer to a recent monograph chapter by Bachelot and Douillard.[39]

A. System development

1. SNOM configurations

There are quite a few experimental configurations for probing high-frequency evanescent fields based on scanning probe microscopy methods. In this section, we start with reviewing the SNOM system development and then delve into its recent advancements (i.e., aperture and scattering-type) for near-field terahertz detection at the nanoscale.

The SNOM is capable of exciting and of collecting evanescent fields and is one of the most promising tools allowing subwavelength sample characterization, beyond the diffraction limit. There are two mainstream types of SNOM configurations, depending on whether the light passes through an aperture of the probe tip or not: (1) aperture-type SNOM (a-SNOM) and (2) scattering-type SNOM (s-SNOM).[15,40,41]

We would also like to highlight that scanning microwave microscopy (SMM) is another seminal scanning probe-based technique for investigating nanoscale microwave responses (in the gigahertz or sub-terahertz range), sharing synergistic insights with SNOM in system development.[42,43]
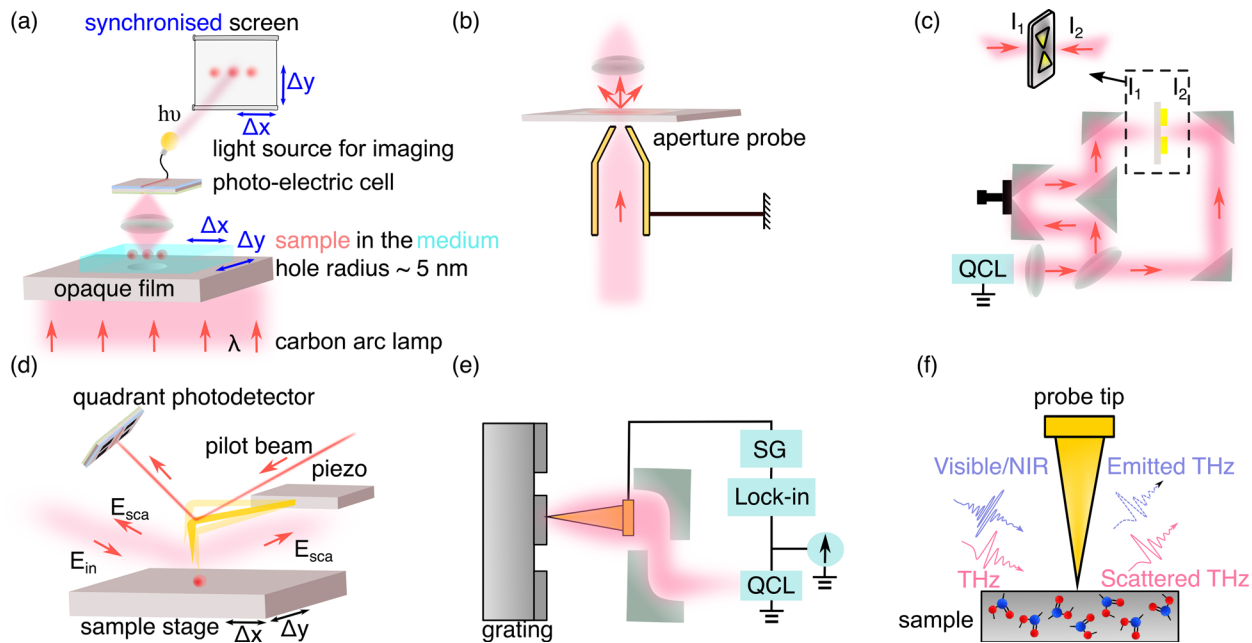
Regardless of the configuration type, three critical elements are required to surpass the diffraction limit using SNOM, namely,

(1) having a concentrated localized field acting as a point source to probe (illuminate) the sample,
(2) maintaining the probe-sample distance within at least a single incident wavelength,
(3) being able to raster scan the sample, and
(4) having an optical detection of sample response.

Satisfaction of above four requirements enables to probe the high-spatial-frequency electromagnetic waves, which do not propagate to the far-field.

The most intuitive realization, which would simultaneously satisfy three of the aforementioned requirements, would be an extension from the conventional-type confocal microscope. Such an idea was initially proposed by Synge in 1928, and was published under the encouragement of Albert Einstein. Figure 1(a) is a depiction of this theoretical design. Synge envisioned[44] that by placing a photo-electric cell in the proximity of an opaque film with a tiny rectangular aperture (the radius roughly equals the incident wavelength), one would be able to resolve sub-wavelength features of the sample by collecting the evanescent fields. Such a system would allow these features to be displayed on a screen synchronized with the raster scanning movement of the aperture. In 1972, Ash and Nicholls[45] demonstrated the first implementation of such an aperture-type near-field detection scheme, resolving $\lambda/60$ features on a grating in microwave frequency as shown in Fig. 1(b).
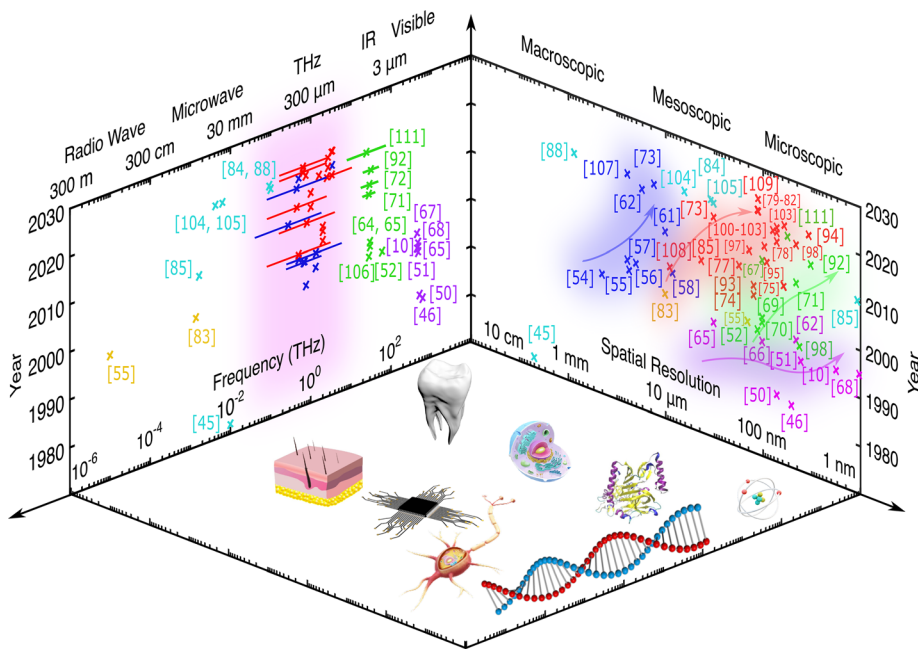
To demonstrate the nano-scale spatial resolution, Pohl et al.[46] employed this aperture-type detection scheme onto a visible laser source (488 nm) and, for the first time, applied a piezoelectric feedback-loop control for the tip-sample distance regulation. Note that, the demand of a precise probe-sample distance control limited the rapid progress of SNOM development until the advent of scanning

FIG. 1. The configuration development track for aperture-type (a)–(c) and scattering-type (d)–(f) THz SNOM: (a) the first theoretical design of SNOM; (b) a typical transmission-type SNOM design for THz detection in early years; (c) modern-type THz aperture SNOM: combining the antenna and probe as a single item; (d): a typical scattering-type SNOM design with different THz sources with a standalone detector; (e) cutting-edge THz s-SNOM design in a detector-less and fast-response scheme; and (f) optical-pump-terahertz-probe s-SNOM for probing ultra-fast dynamics.

probe microscopy (SPM),[47–49] and its core element: a piezoelectric feedback-loop control, as used in Pohl *et al.*'s work. This system configuration triggered the acceleration of SNOM embodiment in the 1980s.

Figure 2 is a temporal evolution map of all SNOM works extending the boundary of spatial resolution limits starting with 1972 until. An observable upward trend of the spatial resolution began in 1983, as shown in Fig. 2, and it has progressed annually in a wide range of

FIG. 2. SNOM spatial resolution competition since 1972 over a broadband spectral range, including visible (purple), infrared (green), terahertz (red: scattering-SNOM, blue: aperture-SNOM), microwave (cyan) and radio-wave (yellow) frequencies. Examples of possible test samples are placed around typical spatial dimensions with potential radiations of the interest. References about THz SNOM spectral bandwidth progression are labeled in Fig. 3.

frequency bands from visible to THz regimes. More noticeably, while a-SNOM demonstrated the sub-wavelength resolution in visible,[46,50,51] infrared,[52] THz,[53–60] microwave,[45] and radiowave[54] regimes, its spatial resolution is still limited at the microscale for long-wavelength electromagnetic waves, especially for THz radiation[61–63] (blue clusters in Fig. 2). This is due to the fact that an a-SNOM relies on a tapered aperture to collect the near-field signals through a tiny hole. Since the light transmission efficiency (σ) decays heavily with a small aperture radius (a) relative to wavelength (λ) as $\sigma \propto (a^6/\lambda^4)$, a trade-off between the aperture size and the transmission efficiency needs to be achieved.[13,64]

Since the first THz a-SNOM work[53] and the pioneering demonstrations of the first THz near-field knife test and white-light imaging,[54,55] many efforts have been made for the advancement of THz a-SNOM (see Table I). One approach is to engineer the probe or the aperture coating materials as well as geometry and to utilize surface plasmon polaritons or hyperbolic media to enhance the transmission efficiency.[56–59,87] Another frequently encountered approach is to integrate the THz nano-detector (an optical detector) into the aperture probe as a single item.[61]

However, recent studies of THz a-SNOM (blue crosses in Fig. 2) show that its spatial resolution still fails to achieve hundreds of nanometers.[62,63,73,88] One recent study incorporated a quantum cascade laser (QCL) as a laser feedback interferometry (LFI) with a THz nano-detector, as shown in Fig. 1(c), achieving 17 μm spatial resolution at

3.4 THz.[73] Such a micrometer-scale resolution ability hampers exploring interesting phenomena from the physical, chemical, and biological perspectives at the sub-cellular level.

Therefore, another type of SNOM capable of revealing nanoscale features is needed. Unlike a-SNOM, s-SNOM focuses and collects the scattering signals from the probe apex and thus avoids the waveguide cutoff effect happening in fiber/aperture transmission.[65] Wessel was the first to theoretically envision a metallic sharp probe that would confine and enhance the electromagnetic field.[89] Wickramasinghe and Williams realized such a theoretical proposition with a signal detection scheme for a scattering-type configuration and patented it.[90] In this signal detection scheme, a carrier wave has a probe oscillation frequency that modulates the near-field scattering signals. Thus, the background noise is expected to be suppressed after demodulating the signals with multiple harmonics of carrier wave frequency. A further brief summary of these signal detection principles is shown in Sec. II A 2. More systematic studies on s-SNOM followed after Wickramasinghe et al., kept pushing the s-SNOM capability limit as demonstrated by performing typical resolution tests, including the knife-edge test and contrast imaging. Developments in s-SNOM systems with nano-scale resolutions were reported in broad electromagnetic spectra among visible,[10,65–68] infrared,[69–72,91,92] THz,[74,76–78,80–82,93–103] and microwave[83,86,88,104,105] regimes. Note that the pioneer work in 1996 by Keilmann et al.[86] did demonstrate that s-SNOM would work in all infrared regions in principle. Figure 1(d) shows a

TABLE I. Selected pioneer SNOM works in the spatial resolution competition.

	Aperture SNOM (sorted by year)		Scattering or apertureless SNOM (sorted by year)	
Frequency	Spatial resolution	References	Spatial resolution	References
Visible	$\lambda/60$ (488 nm) $\lambda/50$ (630 nm)	Pohl et al.[46] Betzig et al.[51]	~ 500 nm (670 nm) 35–100 nm (670 nm) 1–3 nm (633 nm)	Inouye et al.[65] Bachelot et al.[66,67] Zenhausern et al.[10,68]
Infrared	$\lambda/4$ (4 μm)	Piednoir et al.[52]	100 nm (9.2–10.7 μm) 20 nm (9–12 μm) 100 nm (7.6–13.3 μm)	Knoll et al.[69,70] Amarie et al.[71] Huth et al.[72]
Terahertz	$\lambda/2$ (359 μm) $\lambda/4$ (0.6–2.3 THz) 7–60 μm (0.2–2.5 THz) 10 μm (0.05–1.5 THz) 30 μm (0–2 THz) 3.9 μm (0.2–1.5 THz) 17 μm (3.4 THz)	Keilmann[54] Hunsche et al.[55] Mitrofanov et al.[56–59] Walther et al.[61] Sawallich et al.[62] Siday et al.[63] Giordano et al.[73]	150 nm (2 THz) 40 nm (2.54 THz) 300 nm (0.2–3.2 THz) 50 nm (1.3–8.5 THz) 1 μm (2.53 THz) 200 nm (0.11–0.175 THz) 125 nm (3.44 THz) 35 nm (2.7 THz) 120 nm (3.28 THz)	Chen et al.[74] Huber et al.[75] von Ribbeck et al.[76] Kuschewski et al.[77] Dean et al.[78] Chen et al.[79] Rubino et al.[80] Pogna et al.[81] Reichel et al.[82]
Microwave	0.5 mm (10 GHz, 3 cm)	Ash et al.[45]	200 nm (217 mm) ~ 1 μm (3 mm) ≤ 0.1 nm (2.5 GHz, 12 cm)	Knoll et al.[83] Dai et al.[84] Lee et al.[85]
Radiowave	$\lambda/40\,000$, 100 μm (4 m) $\lambda/200\,000$, 10 μm (20 m)	Keilmann[54] Keilmann et al.[86]	$\cdots$ $\cdots$	$\cdots$ $\cdots$

24 November 2024 03:57:31

typical s-SNOM configuration. It contains four main components: (1) a vibrating metallic probe tip driven by a piezo, (2) a pilot laser with a quadrant photodetector to maintain the closed-feedback-loop regulation of the probe tip oscillation, (3) a high-precision sample translation stage in transverse and vertical directions, and (4) a radiation source and detector for optical investigations. Nowadays, it is typical to assemble an atomic force microscope (AFM) with an optical detection system as an s-SNOM.

Figure 2 summarizes published seminal s-SNOM system and instrumentation development studies with corresponding spatial resolutions and bandwidths over the past 50 years since 1972.[10,45,46,50–52,54–59,61,62,65–74,76–84,86,88,92–111] Overall, the spatial resolution and available spectral bandwidth of s-SNOM increased over time in a broad spectral range, from visible to microwave regimes. At the start of the period (1970s–1990s), most efforts to increase the spatial resolution capability were made for visible wavelengths (purple crosses), especially for monochromatic radiation sources.[10,66–68] Since late 1990s, such consistent efforts to push the boundary of the spatial resolution limit started to translate into infrared[69–72,106] (green crosses) and THz[74,76–78,80–82,95–103] (red crosses) regimes. Enabling the broadband spectral range for s-SNOM was until recently the most challenging part of this research effort.

The THz s-SNOM development tracking of spatial resolution began around 150 nm, in the early 2000s,[74] and then kept pushing the boundaries until reaching a plateau at about 50 nm[77,100,103] and even better (about 20 nm) for time-resolved measurements.[98,101,102] On the other hand, the spectral range of THz s-SNOM started to broaden within $0.5-3$ THz in late 1990s.[55] A typical broadband THz investigation approach was THz time-domain spectroscopy (THz-TDS).[76] Favored by the introduction of free-electron lasers (FEL) with tunable radiation, the available THz near-field interrogation spectral range extended up to 8.5 THz recently.[77]

To highlight the spatial resolution advantage for long wavelengths, selected pioneering and representative works of s-SNOM are summarized in Table I and compared with a-SNOM. As Table I suggests, there are two types of radiation sources typically incorporated with THz s-SNOM. Depending on the purpose and funding budgets, it is common to incorporate either powerful continuous-wave laser sources[74,78,81,82,103] or broadband pulse systems[76,77] into an s-SNOM.
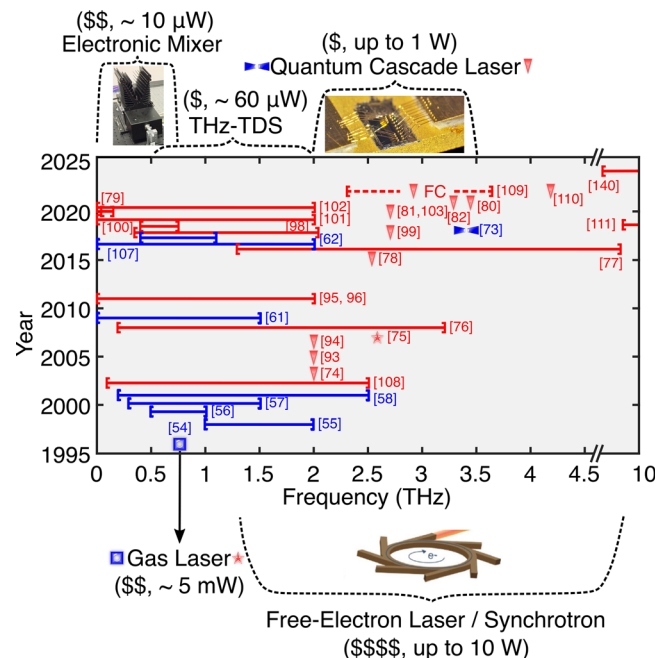
In THz regimes, providing a reliable and affordable radiation source and detector is still considered a challenge.[112,113] THz QCL, for example, is one of the promising sources with high-power radiation and potentially, a room-temperature operating environment.[114–116] One of the detector-less and cryogen-free schemes based on THz QCL is called laser feedback interferometry (LFI), in which electromagnetic radiation from the laser is re-injected into the laser cavity after interacting with external targets.[114] It is a compact technique combining the transmitter and receiver as a single device and allowing coherent detection by analyzing the perturbing intra-cavity electric field. Figure 1(e) displays a typical LFI setup using a THz QCL.[78] Such a cutting-edge THz detection scheme has been reported with sub-50 nm spatial resolutions within $2.5-4$ THz, and has been used to reveal detection dynamics in semiconductor nanowire detectors.[81,82,103]

Another configuration extension is to combine a pump source with THz s-SNOM to probe dynamics in materials.[98,101,102,117,118] To reveal spatial-temporal ultrafast dynamics in time domain usually relies on a visible or near-infrared beam and/or a THz beam to pump the material

concurrently with the incident THz beam as shown in Fig. 1(f). The charge carriers inside the sample would thus generate and accelerate upon the femtosecond illumination. Such a technique is referred to as pump-probe near-field optical spectroscopy. Its scattering fields contain the modulated THz field from pumping, which encodes the sample's ultrafast dynamics. If the incident field has THz components, such a THz near-field scattering configuration is referred to as near-field optical pump THz probe (n-OPTP)[101] in the literature. Otherwise, it is referred to as near-field optical pump THz emission (n-OPTE)[101] or laser THz emission nanoscopy (LTEN)[98,102] according to different literature nomenclatures. Recently, Cai et al. employed such n-OPTE idea to study THz spin current pulses by pumping a type of nonmagnet/ferromagnet heterostructures (in this study, cobalt-iron-boron alloy, a ferromagnetic layer, is sandwiched by tungsten and platinum, two nonmagnetic layers) at the nanoscale.[119] Generally, THz nanoscopy with near-field pumping schemes should be able to study arbitrary heterostructures with potential applications in characterizing spintronic optoelectronic nanodevices in the future.

In summary for THz spatial resolution studies: SNOM serves as a promising tool to provide sub-wavelength THz signatures beyond the diffraction limit. THz s-SNOM is capable of unraveling spatially varying features at the nanoscale level (50 nm) while a-SNOM is more suitable for capturing THz responses at the microscale.

Figure 3 illustrates the annual progression of THz SNOM system developments vs frequency/wavelength for broadband and

FIG. 3. THz SNOM developments since the first demonstration (1995) with typical THz sources covering 0–10 THz bandwidth for aperture SNOM (blue) and scattering SNOM (red). The typical bandwidth of each source is illustrated. Horizontal lines indicate the probing bandwidth for each reference. Subfigures are reproduced with permission from Liewald et al., Optica **5**, 159–163 (2018). Copyright 2018 Optica.[100] Reproduced with permission from Khatib et al., ACS Photonics **5**, 2773–2779 (2018). Copyright 2018 American Chemical Society.[111] Reproduced with permission from Rakić et al., Appl. Phys. Rev. **6**, 021320 (2019). Copyright 2019 AIP Publishing LLC.[114]

single-wavelength radiation sources from 1995 to 2022. We also indicate the relative cost of different types of sources on a $ to $$$$ and their representative output powers. Depending on the generation mechanism, preferable THz spectral range, and funding budgets, there are five typical options of THz radiation sources to be incorporated into an s-SNOM: (1) electronic mixer,[100] (2) THz-TDS,[55,63,76,107] (3) QCL,[78,82,103,120] (4) gas laser,[75] and (5) free-electron laser and synchrotron.[77,111]

Overall, both a-SNOM and s-SNOM have been developed to operate in broadband THz regimes. For example, in the spectral ranges below 3 THz, both a-SNOM and s-SNOM have been demonstrated in near-field THz studies with THz-TDS,[55,76,95,96,107,121] which is a typical, commercially mature and available broadband option ($0 - 6$ THz) at an affordable financial budget for most THz laboratories. A few cases have used electronic mixers and gas lasers. Electronic mixers transmit THz waves based on high-harmonic generation of GHz waves and are usually preferred to provide monochromatic THz radiations at sub-1 THz, e.g., 0.5 THz or lower.[100] Alternatively, gas laser is another commercially accessible option with a promising budget.[75] In terms of monochromatic THz radiation, a noticeable option for SNOM, especially s-SNOM, are quantum cascade lasers (QCLs). Over the past 20 years, consistent efforts in the community have been made to improve the spatial resolution and scattering intensity of THz s-SNOM. As summarized in Fig. 3, s-SNOM has opened up THz responses between 2 and 4 THz at nanoscale, either with a standalone bolometer[73,74,93,94] or using the laser cavity itself as a detector-less scheme.[78,80,82,99,103]

The QCL is a unipolar device and exploits a cascaded series of intersubband transitions for laser emission. It is able to provide high-power THz radiation (up to 1 W) and can operate in a cryogen-free scheme,[114,115,122] with improved designs and modes of operation opening the potential for wide bandwidth tunable operation above 1.5 THz.[123–126]

New advancements in frequency combs (FC) for THz QCL are expected to assist THz s-SNOM with both the advantages of being high-power broadband simultaneously.[127,128] Pistore *et al.* reported the first demonstration of combining the THz QCL frequency comb with an s-SNOM.[109] This QCL-FC-assisted scheme extended the frequency range of THz s-SNOM from 0.4–1.6 THz (THz-TDS system) to 2.5–3.5 THz (Pistore *et al.*, THz QCL frequency comb). Note that, at frequencies except the central frequency of the THz QCL FC, the amplitude of s-SNOM scattering signals collected from a Au mirror is around 25% to that of its counterpart with a THz-TDS system (panel g of Fig. 3 in Pistore *et al.*[109]) Further studies, for example improving signal-to-noise ratio, of phase-locked THz QCL FC are essential to enable QCL-FC-assisted THz s-SNOM to be experimentally useful for material characterization,[126,129] like the retrieval of complex dielectric properties of interrogated samples,[130–132] leveraging short pulses generated by THz QCL[126,133,134] and coherent sensing capability of LFI scheme[114,135–139] for THz s-SNOM in future investigations.

Another noticeable broadband THz radiation source for s-SNOM are the free-electron laser (FEL) or synchrotron. FEL employs relativistic electrons as a gain medium and thus is able to generate ultrashort pulses. The s-SNOM equipped with such a high-power broadband source was demonstrated in the spectral range of up to 10 THz and beyond, including the mid-infrared range.[77,111] Recently, Wehmeier and co-workers (a team led by Mengkun Liu and G.

Lawrence Carr) in Brookhaven National Laboratory (National Synchrotron Light Source II, Upton, USA) have demonstrated to fill an under-explored bandwidth gap at a cryogenic temperature (>5 THz with detector cooled at 4.2 K) for synchrotron-based THz nanospectroscopy measurements by using a liquid-Helium-cooled $Hg_{1-x}Cd_xTe$ ($x \sim 0.173$, MCT) detector,[140] allowing investigations of phonon modes and other various collective features in solid-phase materials in THz regimes in the future. Note that the detection threshold of MCT detector for THz nanospectroscopy is hugely impacted by MCT cooling temperature (5.2 THz at 4.2 K and shifts to 12 THz at 77 K), because the detector material band edge shifts to lower energies with decreasing temperature.

Apart from developing systems, another ongoing task for s-SNOM community is to improve the signal-to-noise ratio of near-field signals. This leads to the discussion of principles about near-field signal retrieval and studies about near-field signal enhancement.

We also would like to mention that, in the context of SMM, the configuration of apertureless SMM is different from scattering-type configurations we discussed in Fig. 1. In apertureless SMM, the probe itself is typically the antenna with microwave (subterahertz) radiation and detection from a vector network analyzer (VNA),[141] without an external radiator to create scattering from the AFM tip.

More recently, in SMM development, Farina and Hwang led the invention of an interesting configuration called inverted SMM (*i*-SMM),[105,142–144] where a microwave signal is injected through a sample holder (also as a microwave waveguide) and thus through the interrogated sample rather than through the conductive probe tip. Note that in *i*-SMM configuration, the sample is held by a transmission line with a broadband impedance matching range, thus allowing both transmission and reflection signals to be measured. We envisage such an inverted near-field detection scheme can be incorporated for high-speed nanoscale THz coherent measurements, if the synchronization between the probe tip dithering and THz raster scanning in the emitter-detector pair can be achieved, including for laser feedback interferometry (THz nano-LFI) detection (in the context of LFI, the laser itself acts as both the emitter and detector simultaneously)[114,135,138] in tandem with a properly designed sample holder. By exploiting LFI, the swept-frequency delayed self-homodyning method[145] allows to operate THz QCL in either continuous-wave[146] or pulsed modes,[137] without requiring an external mechanical modulation scheme (e.g., modulated by a laser drive current rather than an optical chopper)[136,137] for lock-in detection, which greatly reduces the sampling time per pixel and is practically important for realizing high-speed near-field nanoimaging and nanospectroscopy measurements for material analysis employing THz nanoscopy with table-top sources in a compact and experimentally simple scheme.

2. Signal retrieval

One of the important roles of SNOM is to translate the information about the near-field probe-sample coupling into the far-field. For s-SNOM, this is realized by modulating the near-field electromagnetic components onto a carrier wave scattered from the probe. The probe tip acts as an antenna whose scattering depends on both the illuminating field and the near-field interaction between the tip and sample. The illuminating field is formed by propagating waves (directly incident upon the tip and those reflected from the sample surface), constituting background with slow spatial variation on the wavelength scale.

In contrast, the near-field is composed of evanescent waves that decay exponentially at the nanometer scale, and thus induce rapid spatial variation of the tip-scattered light. To separate the near-field from the background, the tip-sample distance is modulated by tip dithering at a frequency Ω, which typically corresponds to the cantilever's mechanical resonance frequency. For small dithering amplitudes, (typically a few tens of nanometers), the slowly varying background is nearly linear with tip-sample distance and mostly contributes to the low order harmonics ($\leq 2\Omega$) of the tip-scattered signals. The fast-varying near-field interaction is highly nonlinear with distance and thus contributes to higher-order harmonics ($\geq 2\Omega$). Thus, the background could be significantly suppressed by demodulating the detector signal at higher harmonics of the tip dithering frequency using, e.g., a lock-in amplifier.[90] Unfortunately, the high-harmonic demodulation on its own does not provide complete background suppression. Because the far-field detector always measures scattered power, $I_{det} = |E_{nf} + E_{bg}|^2$ rather than the field, for coherent near-field scattering, E_{nf}, and background, E_{bg}, the detected signal will always contain products of E_{nf} and E_{bg}. This leads to a, so-called, multiplicative background that could obscure near-field signal. For monochromatic radiation sources, Ocelić et al. demonstrated a pseudoheterodyne interferometric detection technique to retrieve background-free near-field responses in s-SNOM.[147] Before the invention of proper interferometric detection techniques such as pseudoheterodyne (PsHet),[147] multiplicative background constituted a leading cause of s-SNOM imaging artifacts. Note that, synthetic optical holography based on the interference between s-SNOM tip-scattered field and a synthetic reference wave is also suitable for s-SNOM measurements with monochromatic radiations.[148]

To allow for a complete description of material properties, one needs to have access to both amplitude and phase of the tip-scattered light. To do so, an interferometric detection is utilized. Such techniques usually direct a portion of the incident light to the reference arm of a Michelson interferometer, allowing for an interference between a reference beam and the tip-scattered light at the optical detector.[147,149–152] Reference beam further provides a strong boost of the weak near-field signal, significantly enhancing s-SNOM sensitivity. For monochromatic radiation sources, Ocelić et al. introduced a PsHet interferometric detection technique, which completely suppresses all s-SNOM backgrounds.[147] It adds the reference beam phase modulation to the classic high-harmonic demodulation scheme, suppressing the multiplicative background and enabling simultaneous measurement of the scattered field amplitude and phase, even in the case whereas homodyne s-SNOM detection schemes fail to do so.[151] Recently, Sternbach et al. reported the applicability of pseudoheterodyne detection method with pulsed laser sources; they employed this transient detection approach to time-resolved measurements on photo-induced effects in the insulator-to-metal transition of vanadium dioxide at the nanoscale.[153] The compatibility of s-SNOM detection with low-repetition rate pulsed laser systems (which have high-peak power) faces a constraint with lock-in detection, which requires the sampling rate at least twice that of the highest frequency component to accurately reconstruct a signal due to the Nyquist–Shannon sampling theorem.[154] For typical PtIr-coated AFM tips (Rocky Mountain Nanotechnology) of ~ 75 kHz oscillation frequency, the repetition rate of the pulsed laser has to be at least 300 kHz for the second-harmonic demodulation. For higher-order harmonic signals, e.g., the 4th harmonic demodulation with a lock-in amplifier requires the pulse repetition rate to be at least

eight times of the tip oscillation frequency for proper sampling. In addition to pseudoheterodyne detection, to further circumvent the limitation of standard lock-in detection with low repetition rate kHz-class pulsed lasers, Palato et al. recently demonstrated a quad demodulation detection method to retrieve higher-order ($n > 4$, up to $n = 7$) near-field signals with a 200 kHz laser amplifier with the tip oscillation frequency as 325 kHz by exploiting the stroboscopic effect.[155] These innovative detection schemes will be beneficial for observing spatiotemporal dynamics utilizing ultrafast s-SNOM in the future.

The Michelson-type interferometric approach also serves as a core part for s-SNOM measurements with broadband sources, as performed with nano-Fourier transform infrared spectroscopy (nano-FTIR). In nano-FTIR, the detector signal is recorded as the reference mirror translating linearly (thus changing the phase of the reference beam). The resulting interferogram is then Fourier transformed to obtain the amplitude and phase spectra of the interrogated sample. Similar to PsHet, nano-FTIR also provides complete suppression on s-SNOM backgrounds complemented by a strong interferometric boost of the weak near-field signals.[71,72,92]

For broadband THz s-SNOM measurements, usually performed with THz-TDS, the forward elastically scattering field is detected whereas no interference happens between the incident and reference beam.[156,157] This is at first demonstrated by von Ribbeck et al.[76] before the demonstration of broadband infrared s-SNOM by Amarie et al.,[71] which was much later named nano-FITR.[72] As opposed to nano-FTIR, a femtosecond pulse acts as a gated beam in the THz photoconductive antenna to sample the scattering THz field at the receiver. Therefore, the complex tip-scattered THz field is directly measured in s-SNOM combined with THz-TDS systems.[76,96] Note that since THz-TDS systems directly measure THz field rather than power, they do not suffer from the multiplicative background and could simply rely on the high-harmonic demodulation for the background suppression.

However, due to the detection principle of time-domain-spectroscopy, THz white-light nanoimaging obtained by s-SNOM with THz-TDS system usually serves as a qualitative THz contrast scanner with an averaged spectral amplitude but no meaningful phase information, where s-SNOM tip scattered signal is collected when the time delay between the gated pulse (the sub-ps beam, usually in near-infrared) and the to-be-sampled THz field is fixed. Usually, meaningful phase-resolved information from nano-THzTDS relies on THz hyperspectral nanoimaging by taking THz nanospectroscopy at points of interest,[132,158] which usually is time-consuming. Recently, Jing et al. demonstrated a data acquisition method to enable phase-resolved information in THz white-light nanoimaging for nano-THzTDS.[159] The key of this approach relies on an additional modulation of the optical delay path between the gated pulse and the to-be-sampled THz field at a modulation frequency (M) much smaller than the s-SNOM tip resonant frequency (Ω). By combining the carrier-band ($n\Omega$) and sideband ($n\Omega \pm mM$) information, the access to meaningful complex-valued THz nanoimaging information is achieved. Refer to recent studies, like Dai et al.[160] and Larson et al.,[161] for more technical details of s-SNOM signal detection techniques.

3. Probe designs for scattering-type SNOM
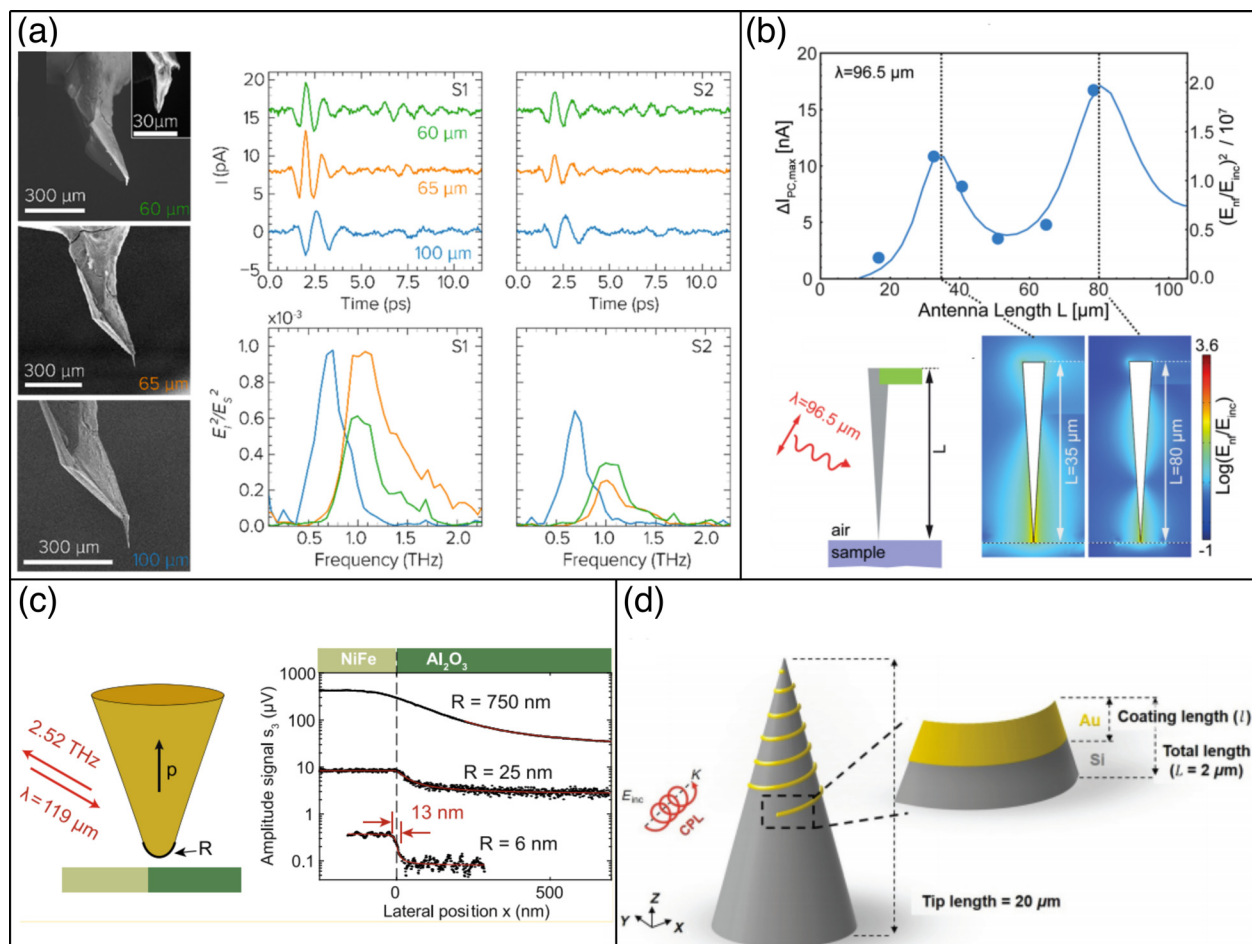
In a scattering-type configuration, SNOM relies on the tip to confine the electric field around the tip apex in order to overcome the diffraction limit and re-radiate the incident field encoded with the sample

<div style="text-align: right">24 November 2024 03:57:31</div>

information. Therefore, the design of probe tips is significant and has the potential to improve the signal-to-noise ratio of scattering signals.

Recently, researchers in the s-SNOM field have attempted to optimize the design of probe tips from different angles, including the tip shank length and surface coating.[162–168] As demonstrated using classical antenna theory for s-SNOM spectra using broadband $(0.2 - 1.2\,\text{THz})$ and single-frequency $(3.11\,\text{THz}, \lambda = 96.5\,\mu\text{m})$ THz radiation sources, the preferred tip shank length L_{tip} is associated with multiple times of the half-wavelength $(L_{\text{tip, n}} = \frac{n\lambda}{2}, n$ is the resonance order), where the spectral varying near-field tip enhancement is possibly to be tuned with the probe length as shown in Fig. 4(a).[165] However, the resonant tip length does not scale linearly with the resonance order (n) but with a shorter probe resonant length $(L_{\text{tip, optimal}, n} < \frac{n\lambda}{2})$, as shown in Fig. 4(b), which is attributed to the presence of a cantilever. Intriguingly, THz near-field coupling does not further shift the probe resonance with the presence of a dielectric or metallic sample under the tip, a phenomenon observed for such devices at visible and infrared frequencies.[162]

A recent study reports the observation of deep-subwavelength THz spatial features around 100 nm by employing a blunt tip whose radius was substantially larger (750 nm) than the obtained resolution.[164] This interesting result was observed at $2.5\,\text{THz}\,(119\,\mu\text{m})$ by increasing the radius of a PtIr tip (standard shank length: $20\,\mu\text{m}$) from 25 to 750 nm, as shown in Fig. 4(c), which breaks with the common belief of s-SNOM users. It is explained by a strong "virtual tip sharpening" through utilization of very small tapping amplitudes compared to the tip radius.

FIG. 4. Probe design for enhancing THz s-SNOM near-field couplings: (a) the tip-shank length dependence of near-field THz spectrum ranges due to antenna resonance effect, which highlights the significance of realistic probe tip geometry shape on frequency-dependent near-field coupling enhancement (probe tip responsivity) in THz nanospectroscopy measurements. Reproduced with permission from Siday et al., ACS Photonics **7**, 596–601 (2020). Copyright 2020 American Chemical Society.[165] (b) THz near-field enhancement dependence on antenna length in addition to the presence of cantilevers, which aligns with the understanding of half-wavelength antenna theory. Reproduced with permission from Mastel et al., Nano Lett. **17**, 6526–6533 (2017). Copyright 2017 American Chemical Society.[162] (c) An experimental observation that 100 nm spatial resolution of THz near-field responses can counter-intuitively be maintained even with a probe tip radius at the micrometer-scale. Reproduced with permission from Maissen et al., ACS Photonics **6**, 1279–1288 (2019). Copyright 2019 American Chemical Society.[164] (d) A probe design proposal to enhance near-field scattering by customizing a chiral coating pattern on the probe surface to be experimentally demonstrated in the future. Reproduced with permission from Zhang et al., Phys. Rev. Appl. **15**, 014048 (2021). Copyright 2021 American Physics Society.[168]

In these s-SNOM probe works, full-wave simulations (COMSOL Multiphysics, CST, etc.) play a significant role and are used to aid the understanding of the experimental observations, e.g., reproducing the spectral peaks observed in THz s-SNOM spectra, which does not originate from the sample permittivity but the antenna-resonance effect.[63,165,167]

Another notable study suggested that a tunable spectral enhancement could be achieved by tuning the metallic coating length or by changing the coating pattern of a chiral helical structure on an achiral silicon probe tip as illustrated in Fig. 4(d).[168]

In addition, a deliberate selection of coating materials to generate surface polaritons at a specific probing wavelength may serve as another potential option. For example, multiferroic materials may introduce an enhanced tip-sample coupling in THz regimes and therefore act as a versatile s-SNOM tip coating option to probe local material properties.[169]

While the dominant near-field response in the scattering signals of s-SNOM is attributed to p-polarized components, recent studies showed that s-polarization responses from s-SNOM could be detectable on specific materials[169] and a special probe design may facilitate the enhancement of s-polarization components.[166] Rather than optimize the probe tip itself, Zhou *et al.* suggested that a grating-slab-tip cascading structure may provide 15-fold near-field enhancement around 0.5 THz.[163] Despite these pioneering works regarding the tip-scattered signal enhancement in the SNOM field, there is still a lack of systematic and conclusive knowledge to guide probe fabrication in a feasible way, especially for THz waves. Significant efforts are required to investigate and provide a refined recipe for reproducible probe tip fabrication and controllable near-field enhancement. This probe tip fabrication reproducibility is essential to broaden the utility of THz s-SNOM for practical use in material characterization at the nanoscale for multidisciplinary projects.

III. NEAR-FIELD INTERACTIONS
A. The three near-field effects

The major element of proper s-SNOM functionality is the metallic sharp probe tip and there are three near-field effects that are essential for enhanced tip-sample coupling and elastic scattering.[11,170]

1. Lightning rod effect

When an electric field is focused onto the probe tip, the tip itself becomes polarized and acts as a lightning rod, leading to a strong localized field enhancement at its apex.[171–176]

2. Dipole effect

According to the method of images, scattering by a polarized tip placed in the sample proximity is equivalent to the scattering of the tip dipole and its mirror image dipole in the sample half-space, essentially representing a dipole antenna. Since the image dipole depends on the sample dielectric properties, the scattered radiation encodes this information and allows for the possibility of recovering the local sample permittivity.[170,177–181]

3. Antenna resonance effect

In s-SNOM spectroscopy, the probe tip acts as a nanoantenna with spectral varying enhancements (alternatively, responsivity) for tip-scattered signals. This probe tip response function is determined primarily by its geometry as well as the coating materials and attached cantilever, which dominates the access to available frequency components of near-field signals. Due to a fixed tip shank length in s-SNOM spectroscopic measurements (equivalently with varying wavelengths of incident radiation), dipolar antenna theory could be adopted to explain experimental near-field enhancements in the frequency domain, whose bandwidth looks as "bandpass-filtered" and "selectively enhanced" (actually due to the probe response function) when compared to its far-field reflection component.[164,165,167,182]

B. Light-matter interactions: Calibration
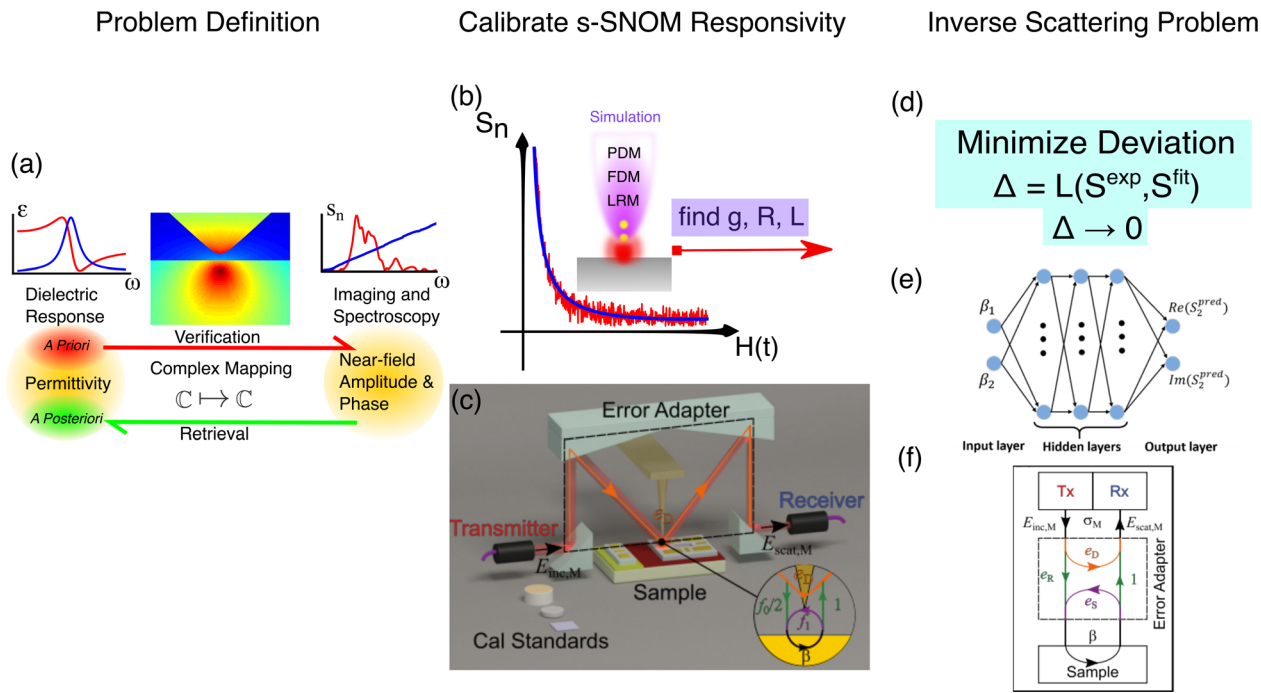
There are two approaches to relate the permittivity with near-field scattering spectra, as shown in Fig. 5(a). The first approach is to fit the complex permittivity (dielectric response) to the experimental near-field amplitude and phase data using an s-SNOM model. This approach has been used frequently in studies aiming to correlate phonon or molecular resonances with measured near-field spectra, identify localized plasmonic resonances, and recover free-carrier spatial and spectral profiles by assuming knowledge of the sample properties *a priori*.[75,100,158,169,184–186] In this review, we define it as solving a verification problem. Another approach treats the complex permittivity in an *a posteriori* manner and recovers this unknown material property from the measured near-field complex-valued spectra.[130,187–196] We define this inverse process as solving a retrieval problem in this review.

Note that both the sample permittivity and the experimental near-field spectra are complex-valued quantities. Therefore, the scattering process involving an s-SNOM probe tip is a complex-complex mapping as denoted in the center of Fig. 5(a).

The essence of multiple interactions between the probe and the sample, before scattering to the far-field, has been well captured by model approximations involving dipole effects[179,180,189,197,198] and its extensions[199–202] as shown in Fig. 5(b). The main significance of dipole models is to calibrate the charge response along the probe tip geometry. Such a probe response calibration in dipole-model families relies on fitting the approach curve,[180,181,190,203] which is the tip-sample scattering variation by moving the probe tip away from the sample to the far end. The simplest model is the point dipole model (PDM), which approximates the probe tip as a dielectric sphere and treats near-field responses in the sample half-space as an induced mirror image with an equal radius.[179,181] A more realistic model of s-SNOM tip-sample interactions is finite dipole model (FDM)[180] and it has three major improvements over PDM:

(1) regarding the probe tip as an elongated spheroid,
(2) considering the charge participation of the tip end close to the sample surface into the near-field interactions, and
(3) distinguishing contributions between the initial polarization from the incident field and secondary polarization due to the tip-sample coupling.

These three improvements are represented by two different monopoles located in the proximity of the tip apex.

Problem Definition   Calibrate s-SNOM Responsivity   Inverse Scattering Problem

FIG. 5. Quantitative analysis for s-SNOM data: (a) a summary of workflow to analyze s-SNOM data, either to reproduce the measured spectra from known material permittivity (*a priori*) or to retrieve unknown sample properties (*a posteriori*) from measured spectra; calibration of s-SNOM system response function: (b) A typical strategy is to characterize the tip by fitting the approach curve in s-SNOM measurements for further modeling purpose, and (c) a vector-nature calibration method to treat probe-sample interactions as a black box, aiming to calibrate system responses including probe geometry from three known standards; (d) a typical method to retrieve sample properties, fitting the measured complex spectra with dipole-based models using searching/optimization algorithms; (e) a black-box method to encode probe-sample interaction inside a neural network, training the network to learn such a complex mapping by assuming a known probe geometry. Reproduced with permission from Chen *et al.*, ACS Photonics **8**, 2987–2996 (2021). Copyright 2021 American Chemical Society.[183] (f) A vector calibration method incorporating all system responses into error terms and avoiding presumed prior knowledge of probe geometries. Panels (c) and (f) are reproduced with permission from Guo *et al.*, Appl. Phys. Lett. **118**, 041103 (2021). Copyright 2021 AIP Publishing LLC.[130]

Finite dipole model essentially calibrates the probe geometry by fitting the experimental approach curve using three parameters: a fraction, g, of the total induced charge in the probe tip that is participating in the near-field interaction, an effective tip radius, R, and an effective tip shank length, L.[181]

Ideally, solving the retrieval problem using FDM would be equivalent to solving an optimization problem since the measured near-field scattering spectra is a function of permittivity as well. By updating the permittivity under a specific rule (search algorithm), minimizing the deviation between the target and fit function would eventually provide extracted permittivity as shown in Fig. 5(d).[185,190] However, FDM was designed for modeling s-SNOM response at mid-IR and has two major issues when applied at THz frequencies:

1. For broadband investigation approaches like THz-TDS, the incident pulse contains all frequency components, which is referred to as whitelight. Therefore, the crucial fitting parameter g obtained via fitting the approach curve in the time domain only captures an ensemble response averaged over the whole frequency spectra. It neglects the frequency-dependent nature of sample permittivity and ignores the spectrally varying tip-sample coupling strength (antenna resonance effect).
   Theoretically, one potential solution for this case could be combining the approach curve measurement with THz point

spectroscopy—for each step size moving away from the sample, a THz nanospectroscopy is performed. However, this approach is unrealistic at the current stage without a high-power stable THz emitter.

2. Another issue is that modeling the probe geometry cannot remove contributions from parts of the system other than the probe, compounded by the fact that the geometry of each individual probe is subtly different (especially for the probes used in THz regime) and that it changes during probe usage.

For further technical details and discussions, readers could refer to the literature for materials regarded as a bulk[180,181,202] or multi-layer structure[189,199,200] employing the dipole-model formalism.

The core of other rigorous s-SNOM models[189,197] aims to calculate the charge distribution and induced polarizability on the probe[198,204] involving the knowledge of the probe geometry[205] using the numerical methods. For example, the lightning rod model (LRM),[189] aims to precisely model the realistic probe geometry while considering the field retardation between the probe and sample under the electrodynamic formalism.

Recently, Chen and his co-workers demonstrated the recovery of complex permittivity in broadband mid-infrared regimes from complex-valued near-field spectra using a neural network (NN).[183] As shown in Fig. 5(e), this end-to-end pipeline is a typical standard neural

network with three hidden layers. Although the pre-trained neural network allows the potential transfer learning and the model deployment to other configurations, the authors also stated that it was based on a standard Neaspec nano-FTIR probe with reproducible and nearly identical probe geometry in each batch.[183]

While Chen's study suggests the retrieved spectra were generated using the neural network (NN), due to the small amount of available s-SNOM training samples (less than several thousands or more in a typical deep learning scenario), such a few-shot learning problem hampers to rely solely and blindingly on a NN black-box. If implicitly informed by a known tip-interaction model,[180,189] the training spectra need to be generated with the assumed prior knowledge of both the probe geometry and the probe surface charge distribution induced by the near-field interaction (for FDM, it originates from the calibrating parameter g describing the effective charge response along the probe geometry). Therefore, it appears that it would be challenging to apply such a neural network directly to the THz s-SNOM setup, considering the probe tip geometry is generally not known nor reproducible.

Hence, considering the compromise between the extraction precision and the model complexity, there is room for an effective calibration approach that is feasible for a broad range of s-SNOM users.

A source-independent s-SNOM calibration methodology to extract the complex permittivity (complex refractive indices) and its derivatives, including free-carrier concentration and conductivity, is worth developing.[130] A typical THz s-SNOM, as illustrated in Fig. 5(c), is composed of an AFM and a THz-TDS system for THz nano-spectroscopy.

The problem is essentially a retrieval problem—by knowing details of complex-valued scattered (reflected) electric field, how
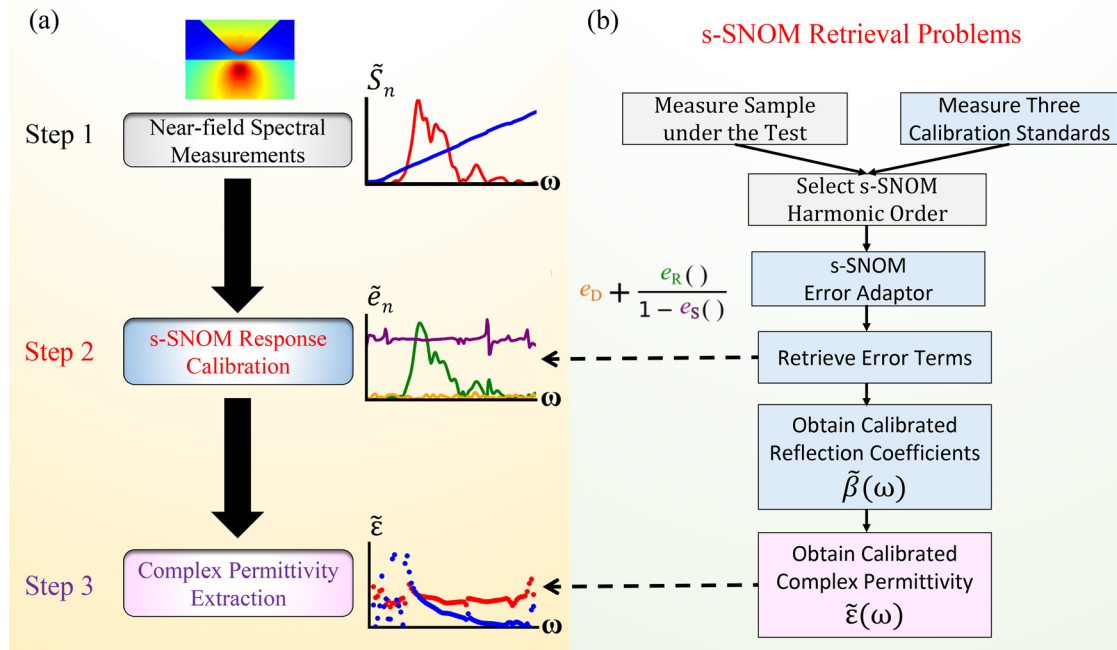
should the material properties of the sample under test be extracted? As the complex permittivity determines the reflectivity of the interrogated sample, it is essentially a procedure to describe this scattering process, as shown in Fig. 5(f), using a physics-informed white box, in the form of an error adapter. From the flow diagram in Fig. 5(f), one can derive the expression that relates the incident and the scattered fields:

$$E_{sca,M}/E_{inc,M} := \sigma_{sca} = e_R \cdot \frac{\beta}{1 - e_S \cdot \beta} + e_D, \quad (1)$$

where β is the unknown quasi-static reflection coefficient ($\beta = \epsilon - 1/\epsilon + 1$) describing the sample material properties (e_D, e_R, e_S) are error terms for the adaptor, and $E_{sca,M}/E_{inc,M}$ defines the measured scattering information from experiments. To perform the calibration, one requires the prior knowledge of material properties—complex permittivity—of three calibration standards with known dielectric constants, in order to obtain error terms (e_D, e_R, e_S).

By doing so, complicated modeling for the probe-sample interaction is avoided and the errors introduced by the uncertainty of theoretical model parameters (especially tip geometry) in solving an inverse problem are eased.

The essential steps to perform s-SNOM vector calibration are figuratively illustrated in a flow chart in Fig. 6. The first step is to measure s-SNOM spectra on the sample under test in tandem with measuring suitable materials with known complex permittivities in the probing frequency regimes. Different from the conventional baseline-removal approach, which directly normalizes the complex-valued spectra of a tested sample to that of a reference (usually a perfect reflector or a spectral-flat sample in the probing bandwidth), the vector-nature

FIG. 6. s-SNOM quantitative analysis flow chart on extracting unknown material properties from tip-scattered spectral measurements: (a) the bridging role of s-SNOM vector-nature calibration between un-calibrated complex-valued s-SNOM spectra (red: amplitude, blue: phase) to extracted sample permittivity (red: real part, blue: imaginary part). (b) The procedure to decipher material properties (i.e., complex permittivity) from s-SNOM scattering spectra by using an s-SNOM error adaptor to solve an inverse problem.

calibration method demands reference spectra from three known standards. Then, tip-scattered spectra ($\tilde{S}_n$) of three standards at a specific harmonic order (n) are employed on the s-SNOM error adaptor to retrieve three error terms (e_D, e_R, e_S). These three error terms (following microwave nomenclature, namely, directivity, reflection tracking, and source match) effectively describe three s-SNOM effects from measurements of the three calibration standards: (1) the sole probe tip contribution without a sample underneath (e_R) under the incident waves, (2) the responsivity (e_R) of the probe tip (a nano-antenna) with a sample, (3) the multiplicative reflection process (e_S) between the polarized tip and the mirror image of sample half-space. Subsequently, with the knowledge of three error terms obtained from experiments, the scattering spectra of an arbitrary unknown sample could be calibrated and thus allows for calibrated complex-valued reflection coefficients $\tilde{\beta}$ and permittivity $\tilde{\epsilon}$. Note that this s-SNOM calibration procedure enables the retrieval of complex-valued permittivity of the sample under test to be ignorant of a prior assumed permittivity model. Additionally, the knowledge of material properties of calibration standards can either come from the literature[206,207] or from far-field measurements like ellipsometry.[208–210]

Measurement-specific calibration steps are always necessary for separating background signals, inherent instrumentation, or measurement errors (which are hardly well-modeled) from the tip-sample interactions.[42] This vector calibration methodology to solve s-SNOM retrieval problems has been applied to extract complex reflectivity and permittivity of multiple organic and inorganic materials at broadband THz frequencies,[130,195] which origins from the so-called S_{11} calibration in the nomenclature of microwave vector network analyzer (VNA) calibration.[130]

The importance of calibration for near-field measurements has also been demonstrated in scanning microwave microscopy (reflection-type),[211–214] where a VNA sends an incident microwave signal through a conductive tip (usually part of a scanning tunneling microscope or atomic force microscope) to the interrogated sample and further measures reflections coming from the tip-sample interface, which passes through the probe tip (calibration plane, before RF cables and connectors) interfaced with an impedance matching network (usually a half-wavelength wave transformer with a $50\,\Omega$ shunt resistor; for overcoming the impedance mismatch between the microwave source and the evanescent microwave probe) and finally back to the VNA (measurement plane).[141,215] One notable effort in SMM calibration technique development is *in situ* calibration, i.e., without referring to extra calibration standards but only with the sample under the test itself.[213,214] Note that the calibration technique for AFM-based SMM requires a highly conductive or lossless dielectric substrate[141] at the probing microwave frequencies for approach curve calibration purpose.[214] Instead of measuring three calibration samples, SMM *in situ* calibration features the ability to extract three error terms (e_D, e_R, e_S) by measuring the input impedance at the probe tip with different probe-sample distances through multiple approach curve measurements, by requiring pure capacitive responses in the probe-sample pair [i.e., $Z_{\text{tip-sample}} = 1/(G + j\omega C) \sim 1/(j\omega C)$, limited to non-lossy substrates ($G \sim 0$), so that the real part of the admittance response can be ignored in approach curve measurements, $Y(\omega, z) = G(\omega, z) + j\omega C(z) \sim j\omega C(\omega, z)$]. This is achieved by simultaneously measuring both SMM microwave responses [$S_{11,m}(\omega, z)$] and tip-to-sample capacitance responses by electrostatic force microscopy[216]

[$C(\omega, z) = \int_h F_{es} dh$ as well as capacitance gradient with respect to the tip-sample distance are derived from electrostatic force measurements, $F_{es} \propto dC/dh$] for the tip-sample pair in approach curve measurements.[141,214] To finish the SMM workflow for extracting dielectric constants (permittivity) for calibrated sample capacitance, a de-embedding process of characterizing the dielectric probe is necessary.[217,218] Proper consideration of tip geometry modeling for de-embedding is therefore essential,[219] for example, approximating as a capacitive sphere[213] or resorting to full-wave electromagnetic simulation.[104] The need for an *in situ* calibration of SMM arises due to the presence of stray capacitance, which can lead to inaccurate calibration results when relying solely on the S_{11} calibration method for SMM measurements. This is because the calibration plane becomes ill-defined in the context of SMM's capacitance-based response mechanism. When exchanging between a calibration sample and the test sample, the stray capacitance introduced by the probe tip cantilever results in varying signals, rendering the calibration plane undefined.[213,214] For STM-based SMM, due to the mechanism for measuring tunnel currents between the tip and the interrogated sample, the sample substrate needs to be conductive, e.g., highly oriented pyrolytic graphite (HOPG)[213] or conductive indium tin oxide (ITO) glass as a ground electrode,[104] whereas s-SNOM can in principle investigate arbitrary AFM-quality solid-phase sample surface without further requirements.

Note that for validly approximating the probe as a capacitive sphere or short monopole, the electromagnetic wavelength needs to be way longer than the probe's physical dimension,[220] whereas this is valid for microwave cases in scanning microwave microscopy using typical STM or AFM tips. However, when the electromagnetic wavelength is close to the dimension of the probe length, which is the case for THz s-SNOM (due to the antenna resonance effect), a point sphere approximation may not be ideal for retrieving quantitative material properties (like complex permittivity) in s-SNOM inverse problems.

We envisage an online de-embedding process taking into consideration three-dimensional probe geometry shape reconstructed by real-time scanning electron microscopy measurements. This could be a similar probe de-embedding strategy (with full-wave electromagnetic simulations) for THz s-SNOM inverse problems. Such a computationally expensive strategy may be realized by the synergistic development of artificial intelligence (AI) and quantum computing on could computing platforms (e.g., Microsoft Azure and Amazon Web Services) in the future.

We also note that recent publications aim to deal with the modeling complexity of tip-sample near-field interactions due to the probe geometry and sample's surrounding environment.[221,222] Chen *et al.* developed for a rapid simulation approach to recover near-field optical contrasts at a qualitative level.[221] Instead of performing a time-consuming full-wave simulation from scratch, the probe tip response parameter is obtained by computing the difference of simulated scattered fields between the consideration and ignorance of the sample under the test. To deal with nontrivial topography in the nanosystems, Mester *et al.* demonstrated an elegant approach using multiple different higher harmonics of near-field mid-infrared scattering signals to remove anomalous observations due to far-field incidence, without adopting complicated electrodynamic simulations.[222]

We emphasize here that, each approach holds its own benefit to analyze near-field scattering signals from s-SNOM. Depending on the

goal and electromagnetic frequencies used in s-SNOM projects, researchers need to adopt a suitable approach to decipher material properties and interpret near-field observations at either the quantitative or qualitative level.

In Sec. IV, significant advances using THz SNOM are reviewed, including bulk materials, thin films, and biological samples.

IV. TERAHERTZ NEAR-FIELD APPLICATIONS

A. Why THz SNOM?

THz radiation refers to electromagnetic waves with the wavelength conventionally ranging from 30 to 3000 μm, corresponding to the spectrum spanning from $0.1 - 10$ THz in the frequency domain.[223–225] The temporal scale of THz radiation is thus on the order of picosecond, matching the energy of various collective motions[17,24] and fundamental excitations in inorganic and organic samples.[30,226,227]

Three representative response mechanisms for THz waves are illustrated in Fig. 7. For example, since electron–electron scattering is around the picosecond scale, THz radiation is suitable for probing intraband transitions including free-electron transport.[21,227] Therefore, THz waves have been used to characterize semiconductors and study electrical properties of organic and inorganic nanowires[24] and films.[228–230] Another frequently encountered collective motion is inter-molecular vibrations, referring to non-covalent bonds across molecules, like van der Waals (vdW) interactions and hydrogen bonds.[28] One of the most intriguing applications of this long-range collective motion in the THz regimes is to determine free and bounded water content in samples.[29,30] By quantifying the absorption of THz radiation, identifiable features of biological tissues (like human skin, brain, etc.) can be determined to distinguish benign and malignant areas.[31–33] Meanwhile, THz radiation has been reported to be sensitive to vibrational modes and stretching modes within a single molecule,

e.g., low-frequency collective vibrations within large molecular chains.[35,231]

Apart from the above three collective motions with spectral resonances as shown in Fig. 7, various organic and inorganic samples hold distinguishable complex-valued refractive indices in THz spectra.[19,232] This allows material identification and sensing applications in a wide range of areas including biomedical imaging,[31,32,233] pharmaceutical analysis,[234–236] pollutant monitoring,[237] food quality assurance,[238] and art conservation.[239–242]
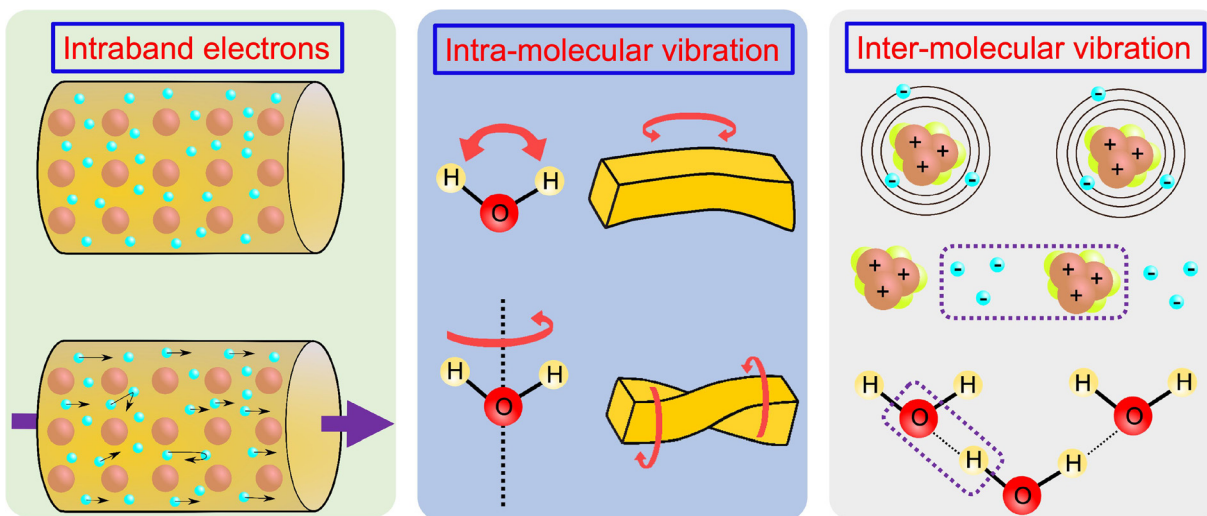
In the past, due to the diffraction limit, the above-mentioned phenomena were typically investigated at the macroscale. To progress the understanding and unveil the microscopic origin of the THz responses, it is crucial to resolve the constituents of these ensembles at the nanoscale. Thanks to the advent of SNOM, we are able to unravel subwavelength THz features within tens of nanometers.[13,15,34,40]

B. Material characterization

Sections IV B 1–IV B 3 review THz near-field studies beyond the instrumentation development. One of the major applications for SNOM is surface characterization. Depending on the sample properties, we classify the studies into three different types:

(1) solid-state bulk materials,
(2) thin films and van der Waals (vdW) materials,
(3) and weakly scattering biological samples.

Since THz radiation is sensitive to free-electron transport and lattices, THz s-SNOM serves as a desirable tool to probe local plasmons and thus free-carrier profiling in semiconductor nanodevices,[75,91,130,158,195,243–245] visualize plasma waves, invoke the field distribution,[246–248] investigate the light coupling with electrons,[132,159,249–252] phonons,[120,169,253,254] and excitons,[255,256] strain-induced topological transitions,[257] and phase transitions[258–260] in solid-state materials.

FIG. 7. Typical response mechanisms of light-matter interactions in the THz spectral range: (1) intraband transitions: the excitation of electrons into a higher energy level within the same energy band. This leads to the intraband absorption of free electrons and free-electron movements, as shown in the left panel, which is able to be probed by THz waves. (2) Intra-molecular vibration modes, including stretching and rotation within a single molecule. (3) Inter-molecular vibrations including weak non-covalent interactions, hydrogen bonds, and van der Waals forces.

1. Solid-state bulk materials

One of the most interesting THz s-SNOM application studies is nondestructive and ultrasensitive characterization of semiconductor devices at the nanoscale, which was for the first time demonstrated by Knoll and Keilmann with contrasting mobile carriers in semiconductors.[91] Huber and his co-workers demonstrated the first spatial contrasts of different doping concentrations by scanning a cut-through of a multiple-transistor device at 2.54 THz as shown in Fig. 8(a).[75] This study reveals the spatial THz responses originating from the near-field excitation of THz plasmons. Although it is limiting to use a bolometer to collect the spatial scattering intensity of a gas laser, this pioneering work established the experimental possibility of quantitative studies to rigorously extract local free-carrier concentration and conductivity of semiconductor nanodevices using THz s-SNOM.

Ten years later, Liewald et al. reported a study of a silicon chip with various doping concentrations using interferometric s-SNOM equipped with a microwave mixer.[100] With the tunability to obtain monochromatic radiation up to 0.75 THz, this study displayed both the spatially varying amplitude, in Fig. 8(b), and the phase mappings for different doping concentrations of a semiconductor nanodevices.

The same commercial device was further investigated by Aghamiri et al., who utilized a THz-TDS system in a purge box to demonstrate the s-SNOM capability of relating the THz spectral contrast with distinctive doping carrier concentrations.[158]

Since the sample electrical properties like carrier concentrations and conductivity are fundamentally determined by the complex permittivity, the premise is to measure complex permittivity of the interrogated sample using s-SNOM.

To enable THz s-SNOM as a useful nanoscopy to quantitatively characterizing arbitrary unknown samples, it is vital to solve the s-SNOM retrieval problem (an inverse problem), as defined in Fig. 5(a), without the prior knowledge of unknown samples' dielectric properties (i.e., complex permittivity) nor presuming permittivity values following the mathematical form of a phenomenological model (e.g., Drude, Lorentz–Drude, or Brendel–Bormann model). To address above issues, recently, Guo et al. demonstrated a quantitative nanoprobe method[130,132] for s-SNOM to measure sample complex permittivity and thus other sample characteristics (free-carrier concentration and conductivity)[195] in a broadband THz spectral range $(0.5 - 1.6 \, \text{THz})$ under an ambient environment.

Additionally, Wiecha et al. demonstrated the capability to determine carrier density from both photo-excited and impurity-doped Si utilizing the prior knowledge of the interrogated silicon sample's momentum scattering time and doping species from single-frequency THz measurements at 0.25 THz in a home-built s-SNOM system.[245]
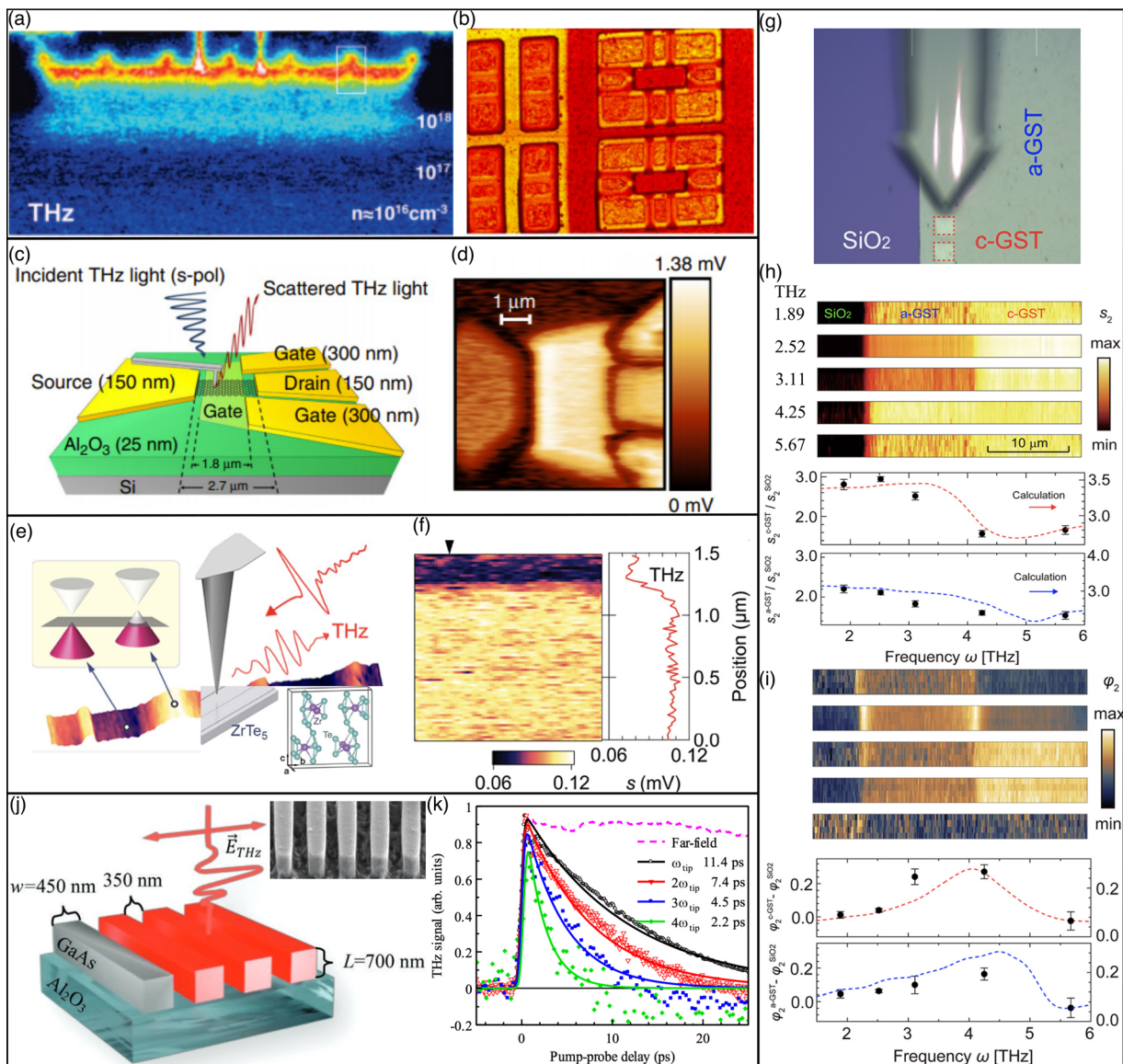
Owing to the nm-scale sensitivity of detecting free electrons, THz s-SNOM is anticipated to probe minute heterogeneity results from the external modulation of electronic structures as well. Facilitated by THz broadband spectroscopy $(0.5 - 1.6 \, \text{THz})$ and white-light contrast $(\sim 0.5 \, \text{THz})$, Kim et al. reported strain-induced THz near-field responses across the strip conjunction of a $ZeTe_5$ single crystal by probing THz nano-scale conductivity heterogeneity using an s-SNOM, which demonstrates the capability of tracking the nanoscale transition of Dirac fermion density using THz waves[257] [Figs. 8(e) and 8(f)] as well as visualizing the conductivity heterogeneity understood as charge fillings in grain boundary traps for $MAPbI_3$, a perovskite material.[263]

Pushkarev et al. combined THz s-SNOM with a visible pump laser to achieve time-resolved THz measurements and gain insights into the electron motion at nanoscale with a single-crystalline GaAs nanobars.[262] They observed faster transient decay of s-SNOM signal in GaAs nanobars at higher demodulation orders [see Figs. 8(j) and 8(k)] and attributed it to different relaxation dynamics at surface vs bulk, emphasizing a crucial role of interfaces in the electron response of nanostructures. To further quantitatively correlate the nanobar geometry and permittivity with the fast relaxation dynamics, future studies on THz s-SNOM probing volumes (both spatial resolution and probing depth) are required.

In addition to probing the free-electron movements in nanodevices, THz s-SNOM has also been demonstrated to reveal photon-plasmon couplings.[261] As predicted by the theory, a gated plasma wave originates from the coupling of THz radiation into an antenna-coupled field effect transistor. It involves the collective interaction between the two-dimensional electron gas and gate electrode. One approach allowing the discovery of such a light-matter coupling is tuning the gated voltage to control the carrier density and plasma frequency. By doing so, Soltani et al. reported the first visualization of plasma wave field distribution in the channel of graphene FET detector excited at 2 THz,[261] as shown in Figs. 8(c) and 8(d), with a propagation distance of several hundred nanometers and a short sub-100-fs lifetime. Recently, Feres et al. reported the enhanced THz nanoimaging contrast in graphene/hBN device with buried structures at 3.8 THz using free-electron lasers by harnessing the polariton-assisted THz field enhancement in graphene.[254]

Apart from plasmons, THz radiation can also probe collective lattice vibrations and thus highlight the spectral features of amorphous or crystalline phases of a material. Chen and his co-workers observed clear THz near-field spectral differences between the amorphous and crystalline phase of a chalcogenide phase-change material, $Ge_1Sb_2Te_4$ (GST) on a SiO_2 substrate, in Fig. 8(g), using s-SNOM equipped with a gas laser spanning the spectra from 2 to 6 THz.[209] By comparing obtained experimental near-field data to the modeled near-field spectra using dielectric function extracted from far-field transmission FTIR measurements $(0.9 - 350 \, \text{THz})$, they confirmed that the spectral differences are correlated with the distinctive optical phonon modes between the amorphous and crystalline phase of the sample as shown in Figs. 8(h) and 8(i). This study highlights the significance of knowing the complex permittivity to perform further conclusive analysis in near-field interrogations.
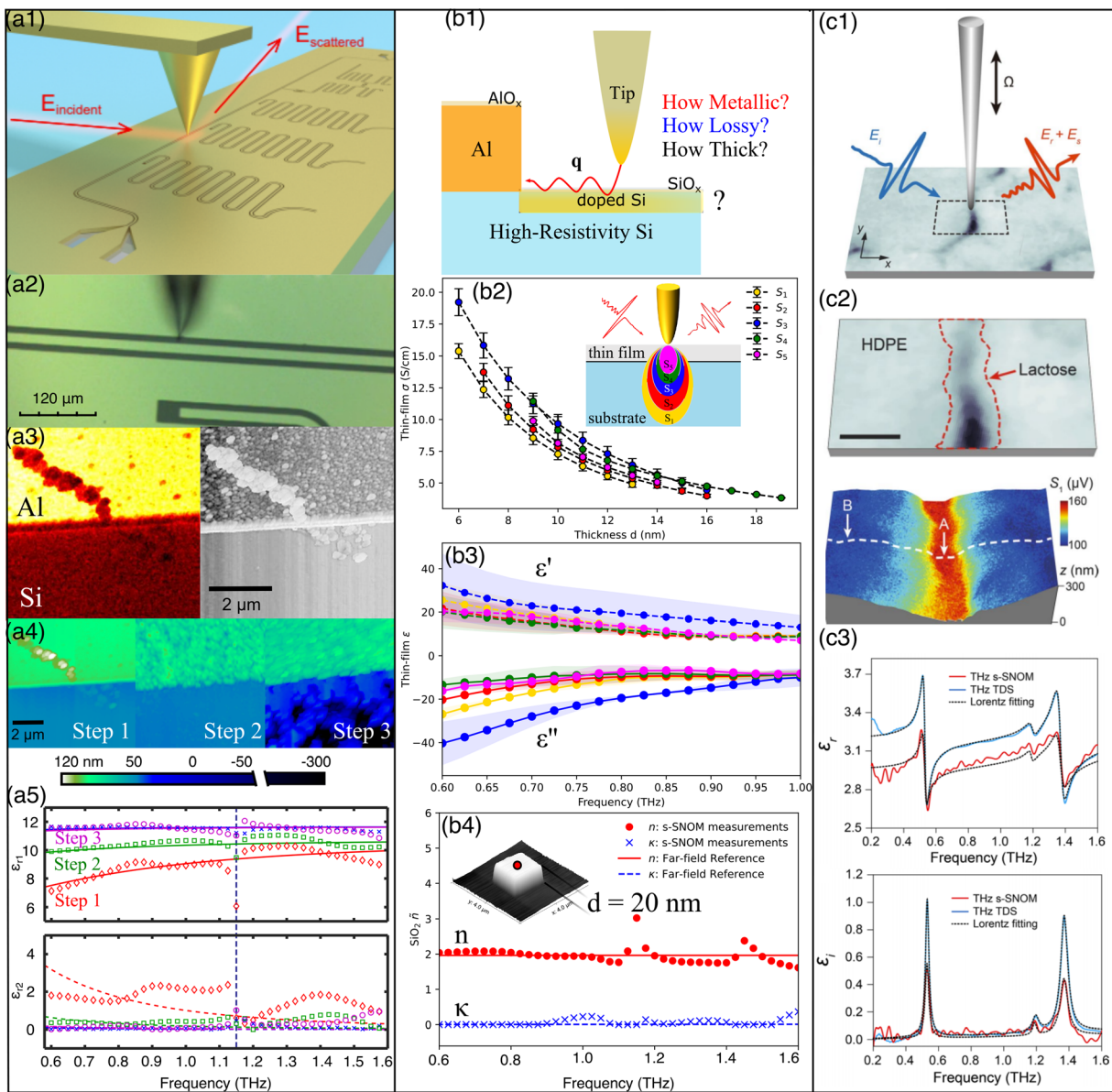
Benefiting from nanoscale probing sensitivity of THz s-SNOM, Guo et al. harnessed quantitative results from THz nanospectroscopy to aid high-precision advanced manufacturing protocols of quantum devices for superconducting quantum computing.[195] By collecting the elastic forward scattering on test devices [Fig. 9(a1)], Guo et al. found organic photoresist residue (tens of nanometers) which is invisible under the conventional optical microscope, in Fig. 9(a2), and managed to track the evolution of complex-valued permittivity of a coplanar microwave resonator after multiple surface treatments as shown in Fig. 9(a4) to further evaluate the effective removal of fabrication-induced doping in Fig. 9(a5).[195] This work reported unintentional doping originating from wet chemical etchants as an undesired effect, which may serve as potential loss channels of superconducting quantum computing devices. Moreover, this study shows that THz s-SNOM are ready to be employed to

24 November 2024 03:57:31

FIG. 8. THz nano-scale investigation of solid-state integrated circuit devices, including: (a) a cut-through for multiple-transistor devices at 2.54 THz with spatially varying THz contrast originating from Drude responses due to the doping concentration heterogeneity. Reproduced with permission from Huber *et al.*, Nano Lett. **8**, 3766–3770 (2008). Copyright 2008 American Chemical Society.[75] (b) Doped silicon random access memory at 0.6 THz with the Durde response spatial contrast. Reproduced with permission from Liewald *et al.*, Optica **5**, 159–163 (2018). Copyright 2018 Optica.[100] (c) and (d) Device configuration as well as THz responses of a graphene TeraFET bow-tie antenna among source, gate, and drains at 2 THz. Reproduced with permission from Soltani *et al.*, Light: Sci. Appl. **9**, 97 (2020). Copyright 2020 Nature Publishing.[261] (e) and (f) THz white-light contrast (frequency-averaged response, mainly dominated by the component ∼ 0.5 THz) of Dirac semimetal ZrTe₅ across the strip junctions. Reproduced with permission from Kim *et al.*, ACS Photonics **8**, 1873–1880 (2021). Copyright 2021 American Chemical Society.[257] (j) and (k) Optical pumped THz far-field and near-field measurements to resolve ultrafast dynamics in GaAs nanobars, aiming to understand nanoscale charge transport in a volume-confined system. Reproduced with permission from Pushkarev *et al.*, Adv. Funct. Mater. **32**, 2107403 (2022). Copyright 2022 American Chemical Society.[262] (g) THz nanoscopy investigation of chalcogenide phase-change materials, $Ge_1Sb_2Te_4$ (GST) compounds on a SiO_2 substrate, with distinctive nano-scale dielectric response contrast between amorphous [(h): a-GST] and crystalline [(i): c-GST] states originating from THz optical phonon modes within 2–6 THz. Reproduced with permission from Chen *et al.*, ACS Photonics **7**, 349903596 (2020). Copyright 2020 American Chemical Society.[209]

characterize advanced materials and nanostructures with high charge carrier mobility, where the inference of nanoscale surface doping and interfacial bonding are essential to understand the microscopic mechanisms.[264,265]

Recently, Guo *et al.* extend s-SNOM calibration method[130] to multilayers,[132] allowing direct quantitative analysis of both complex-valued permittivity and thickness of an unknown thin film from a complex nanostructure considered as being multilayer [Fig. 9(b1)].

FIG. 9. Complex-valued permittivity extraction from THz s-SNOM broadband spectra: (a1) and (a2) Near-field investigation of coplanar microwave resonators used for super-conducting quantum computing: (a3) THz nanoimaging (second-harmonic signals) to identify fabrication-induced doping in clean Si channels and surface treatments (a4) aiming to remove induced doping. THz nanospectroscopy (a5) for quantitative evaluation of fabrication-induced excess carrier concentration. Reproduced with permission from Guo *et al.*, Appl. Phys. Lett. **119**, 091101 (2021). Copyright 2021 AIP Publishing LLC.[195] (b1) THz near-field investigation of an unknown surface doped layer on a high-resistivity sili-con substrate: (b2) retrieved surface doped thin film feasible thickness and conductivity using (b3) complex-valued permittivity measured via multiple THz s-SNOM high-order harmonic signals (S_1–S_5). (b4) THz s-SNOM multilayer extraction validation on a known multilayer nanostructure (20 nm SiO_2 squares on Si). Reproduced with permission from Guo *et al.*, Nanophotonics **12**, 1865–1875 (2023). Copyright 2023 De Gruyter.[132] (c1) near-field identification of localized molecular resonance peaks in crystalline-lactose stereoisomer with first-harmonic scattering contrast (c2) with the permittivity data (c3) to reproduce the measured near-field scattering. Reproduced with permission from Moon *et al.*, Sci. Rep. **9**, 16915 (2019). Copyright 2019 Nature Publishing Group.[192]

Once the thin film complex-valued permittivity is obtained, a further infer of conductivity, mobility, or dielectric loss is allowed [Figs. 9(b2) and 9(b3)]. Guo *et al.* also validated the capability of this s-SNOM extraction method on a well-characterized AFM standard calibration sample (TGQ1, SiO_2 squares on Si). The development of s-SNOM

extraction method on complex-valued permittivity and thickness enhances the practical usage of THz s-SNOM for characterizing unknown materials at the nanoscale when the knowledge of the per-mittivity model of the interrogated sample is not available in reality. This allows the expectation of utilizing THz s-SNOM for analyzing

permittivity-related information of samples, as viable as far-field THz probe methods.[17,145]

Another pioneering work on the extraction of THz permittivites from s-SNOM scattering spectra demonstrated the capability of recovering molecular resonance of crystalline-lactose stereoisomer as shown in the bottom panels of Figs. 9(c1)–9(c3).[192] In this study, Moon et al. demonstrated that the permittivity of homogeneous bulk materials, which was inferred by comparing measured near-field data with far-field THz-TDS measurements in Fig. 9(c3), would not change at the nanoscale. This suggests that, once the s-SNOM reference materials are homogeneous and bulky, the choices of calibration standards, for s-SNOM permittivity retrieval problems, can be either spectral-flat materials (high-resistivity silicon, gold, air) or well-documented doped semiconductors in THz regimes.[130,132] By doing vector calibration on known bulky materials, it allows to interpret non-trivial near-field THz spatial contrasts due to the complex sample micro-structure topography[266–268] at a quantitative level. Such an independent extraction (without presuming a permittivity-model form) is essential in THz s-SNOM, allowing to infer the information (e.g., mobility or electron scattering rates) robustly before moving across the niche point to overfit a permittivity or conductivity model with quite a few parameters. For example, an independent and nanoscale probe of THz and lower-frequency conductivity allows to directly study locally confined systems with proposed microscopic pictures, including the carrier diffusion within a single THz pulse[269] or carrier backscattering,[270,271] or other models[23] based on either classical[272] or quantum-mechanical pictures.[273–276] In summary, direct complex-valued permittivity measurements in THz s-SNOM is the premise to study potential sample responses exhibiting non-Drude behavior,[277] which provides independent experimental evidence to answer at which spatial and temporal scale shall we adopt a complicated model to describe complex nanoscale dielectric behavior[278] in a nanoscale confined system.[279]

2. Thin films and two-dimensional (2D) materials

THz radiation oscillates at the picosecond timescale, matching the energy scales of various fundamental excitations and quasiparticles.[20] The investigation of these surface phenomena at the nanoscale contributes to a better understanding of their fundamentals.[280,281] For example, the phonon has a considerable impact on a wide range of crystallographic properties, including electrical and thermal conductivity, ferroelectricity, and superconductivity. Therefore, controlling the coupling strength between photons and electrons/phonons/excitons on emerging materials may thus offer as an intriguing fundamental platform for future applied research. Unlike bulk materials, instead of covalent bonds, the interlayers of van der Waals materials are weakly bonded by van der Waals forces. These materials also are referred to interchangeably as two-dimensional materials in the literature.[282] Such unique structures possess fascinating optical properties at the nanoscale.
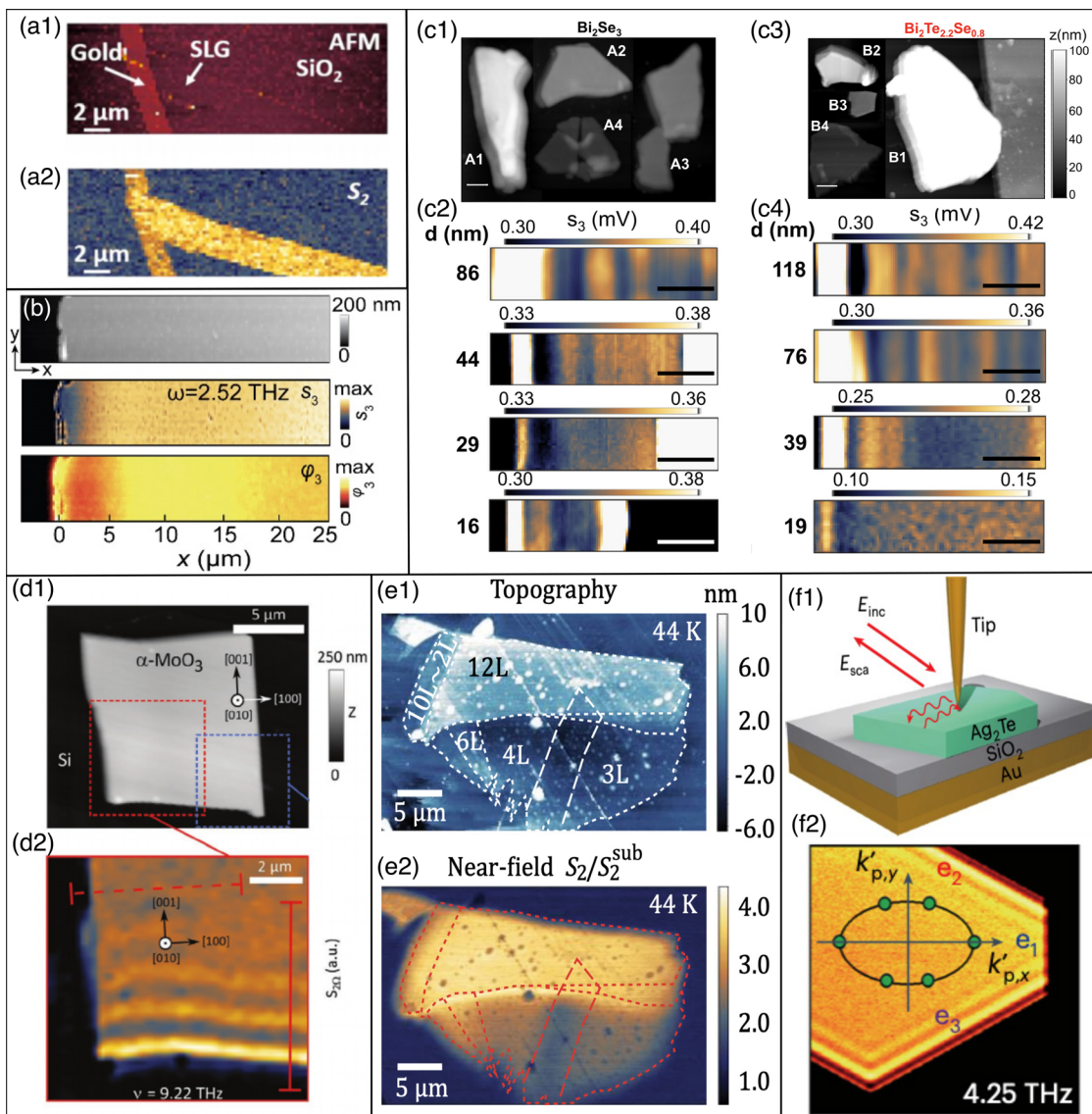
As a pioneer work, Zhang et al. demonstrated that due to unique Dirac band structure, graphene exhibits high carrier mobility in the range of $0.2 - 1$ THz, thus becoming a good THz reflector for near fields with high in-plane momentum.[243] As shown in Fig. 10(a1), THz nano-imaging was performed on a SiO_2 substrate with pre-patterned 30 nm Au lead and single-layer graphene (SLG). The corresponding second-order harmonic THz scattering amplitude is shown in Fig. 10(a2). It shows that the near-field reflectivity for THz waves is

comparable to that of a gold film. This study demonstrates the potential feasibility of graphene as the reference material in THz near-field experiments. Specifically, highly oriented pyrolytic graphite (HOPG) is accessible at an affordable price, and unlike thick noble metal, the atomic-layer flatness could be easily achieved by just peeling off the top few graphene layers. Moreover, graphene could be easily transferred onto other surfaces or structures without edge artifacts. Considering that it acts as a metallic reflector in the THz regimes, graphene would be an ideal candidate for both substrate and reference materials in THz near-field investigations involving weakly scattering biomedical samples.

In Figs. 10(d1) and 10(d2), de Oliveira et al. demonstrated that by exploiting phonon polaritonic excitations, THz radiation could be confined at the nanoscale on a vdW semiconductor film like α-MoO_3, suggesting the importance of next-generation vdW hererostructure engineering to enable ultralow-loss THz polaritons for directional in-plane propagation at the nanoscale.[282] Meanwhile, surface plasmon-polariton fringes with thickness-dependent spacing are observed in thin films of topological insulators, including Bi_2Se_3 at 2.55 THz, as shown in Fig. 10(b), highlighting the importance of near-field phase from s-SNOM spectra to analyze THz polaritons.[283] Similar oscillation fringes around the flake edge for Bi_2Se_3 [Figs. 10(c1) and 10(c2)] and $Bi_2Te_{2.2}Se_{0.5}$ [Figs. 10(c3) and 10(c4)] are reported at 1.99 THz with multiple different film thicknesses, revealing the contribution of two-dimensional electron gas to hyperbolic THz polaritons hybrid with plasmons and phonons.[120]

Thin film thickness, as another freedom of parameters, tunes the effective plasma frequency and thereby THz near-field response for the whole interrogated system in tandem with sample dielectric constants. Therefore, it is crucial to decouple the contribution of a thin film from the whole interrogated system to interpret THz near-field responses. However, it is not straightforward to extract both thin film thickness and dielectric constants simultaneously from tip-scattered THz s-SNOM signals. To achieve this, Guo et al. recently proposed an s-SNOM inversion extraction procedure for multilayer structures and characterized THz surface plasmon polaritons in silicon quantum devices due to a highly doped surface layer.[132] With the information of thin film thickness, Schäffer et al. reported the quantitative nanoscale conductivity mapping of cesium lead bromide ($CsPbBr_3$) thin film at grain boundaries, which indeed probed the spatially varying permittivity at the nanoscale.[284] Recently, by precisely controlling the number of layers (sample thickness), Jing et al. reported tunable THz metallic responses on layered transition metal dichalcogenide WTe_2 at 44 K using a cryogenic s-SNOM in Fig. 10(e1), demonstrating layer-dependent Fig. 10(e2) transition of WTe_2 energy bandgap.[251] This study performed by Jing et al. highlights the significance of introducing another measurement freedom—temperature dependence for THz s-SNOM measurements, which allows for finer understanding of material low-energy behaviors and will be discussed in more details in Sec. V about the road ahead.

Another experimental observable freedom is the anisotropic electronic and vibronic properties of the material platform. Recently, phase-resolved nano-THz measurements allows the real-space characterization of surface phonon polaritons[285] and acoustic plasmon polaritons[252] in semiconductor materials where the real part of the directional permittivities holds an opposite sign to the imaginary part. Nörenberg et al. reported the low-loss THz phonon polaritons in

FIG. 10. THz near-field studies on low-dimensional materials: AFM topography (a1) and THz near-field response (a2) between single-layer graphene (SLG), gold, and SiO_2 by white-light THz nano-imagining (0.2–2 THz, the spectral peak is around 0.9 THz). Reproduced with permission from Zhang *et al.*, ACS Photonics **5**, 2645–2651 (2018). Copyright 2018 Americal Chemical Society.[243] Observation of THz surface polaritons in thin flakes of topological insulators like Bi_2Se_3 at 2.52 THz (b) [Reproduced with permission from Chen *et al.*, Nat. Commun. **13**, 1374 (2022). Copyright 2022 Nature Publishing Group.[283]] and 1.99 THz (c1 and c2), $Bi_2Te_{2.2}Se_{0.8}$ at 1.99 THz (c3 and c4). Reproduced with permission from Pogna *et al.*, Nat. Commun. **12**, 6672 (2021). Copyright 2021 Nature Publishing Group.[120] An α-MoO_3 film at 9.22 THz (d1 and d2) with uniform topography [Reproduced with permission from Oliveira *et al.*, Adv. Mater. **33**, 2005777 (2021). Copyright 2021 Wiley Online Library.[282]] and layered transition metal dichalcogenide WTe_2 (e1) at 44 K with thickness-dependent THz near-field responses (e2) revealed by white-light THz nano-imaging (0.2–2.5 THz, the spectral peak is around 0.6 THz). Reproduced with permission from Jing *et al.*, Nat. Commun. **12**, 5594 (2021). Copyright 2021 Nature Publishing Group.[251] (f) THz real-space nanoimaging of in-plane anisotropic THz image polaritons supported in monoclinic Ag_2Te crystals on Au substrate with an insulator spacer. Reproduced with permission from Chen *et al.*, Nat. Mater. **22**, 860 (2023). Copyright 2023 Nature Publishing Group.[252]

germanium sulfide (GeS, a type of van der Waals semiconductor materials) from 6 to 9 THz.[285] Another interesting observation is reported by Chen *et al.*, where the hybrid of THz plasmon polaritons to its mirror image [Fig. 10(f1)] below an insulating spacer (SiO_2) is observed in low-symmetric hessite (Ag_2Te) crystal at 4.25 THz with in-plane

anisotropic THz responses [Fig. 10(f2)].[252] This so-called THz acoustic plasmon polariton (or image polaritons) was demonstrated to facilitate the further confinement of THz radiation ($\lambda_p/\lambda_0 \sim 1/65$) and decrease the polariton damping (lifetime > 0.4 ps). In a more delicate device structure, facilitated by a similar insulating spacer (2 nm hBN)

in high-mobility graphene devices, Ruiz *et al.* observed acoustic plasmon phase velocity shift at room temperature in THz regimes and understood as the transition from the hydrodynamic regime to the collisionless regime in electronic Fermi liquids.[286] Essentially, this transition is realized by tuning the relationship between probing THz wavelength and electron-electron scattering rate as well as interparticle collision rate, which is experimentally realized by controlling the thickness of the insulating spacer and the resulting Coulomb interaction screen degree. This work demonstrates that THz photocurrent nanoscopy based on s-SNOM is particularly useful for studying phenomena in low-dimensional electronic systems.[103,287] Recently, Guo *et al.* reported the near-field localization of the boson peak,[277] due to the low-frequency vibrational density of states,[288–290] in rare-earth metal (tantalum) films, providing a microscopic insight into two-level-system fluctuation as one of leading loss channels inhibiting superconducting qubits coherence lifetime. Moving from coplanar microwave resonators, another typical meta-structure in superconducting devices for quantum computing is Josephson junctions (metal/few nanometer-thick insulator/metal sandwich structure). Kim *et al.* demonstrated again THz s-SNOM advantage in quantum device, visualizing asymmetric nano-THz scattering responses across a $Al/AlO_x/Al$ junction surface in room temperature.[291] THz s-SNOM also plays a significant role when material heterogeneity is non-negligible at mesoscopic length scales. Examples include characterizing quasi-particles such as exciton-polaritons[256,292] in semiconductor materials or layered transition-metal dichalcogenides with THz excitation which could be promising for many novel THz applications in photonics, information, and quantum technologies.

Since being low-loss and low-damping is technologically essential to achieve the practical realization of polariton-based on-chip circuitry or other nanophotonic devices, the direct characterization of THz polaritons at the nanoscale is significantly important to explore further candidate materials with ultraconfined and long-lifetime polariton responses. As recently demonstrated by Obst *et al.*[293] on a typical anisotropic layered semiconductor (α-molybdenum trioxide), tunable in-plane hyperbolic polaritonic dispersion has been tuned by adjusting the twisted angle between two mechanically exfoliated layers (80–120 nm per layer) to achieve the canalized propagation. Note that Duan *et al.* recently demonstrated the existence of multiple photonic magic angles in trilayer α-molybdenum trioxide devices visually by near-field nano-imaging on stacks with different inter-layer angles.[294] The same strategy should be translatable to other vdW materials holding non-trivial permittivity tensors in THz regimes.

From the point of structural and optical response symmetry breaking, lowering the material system's structural and therefore optical response symmetry is the key to realize extreme polaritonic responses.[295] Finding non-trivial twist angles of THz polaritons is an effective approach to tailor broken symmetry and thus tuning the degeneracy of phonon resonators. The field is witnessing the presence of in-depth studies on the quantitative investigation of nanoscale THz anisotropic responses in materials characterized by non-trivial permittivity tensors and intentionally modified optical response symmetry at the moment. In platforms using native materials, one should anticipate optical response symmetry breaking characterized by non-trivial THz permittivity tensors without identical diagonal components nor rotation invariance (anisotropy), particularly in low-symmetry materials

such as orthorhombic, monoclinic, and triclinic crystals, while its interplay with non-Hermiticity (dictating absorption or loss in materials) on THz nanoscale responses is also an under-explored area. For achieving exotic THz material platforms by van der Waals engineering in the future,[296,297] quantitative s-SNOM approach to elegantly and robustly recover anisotropic complex permittivity tenors is necessary. By engineering the axial complex-valued permittivity in meta-structures[298] or van der Waals heterostructures,[299] tunable lattice vectors in the reciprocal space matching with THz polariton dispersions[300] for nano-waveguiding and energy transfer functionality is possible in the future.
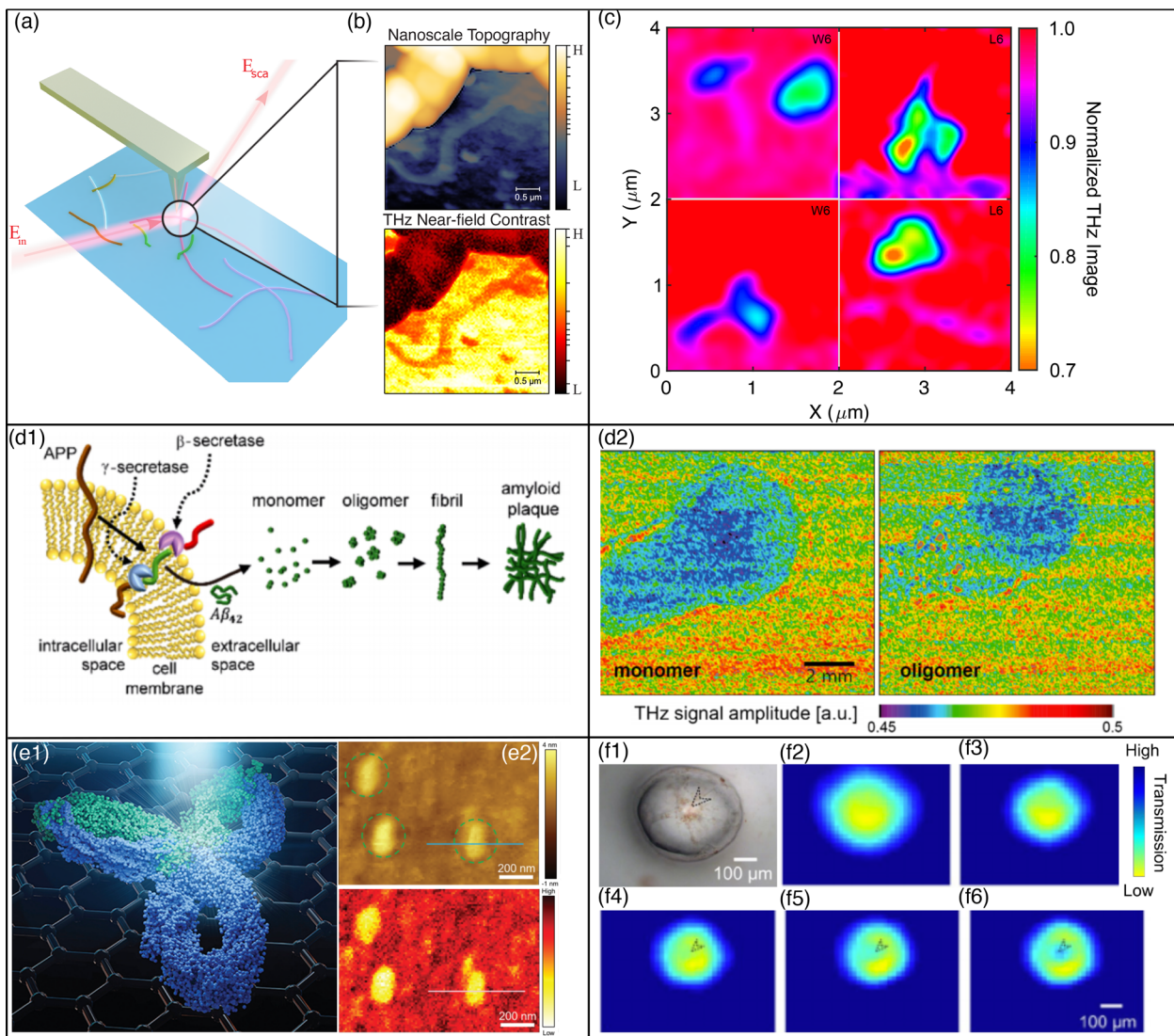
In this part, aforementioned pioneering THz near-field studies suggest that two-dimensional materials can serve as a potential platform for tunable control of long-wavelength radiation like THz waves and pave the way for surface-enhanced spectroscopy in THz regimes. The capability of THz s-SNOM for nondestructive quantitative characterization devices performance sensitive to nanoscale electronic heterogeneity (e.g., surface doping, mobility, charge-carrier effective masses) and thin-film thickness opens the door to facilitate next-generation applications, including thin-film transistors,[301] perovskite-based nanodevices,[302–305] and flexible electronics based on piezoelectric[306–309] and triboelectric effects[310] where microscopic conductivity and material heterogeneity in multilayer nanostructures matter for nanodevice performances.

3. Biological samples

Recently, studies have been showing the capability of SNOM to interrogate biological samples. In THz regimes, apart from intermolecular vibrations like hydrogen bonds and van der Waals forces, long-chain intra-molecular vibration and rotation also hold fingerprints. These molecular responses have been exploited to aid the identification of biomacromolecules including DNA, lipid, melanin, and saturated fatty acid[28,35,233] as well as multiple skin constituents (e.g., melanin, keratin, collagen).[314]

THz SNOM has been employed to investigate mouse brain tissue, bacteria, proteins, fruit cells, and peptides of different secondary structures.[196,311–313,315,316] THz s-SNOM researchers first demonstrated the observable contrast between the interrogated biological samples and the underlying substrate[312,313,316] and then started to retrieve quantitative metrics relating to material properties (e.g., conductivity) from the near-field contrast.[196,311] A typical pipeline to study biological nanowires using a THz s-SNOM is shown in Figs. 11(a) and 11(b), where the observable THz contrast across the sample and substrate is the premise before the discussion of further scientific analysis. The first experimental near-field THz investigation of biological samples was the nano-THz response in immobilized Pseudomonas fluorescens bacteria.[316] The authors tried various substrate choices and found that GaAs and Au were preferred candidates in detriment to early and widely adopted mica to highlight THz near-field responses at the nanoscale. In this study, Schäffer *et al.* showed a preliminary attempt to extract the bacteria's permittivity. Due to small dielectric constants of the interrogated bacteria in THz regimes and thus the low signal-to-noise ratio, the authors only managed to recover similar scattering amplitude of the result by mimicking the interrogated bacteria as PMMA.

Recently, researchers employed SNOM to reveal the relationship between the secondary structures of peptides and their electrical

FIG. 11. THz near-field contrast for biological samples using SNOM: THz s-SNOM contrast nanoimaging (a) on native bacteria nanowires, electrically conductive Geobacter protein nanowires, with simultaneously measured topography and (b) near-field THz responses on an individual bacteria nanowire without requiring a direct electrical contact at the nanoscale. (c) Synthetic bacteria peptide nanowires with different secondary structures with THz nanoscale responses achieved by s-SNOM. Reproduced with permission from Solemanifar *et al.*, Nanotechnology **33**, 065503 (2021). Copyright 2021 Institute of Physics.[196] THz near-field imaging to track the biological process (d1) for monomer and oligomer before deforming to be as peptides with THz spectral-averaged contrast (d2) at the millimeter-scale achieved by an a-SNOM. Reproduced with permission from Heo *et al.*, ACS Nano **14**, 6548–6558 (2020). Copyright 2020 American Chemical Society.[311] (e1) Individual Y-like shape antibody (IgG, as a majority of serum antibodies in humans) molecule on graphene with (e2) THz spatially varying near-field response around 150 nm using an s-SNOM. Reproduced with permission from Li *et al.*, Small **17**, 2005814 (2021). Copyright 2021 Wiley Online Library.[312] (f1) The topography and THz near-field responses of watermelon pulp cells in a 5 h dehydration process (f2)–(f6) with noticeable spatial features around tens of micrometers using an a-SNOM. Reproduced with permission from Li *et al.*, Cell Proliferation **53**, e12788 (2020). Copyright 2020 Wiley Online Library.[313]

properties, like conductivity. Figures 11(c) and 11(d) show the spatially varying THz responses of peptides at nanoscale [panel (c)], achieved by THz s-SNOM, and at millimeter-scale [panel (d)], achieved by THz a-SNOM, reported in recent ground-breaking THz SNOM biological studies with quantitative analysis on near-field data to retrieve peptide electrical properties.[196,311] Heo *et al.* distinguished oligomerization and

fibrillization state of amyloid beta protein in the buffer solution from near-field THz conductance measurements using an aperture SNOM.[311] With the cost of spatial resolution and loss of topography, aperture-type SNOM demonstrated its potential to investigate biological samples *in vivo* with resolvable features at tens of micrometers in THz regimes. Meanwhile, by employing s-SNOM, Solemanifar *et al.*

demonstrated to resolve smallest 10 nm high topological features of synthetic peptides [Fig. 11(c)] along with THz spatial varying contrasts within 100 nm.[196] This work also managed to recover the THz conductivity of different synthetic peptides with different secondary structures. While it shows the potential of developing novel bioelectronic devices, implantable sensors, and green electronics, it also draws the attention of biology research community on the power of THz s-SNOM as a novel and nondestructive technique to characterize bacterial nanowires.

Similar progress utilizing THz near-field contrasts to study biological processes is shown in Figs. 11(e) and 11(f). Yang *et al.* reported resolution of individual immunoglobulin G (IgG) and ferritin molecules on graphene substrates [Fig. 11(e)] at around 150 nm spatial resolution using THz s-SNOM with white-light contrasts from a TDS system.[312] Although no quantitative metric, such as complex permittivity, was extracted, this study highlights graphene (atomic-flat roughness and metallic reflectivity) potentially desired as a substrate for THz biological contrast imaging using s-SNOM. The same group also attempted to apply THz aperture-type SNOM on biological samples and Li *et al.* managed to monitor temporal drying evolution of a single watermelon pulp cell at 1.66 THz over 5 h, in Figs. 11(f2)–11(f6), with a spatial resolution of $\sim 20\,\mu m$ using an a-SNOM.[313] However, due to the low spatial-resolution capability of THz a-SNOM, a negligible THz near-field spatial contrast was reported within a single cell due to dehydration. Although this study failed to distinguish cellular organelles in the cytoplasm of a single cell, it represented a good starting point for THz near-field biological studies.

We also note that SMM researchers have undertaken endeavors to achieve quantitative microwave measurements in liquids for biological applications.[104,144,317–320] To address the challenges of strong absorption encountered when directly immersing the probe tip in liquids[318] and the complex interactions (beyond pure-capacitive responses) with live cells in physiological buffers,[104] Tselev and colleagues demonstrated an elegant approach. They separated the probe tip and the samples using an ultrathin membrane (made of nanometer-thick silicon nitride or silicon dioxide) mounted on silicon frames (liquid cells), which were initially developed for supporting samples in TEM (transmission electron microscopy) studies.[317] This innovative approach enabled the imaging of single yeast cells in glycerol solutions, capturing their responses to 5 GHz microwaves. Recently, the inverted-SMM technique was showcased for interrogating mitochondria in an isotonic glucose solution,[144] alongside ongoing advancements in calibration methods that account for the lossy nature of the medium.[320] Another recent interesting SMM study involving liquids shows how a nanometer-thick water meniscus acts as a nanoscale microwave iris formed between the probe tip and a twist-layer graphene (TBG) system for concentrating microwave electromagnetic fields within small areas, which is used for explaining imaging results of Morié patterns at different twisted angles with 1 nm spatial resolution.[319] Note that this strong coupling enhancement effect is attributed to the high dielectric value of water (~ 81) at 3 GHz. This diminishes the impact of the sample's geometric capacitance, in turn enhancing the contribution of quantum capacitance—which is closely associated with the electronic properties of the sample—to measured near-field microwave signals. As a result, the contribution of the sample's free carrier concentration to the microwave signal is increased due to the increased contribution from quantum capacitance.[321] For THz

s-SNOM, such a near-field coupling enhancement realized by introducing an additional adventitious liquid layer with impedance-matched permittivity values at THz frequencies is a potential new strategy to be explored and verified. For achieving nanoscale impedance matching and enhanced THz near-field couplings, we envision recently demonstrated virtual gain approaches for amplifying evanescent fields[322–324] as well as next-generation nanoscale metalens techniques[325] may serve as viable options in the future.

To further unveil the origin of both THz temporal and spatial response change, it would be interesting and necessary to observe THz near-field spatial contrasts among nucleus, vacuole, and Golgi apparatus in the future, harnessing high spatial-resolution capability of an s-SNOM. THz-specific protocols (e.g., liquid permittivity, membrane permittivity, membrane thickness) are therefore essential to be explored iteratively in practical experimental investigations for optimal near-field imaging and spectroscopic measurements.

While the near-field response contrast between the sample and substrate could be enhanced by tuning the permittivity difference between these two, a quantitative interpretation of the convoluted near-field responses in the tip-sample-substrate triplet is non-trivial and usually relies on a well-documented vibration mode database[326] to infer the information of molecular vibration modes in the interrogated sample system.[327] Such auxiliary knowledge of THz molecular responses is not as well-documented as that for mid-infrared cases, which requires continuing efforts of THz spectroscopic studies in the community for creating a database with reproducible molecular vibrational mode information.[231,328,329]

Apart from investigating dried biological samples using s-SNOM, probing living cells or organic samples in liquid environment has been demonstrated so far in mid-infrared regime using s-SNOM. Meanwhile, it would be exciting to expect *in vitro* THz near-field studies employing s-SNOM to unveil nanoscale features of biological samples in the future.

V. THE STATE-OF-THE-ART AND THE ROAD AHEAD

The pairing of s-SNOM and THz radiation sources with a coherent detection scheme has distinct advantages, particularly for THz nanoscale quantitative analysis on interrogated samples. Applications reported to date range from probing collective modes in materials such as conductivity, phonon resonances, and surface polaritons in solids, quantifying localized THz permittivities at the nanoscale for material analysis, undertaking THz nano-imaging on inorganic samples, and performing nano-spectroscopy on biomarco-molecules. Within these applications, the majority are performed with a solid-state sample at room temperature.

Now, we are able to experimentally measure THz sample responses, in contrast to the substrate or other reference materials, at the nanoscale as well as able to interpret such tip-scattered responses at a quantitative level, the next question we need to answer is—what kind of research questions can THz s-SNOM solve with appealing advantages over other methods? Are we finishing the instrumentation or the methodology developments? What else do we need to achieve before employing THz s-SNOM to address urging scientific questions and potentially push the domain knowledge boundary in other disciplines? We would like to point out open challenges other than pushing spatial resolutions. In this section, we envision the road ahead for THz s-SNOM in the future and sort them in order of fundamental significance along with readiness in light of previous s-SNOM studies.

A. Soft materials: Live cells in liquid

Since the demonstration of near-field infrared spectroscopic investigation on a single tobacco mosaic virus,[330] s-SNOM has been employed in various solid-state soft biological samples,[330–334] including insulin aggregates, purple and lipid-like peptoid membranes,[331–333] and ferritin protein complexes.[332,334] These studies demonstrate that s-SNOM is capable of revealing a secondary structures such as α-helical and/or β-sheet structures from near-field optical responses.[331,334] However, to truly enable nanoscale s-SNOM investigation of living cells or tissues, the premise is to collect measurable near-field s-SNOM signals in liquid environments. However, s-SNOM cannot directly probe wet samples, including biological objects like living cancer cells or bacteria. This is because wet samples contaminate the tip and the samples can change upon evaporation during scanning.[335,336]

Recently, several researchers aimed to circumvent these problems and report the successful observation of near-field contrast in mid-infrared regimes using s-SNOM.[335–340] One of the remarkable advances is reported by Kaltenecker et al.,[336] who demonstrated the interferometric s-SNOM measurements of living *Escherichia coli* cells. Unlike encapsulating the sample with two graphene sheets as proposed by Khatib et al.,[335] Kaltenecker et al. proposed to cover the sample with a 10 nm SiN membrane, and utilize sub-surface imaging capability of s-SNOM to probe living *E. coli* cells in the liquid solution below a thin membrane. This method avoids the previously reported issues encountered using the encapsulation approach, including the deviation from samples' native topography due to the compression by encapsulation materials.[335]

Regarding the use of THz nanoscopy, to our knowledge there are no s-SNOM studies to report the measurable amplitude and phase from the biological samples in liquid yet. It would be intriguing to use THz s-SNOM to characterize biomolecular processes in liquid, either in an enclosed cell or a fluid channel with flowing buffer solutions. Considering that THz waves are sensitive to free-electrons and have the potential to reveal various unique features in biological samples, THz s-SNOM may be employed to unveil the micro-mechanism and track the progression of the electron transport property of bacteria induced by free nitrous acid,[341,342] extra-cellular electron transport within microbial bacteria in bacterial biofilms and sludges,[343–348] or further study microbial nanowires with long-range electron transport[349–353] combing with a direct conductivity measurement[354] and chemical composition localization[355] at the nanoscale in a nondestructive way. Additionally, liquid-based THz radiation emission[356,357] and detection,[358,359] the so-called THz aqueous photonics, has been demonstrated as an emerging area recently. One question is left to be answered—is it possible to utilize such THz-liquid interaction as a nanoprobe for biological samples in liquid using an s-SNOM?
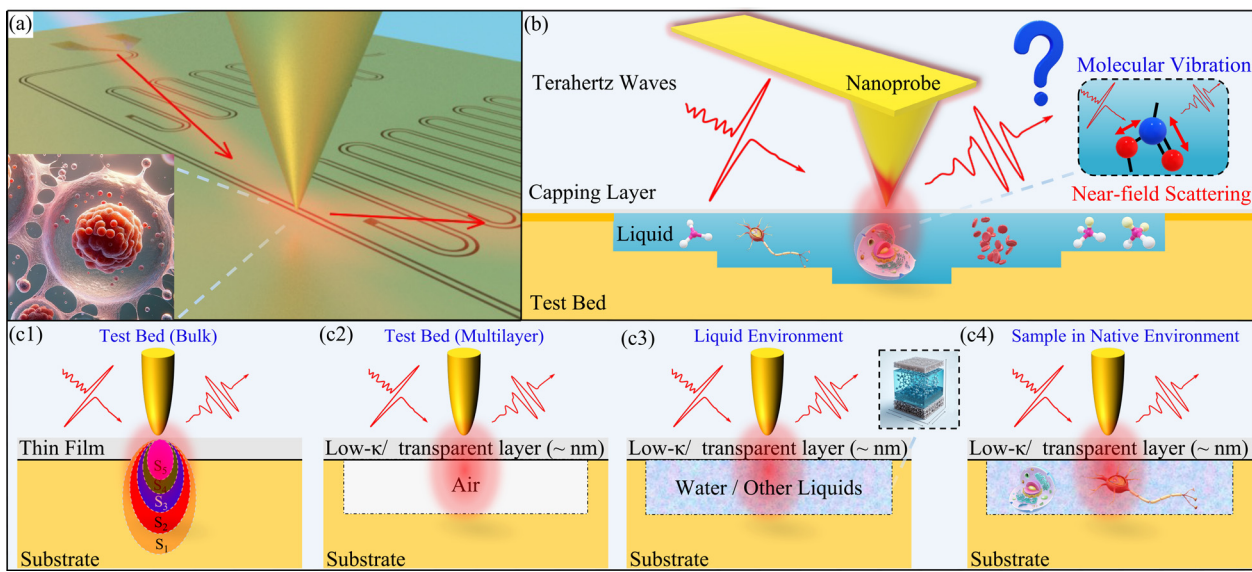
Apart from future demonstrations of THz in-liquid studies using s-SNOM, an interpretation of such scattering signals from the liquid using either encapsulation or sub-surface approaches requires the adequate knowledge of the probing depth and volume of THz s-SNOM, which is essential to recover complex permittivity of such a multi-layer structure (encapsulation layer/sample/solution), including the biological samples in the liquid environment. Considering the complex nature of the s-SNOM scattering signal,[360] a versatile approach dealing with both the phase and amplitude of s-SNOM scattering signals from the liquid with encapsulation layers is in demand in the future.

B. Probing depth and effects of multilayer structures

One of the open challenges for THz nanoscopy is local quantitative characterization as well as capturing fast events at ordinary conditions (also in liquid, in the case of biology), which requires the capability to quantify near-field responses in multilayer and buried nanostructures. High-resolution subsurface imaging remains a nanometrology challenge to electromagnetic and acoustic dispersion and diffraction, although single-molecule-scale probing of material surface properties has been achieved.[361,362] Measuring the subsurface domain poses an inverse problem, which is usually a nonlinear challenge.[363] As a result, in order to nondestructively acquire insights into the interior of a material, it requires quantitative knowledge of how deeply the detected signals are responsible for the material's inner structure. On the other hand, spectral features of solvated molecules from typical far-field THz spectroscopy measurements with micro-fluidic platforms are mostly in the absence of resonant absorption peaks.[364] This feature-less THz spectral continuum may be due to an increasing density of hydrogen bonds[364] with an averaged dielectric response between the host medium and the scatterers (solvated molecules) over hundreds of micrometers. To explore THz opportunities for potential molecular fingerprints in the native environment and other important transient and dynamical processes in liquids, prior studies on THz near-field probing depth and multilayer (also buried) nanostructure effects are important.

Recent s-SNOM calculations and experimental studies carried out in visible[365–367] and mid-infrared[188,190,366,368–370] regimes correlate the probing depth with various factors including the tip tapping amplitude, tip radius and demodulated harmonics.[190] The estimated s-SNOM sensing depth varies from tens of nanometers to more than a hundred nanometer on different samples. Recently, Guo et al. demonstrated an s-SNOM multilayer extraction procedure to recover both thickness and complex-valued permittivity of fabrication-induced surface layer in silicon-based nanodevices.[132] Nevertheless, further THz s-SNOM experimental efforts are needed to answer quantitatively what is the sensing limit in surface normal direction, especially for subsurface layers in multilayer nanostructures. Remarkably, a detailed study of probing depth at THz frequencies and recovery of THz permittivity of multilayer structures is a relatively unexplored terrain. Moon et al. reported sub-surface contrast of 30 nm Au grating buried in a thick Si_3N_4 layer.[97] However, there is no quantitative mapping between the probing depth with the s-SNOM operational parameters and the samples' complex permittivity. This might relate to the difficulty of collecting sufficient scattering power of THz near-field radiation from the Authors' home-built s-SNOM.

To enable the quantitative interpretation and THz nano-scale local mapping of biological samples in liquid, it is essential to advance a detailed understanding of THz probing depth with multilayer nanostructures to encapsulate under-study samples in buffer solutions. We envisage an experimental design and plan for THz s-SNOM investigating (Fig. 12) materials in liquid environments in light of pioneer demonstrations in mid-infrared regimes.[336,340] Monolayer membrane and nanosheets[371–373] with tunable low-dimensional THz dielectric properties, i.e., tunable nanochannels for THz photon penetration, are envisioned as the capping layer candidates. To avoid being broken by tip tapping motions, the mechanical properties of the capping layer need to be compatible with the spring constants of s-SNOM probe tips.

FIG. 12. An envisioned experimental design for THz near-field investigations on biological samples in water or other liquids: (a) Intrinsic SNOM probing of a molecule without destructive or invasive touch. (b) A THz s-SNOM measurement strategy for probing near-field light-matter interactions in the solvent (liquid) environment. (c1) THz near-field dielectric characterization of multilayer structures using prepared substrate (bulk) and capping layer materials. (c2) and (c3) Find the optimal liquid cell etching depth allowing substrate-enhanced near-field interactions with air or liquids encapsulated by both the capping thin-film layer (at the top) and the substrate with etched nanochannels (at the bottom). (c4) Non-contact near-field investigation of samples in their native environments (with liquid or buffered solutions). Reproduced with permission from Guo *et al.*, Nanophotonics **12**, 1865–1875 (2023). Copyright 2023 De Gruyter.[132]

A desired s-SNOM liquid cell is expected to be optimized with an iterative strategy (Fig. 12): (1) find the optimal capping layer thickness and substrate, subject to observable thickness-dependent near-field responses from the covered substrate; (2) quantify the probing depth of the dipole–dipole interaction in the designed liquid cell in air. Find the critical shallow trenching depth where the air gap screens the doped substrate near-field interactions [Figs. 12(a) and 12(b)]; (3) fill the buffer solution in the liquid cell (multilayer nanostructure) and refine the etching depth to achieve substrate-enhanced near-field interactions due to the strong water absorption for THz waves; (4) with optimized geometrical structures iterating through (1–3), measure THz near-field responses in the refined liquid cell at the nanoscale [Fig. 12(d)]. To spatially quantify complex-valued dielectric constants or absorption coefficient of the sample in liquid, the liquid cell may be fabricated with two-dimensional materials and semiconductors of several known doping concentrations for the calibration purpose. Due to well-documented dielectric properties in THz regimes, doped Si and GaAs are envisioned as possible candidates to stay at a niche point, where subsurface near-field interactions enhanced by their high-value permittivity (larger than high-resistivity Si)[374–380] as well as the semiconductor shallow etching performance is predictable.[381,382] Another motivation for multilayer nanostructures engineering[383] is to realize THz polariton-based nanoscale interferometry. Considering the ultra-compressed capability of free-space THz wavelength[132,252,254] and remote probing sensitivity on molecules[384] by surface polaritons, THz polariton-based interferometry is envisioned as a non-contact solution for remote probing the existence of adjacent molecules at the nanoscale. The future development of an analysis framework for ultra-confined and highly damped THz evanescent waves is necessary to allow the quantitative characterization of deposited molecules using THz polariton interferometry.

C. Probe geometry and coating design

Over the past two decades, the s-SNOM community has managed to demonstrate THz spatial features down to tens of nanometers using sharp tips, with a notable progress that Maissen *et al.* showing spatial resolutions down <15 nm at THz frequencies.[63,162,164,165] In the past, it was considered that the spatial resolution of an s-SNOM is determined by the tip radius. However, as reported by Maissen *et al.*,[164] a blunt tip (radius: 750 nm) can resolve THz features down to 100 nm in an s-SNOM. This suggests that the spatial resolution of THz s-SNOM could be affected by a combination of multiple factors, including the probe tip radius, tapping amplitude, signal demodulation harmonic orders, permittivities of probe and interrogated samples at THz wavelengths, as well as the probe tip geometry.

To advance THz s-SNOM capacity, exploring the exact probe tip shape (arrow, elephant-nose, Akiyama, etc.) is essential to increase the signal-to-noise ratio for THz scattering signals.[385,386] Usually, the probe tip used in THz s-SNOM is platinum/iridium metalized. Recently, researchers reported the capability to tune the spectral enhancement by designing a customized metal coating on the tip.[168] The influence of coating patterns on the confined field enhancement near the tip end, in combination with the tip shank length and incident wavelengths, needs continuing exploration in the future.

D. Cryogenic probing for low-temperature physics

Over the last two decades, imaging using s-SNOM under ambient conditions has resulted in a slew of scientifically significant findings.

On the other hand, intriguing phenomena of fundamental physics often happen solely at cryogenic temperatures[387–391] and require nanoscale optical techniques for their interrogation. Therefore, it is important to enable s-SNOM operation at cryogenic conditions. The progress in this direction began with pioneering home-built systems,[392,393] including remarkable demonstrated operation at as low as 5 K for non-interferometric operation.[394,395] Recently, a commercial cryogenic s-SNOM system was developed by attocube systems AG (Haar, Germany). It demonstrated the capability of interferometric s-SNOM imaging and spectroscopy at temperatures between 6 and 10 K,[396] significantly improving operating temperature range, data quality, and, most importantly the accessibility of cryogenic optical nanoanalysis. The cryogenic operation outside MIR regimes, including THz or even visible ranges, is currently under development with prudent tests. The ability to perform temperature-dependent THz s-SNOM measurements allows to *in situ* probe temperature-dependent permittivity (absorption coefficient) quantitatively. The information of absorption coefficient in low-frequency regimes, for example, from 0 to 2 THz regimes, allows to probe the information of density of states[397] experimentally at the nanoscale using s-SNOM.[277] The access to such experimental observable[398–400] is significant to further study low-frequency vibrational dynamics and mode excitations in complex systems (e.g., glass),[401] including ordered and disordered systems[402] with insights obtained from molecular simulations and theoretical modelings.[403,404]

Currently, no SNOM measurements have been performed at millikelvin temperatures. The cryogenic probing using THz s-SNOM in tandem with strong magnetic field is the also terrain with limited studies. Recently, an experimental breakthrough down to sub-2-Kelvin nano-THz contrasts has been reported by Kim *et al.* with the capability of externally applied magnetic field (up to 5 T) using an s-SNOM.[405] Continuing efforts addressing the signal-to-noise ratio of THz s-SNOM are the premise for the community to draw conclusions further from THz near-field responses observed in cryogenic temperatures. In addition to the tunability of magnetic field,[406] THz cryo-SNOM is able to visualize the profound effect of orbital motion of the charge carriers at their native nanometer length scales, allowing to offer direct experimental observations for physics phenomena where quantization is non-negligible, for example, Landau quantization.[407,408] While the manner to cool temperatures below liquid helium from the room temperature is expensive and time-consuming, another technical complication to performing s-SNOM measurements at such low temperatures is due to the limited cooling powers of dilution fridges and the corresponding required optical access for THz radiations. For nanoscale material heterogeneity characterization, it would be expected to allow THz s-SNOM to operate at close to the device operating temperature, which would aid both fundamental and applied science projects, for example spintronic devices made by spin gapless semiconductor,[409] qubit devices optimization for superconducting quantum computing[410,411] or other polariton-based nanophotonic devices fabricating by III–V semiconductors, topological insulators or other quantum materials, and providing direct experimental evidence to understand THz intra-nanowire dynamics for nanowire-based THz devices.[412]

To harness THz s-SNOM uniqueness of resolving complex-valued permittivity at the nanoscale, cryogenic nano-THz probing on exotic phenomena happening at the nanoscale, like the Casimir effect,[413,414] summon the development of THz cryo-SNOM with high signal-to-noise ratio to derive reliable physics interpretations. One option to obtain a quantitative interpretation of near-field responses in THz cryo-SNOM is effectively removing non-idealities of the measurement system with vector calibration, which has recently been reported in low-temperature microwave reflection measurements by near-field SMM.[415] We note that, recently, Wit *et al.* reported an SMM calibration method to calibrate system response for recovering complex impedance without referring to three documented standards. Instead, Wit *et al.* concurrently measured retraction curves (in s-SNOM literature, it is usually referred to as approach curves) of both microwave reflection signals and conductance (real part of complex conductance) signals of the interrogated sample while assuming the unmeasured capacitance as a constant.[415] However, this method is hard to directly translate for calibrating s-SNOM responses for general cases, since practically it is difficult to derive the real part of the complex permittivity of the interrogated sample (which is also frequency-dependent) before calibrating the system response. Therefore, we still suggest the essence of three well-documented standards for s-SNOM vector calibration.

Finally, we anticipate the vector calibration for THz s-SNOM, demonstrated at room temperature,[130,132] to be extended to low-temperature nanoimaging and nanospectroscopy measurements.[405,416,417] This will allow us to study microscopic physics phenomena happening at low temperatures more quantitatively, for example, terahertz magneto-optical activity at the nanoscale in the future.[418,419]

E. AFM-THz: An analogy to AFM-IR

Unlike s-SNOM that collects scattering optical signals from the sample, AFM-infrared spectroscopy (AFM-IR) probes the local thermal expansion of a sample resulting from absorption of infrared radiation upon external illumination. The detection is performed by monitoring the probe tip tapping response under pulsed illumination via AFM.[420] In the same way, with the illumination of THz radiation, a similar detection scheme could be implemented. During the scanning, the absorption of incident THz radiation on the sample leads to the modulation of probe cantilever oscillation. A high-power THz stimulus, for example, from pulsed QCL can be an ideal THz radiation source to implement AFM-THz. The probed thermal expansion of the sample due to absorption of THz radiation allows to further study on low-frequency vibration modes of the interrogated sample. Amorphous materials like glasses or other material systems with potential low-frequency modes may be suitable candidates for AFM-THz.[404] We envision that AFM-THz would need to be operated in a cryogenic environment.

F. Tissues characterization at the cellular level

Skin cancer which includes melanoma, squamous cell carcinoma (SCC), basal cell carcinoma (BCC), is a common malignancy that has shown a continuing drastic increase in Europe, Canada, and the United States, along with the highest incidence rates reported in Australia.[421] Melanoma is considered as the most dangerous of the skin cancers,[422] and the early stage recognition of atypia in dysplastic nevi[423] helps provide a better diagnosis of patient survival.

The ability to observe preliminary structural features during the benign-malignant transition, therefore, is essential for assisting in the early stage diagnostic recognition and further medical intervention. Typically, the conventional characterization technique on skin tissue is histology staining, which only offers evidence only on formed malignant/cancerous regions. However, there is no reliable and mature techniques yet to highlight the early stage formation of skin lesions in the benign-malignant transition.

THz radiation, as a non-ionized electromagnetic wave, has been reported to respond with various types of tumors,[27,31,32,424] including skin (SCC, BCC), gastric,[425] oral,[426,427] brain,[428] breast,[429] and liver[430] cancers. Its non-ionized nature promises a biologically safe investigation and the unique light-matter response enables a label-free tissue characterization technique for lesions.

Notwithstanding the fact that THz contrasts existed in various malignant tissues, the underlying contrast mechanism and origin are not well understood in cellular level. The initial belief blamed to the accelerated metabolism of tumorous/cancerous tissues than the benign ones, and therefore resulted in an excessive amount of water.[431] This explanation was adapted by pioneering medical physicists from Cambridge to explain the first observed THz tumorous contrast in early 2000s.[432–434] This water-induced THz contrast mechanism was continuously attributed to by most THz tumor/tissue studies till 2010. Sy *et al.* at the first time experimentally verified non-water-related THz response on liver cirrhotic tissues fixed in formalin,[430] and it guided the community to study THz non-water-related contribution like the increase in cell density, lipids and proteins,[435,436] and other biomacromolecules,[28,29] including fatty acids,[35] DNA,[328] etc.

Specifically, for melanoma skin cancer, both its precursor—nevus—and original pigment—melanin—have been reported with THz responses.[437,438]

In spite of these progresses, there are still several fundamental and key questions to be studied and answered for bridging THz and medical researchers as well as realizing the anticipated label-free early stage diagnosis of melanoma skin cancer:

1. How does microscopic spatial structural change of a potential melanoma tissue affect THz response and relate to signatures for early stage recognition?
2. Within a single nevus cell, does THz radiation respond to any specific kind of organelle, like nucleus, cell membrane, nucleolus, mitochondria, lysosomes, vacuoles, etc.?
3. How does a cellular-level (nanoscale) THz response from different spatial locations of tissue form the averaged electromagnetic-tissue response in hundreds of μm scale, for the sake of real-time THz scanning in the future?

Currently, a majority of mechanism studies attempting to unveil the origin of THz tissue contrast are drawing conclusions from far-field measurements, with spatial responses averaged over a couple of hundred μm and ignorant of the ramification of samples' cellular-level inhomogeneity.[32] Thus, attempts to explain THz contrast origins, which are drawn from far-field THz measurements, screen out the cellular-level features, average the responses within a beam spot, and thus hamper direct evidence of proposed THz contrast origins. Although water is still considered as the major THz-tissue response contributor,[30] tissue inhomogeneity and water-free THz responses from microscopic structural variations in tissues[32] at the nanoscale require study for the delineation of cancer margins

and the direct evidence of THz non-water-induced skin cancer contrast. Recently, Kucheryavenko *et al.* revisited the applicability of the effective medium theory for describing THz wave interacting with soft turbid tissues by using THz immersion microscopy to extract optical constants of tissue-mimicking phantom (subwavelength and mesoscale SiO_2 particles embedded in a hydrated gelatin slab) by considering the relative volume fraction of a constituent in a composite material in spatial-averaged measurements.[439] We anticipate that THz s-SNOM can provide microscopic observations for further revisiting theoretical predictions based on Lorenz–Mie scattering and effective medium theory. More importantly, a direct sub-molecular-level mapping of complex permittivity via THz s-SNOM allows studying an interplay between THz-wave absorption and scattering mechanisms in multilayer turbid tissues with an anisotropic geometry with direct microscopic evidence in the future.

The sub-cellular understanding of the THz response on lesions/tumors is essential to interpret the experimentally observed THz contrast in various tumorous tissues either *in vivo* or *ex vivo*. It is significant to further bridge THz studies with medical communities realizing this label-free *in vivo* recognition of lesions/tumors for pragmatic early stage diagnosis and medical intervention.

Owing to the deep-subwavelength resolving capability of s-SNOM, direct access to the cellular-level features of tissues is possible. In a pioneer work, Kanevche *et al.* has demonstrated measurable sub-cellular contrasts at mid-infrared wavelengths from the intracellular structures of eukaryotic (*Chlamydomonas reinhardtii*) and prokaryotic (*E. coli*) species.[440] To further pinpoint and decipher microscopic responses from macroscopic spatially averaged THz signals, the preliminary requirement is to confirm THz waves are responsible for tissue constituents (e.g., collagen, melanin and typical proteins).[314]

Hence, it is rational to harness the capacity of THz s-SNOM to resolve the sub-cellular THz features on un-stained skin tissues showing a nevus or nevi. With the advancement of THz radiation sources toward operating in high-power, high-temperature, and broadband regimes based on semiconductor hetero-structures,[441,442] inorganic and organic crystals,[443,444] electron bunch trains,[445] graphene hyperbolic grating,[446] or topological semimetals nanowires[447] we envisage great attention to be attracted on nano-THz biological studies, including direct characterizing cellular structures at the nanoscale. To realize unprecedented THz-tissue response at the cellular or molecular level in liquids,[448,449] considering s-SNOM probing volume is typically restricted by the tip tapping amplitude around several hundred nanometers, a deeper (μm) volumetric characterization,[450] i.e., THz near-field tomography, would be necessary and insightful when approaching to decipher superficial contribution from volume-averaged THz responses. This is a premise to empower direct microscopic characterization of THz-tissue interactions by visualizing cell responses in liquid at the nanoscale. If the near-field observations of nanoscale THz response variations within a single cellular structure regardless of topological variations could be realized, there might be an opportunity to answer the cellular-level origin of THz far-field contrasts on tissues, which might provide vital shreds of evidence and incentives for prudent decisions on employing THz waves as a standard medical diagnostic tool for early stage lesions in the future.

G. Metal oxides and defects

For solid-state materials, we find s-SNOM researchers usually start with well-documented and standard materials. The pioneer THz s-SNOM studies work with probing spatially varying surface doping in

24 November 2024 03:57:31

metallic nanostructures,[79,451] doped semiconductor-based nanostructures, like silicon[91,195,245,267] or gallium arsenide,[117,262] vanadium dioxide[259] and graphene[158,243,254] with well-documented dielectric properties, then progressing at the stage to study materials whose nanoscale properties with less-documented information at THz frequencies, including phase change materials,[209,260] perovskites,[263,284] rare-earth metal oxides (Fig. 13),[277] carbon black in rubber,[452] and antiferromagnetic thin films with anisotropic conductivity.[453]

Considering these applications originally rely on the high sensitivity of THz waves to conduction electrons or surface mobility, THz s-SNOM is considered as a promising candidate to quantify local changes in the electrical conductivity of metal oxides caused by oxygen vacancies, which are typically invisible to conventional methods.[454] With the spatial resolution of tens of nanometers, THz s-SNOM could be used to probe electrical properties of oxides, potential insulator-to-metal transition of oxygen vacancies, and resulting conductivity changes due to the increase in vacancy concentrations at the nanoscale,[455,456] allowing to potentially unveil the microscopic origin of near-surface vacancy structure[457] and to clarify the role of oxygen vacancies as well as dopants in high-temperature superconductors[458,459] and in metal-based biodegradable memory alloy[460] to sharpen the microscopic understanding of metal aging, corrosion rates, and Schottky barrier distribution with *in situ* THz nanoprobing. The nondestructive and nanoscale resolving ability of THz s-SNOM allows for developing the fundamental understanding and optimizing the fabrication process of future metal and oxides-based electronics and implantable biomedical devices.
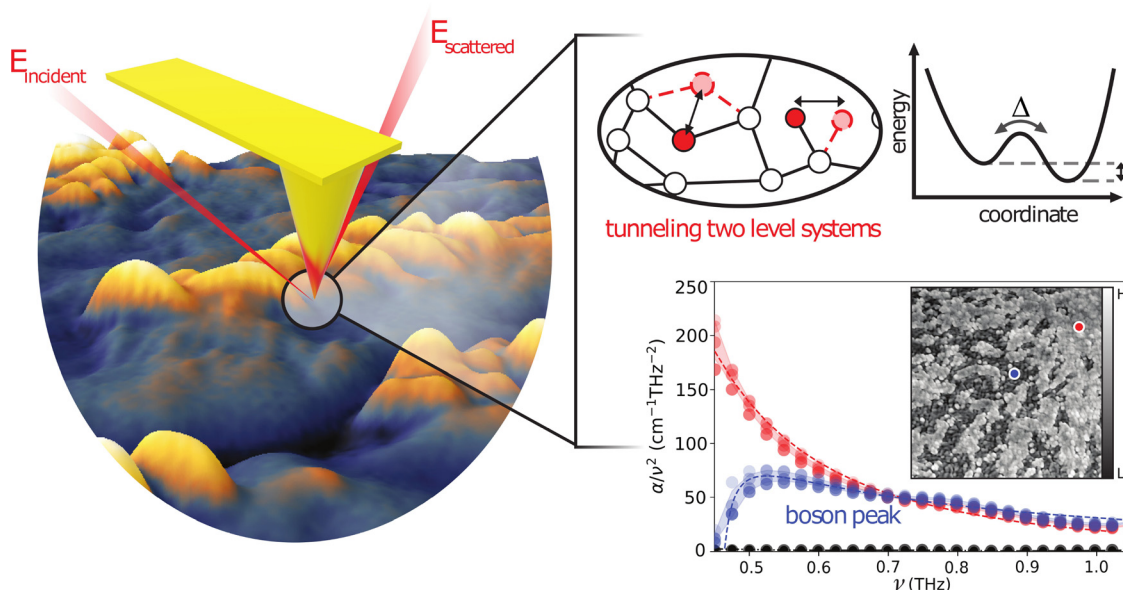
H. Topological insulators

Topological insulators are a group of exotic materials where metallic states appear on the surface of what is notionally an insulator.[461] They serve as exotic material platforms to experimentally study novel transport phenomena, including the anomalous quantum Hall effect and spin Hall effect observed in topological insulator systems.[462] THz s-SNOM allows for tracking changes of the induced local electrical properties at the nanoscale during the fabrication of topological insulators and reveals the underlying physics of these materials nondestructively.[120] This ability of THz s-SNOM paves the promise to assist a wide range of application studies including the development of high-efficiency for thermometric-film wearable electronic devices,[463,464] spintronics,[465] quantum computing,[466–468] flexible piezoelectrics[469] and thermoelectrics based on topological insulators.[470,471]

While THz a-SNOM has been demonstrated as a suitable probe to study evanescent electromagnetic responses in meta-structures[472] based on topological insulator,[473] near-field plasmon responses from topological insulators were found to be more pronounced by using THz s-SNOM.[120,283] This may motivate THz a-SNOM developers to consider the incorporation of QCL or gas laser; however, switching the a-SNOM radiation source may also urge the advance of aperture-based near-field detection technique, where the photoconductive nano-antenna in a-SNOM probe was originally inspired and designed for the broadband detection using THz-TDS systems.

We also note that frequencies below 4 THz (including microwave regimes realized by scanning microwave microscopy) are crucial for studying quantum materials,[474–481] including edge and bulk states as well as other emergent phenomena in topological insulators at the microscopic level, including imaging quantum Hall edge channels[474] and quantifying surface electronic transport (the imaginary part of SMM signals is a good measure of local resistivity) in gated graphene devices[475] by microwave microscopy. A recent example demonstrated by Wang *et al.* showcased the SMM advantage to visualize Chern insulators' one-dimensional chiral (quantum anomalous Hall) edge mode

FIG. 13. Near-field localization of the boson peak, a signature of low-frequency vibrational modes relating to excess vibrational density of states, using THz nanospectroscopy. The direct microscopic observation of two-level systems as one of the leading loss channels for quantum devices at the operating temperature. Reproduced with permission from Guo *et al.*, J. Phys. Chem. Lett. **14**, 4892–4900. Copyright 2023 American Chemical Society.[277]

features manifested experimentally as a sharp microwave response enhancement at the crystal sample boundaries[478] ($400 \times 20\ \mu m^2$ $Cr - doped\ (Bi,\ Sb)_2 Te_3$, a typical ternary compound alloy composed of bismuth, antimony, and tellurium with electrical and magnetic properties tuned by chromium doping) and edge state conductivity. In the meantime, the capacity of microwave microscopy with continuous frequency tunability in SMM experiments is expected to shed light on the non-trivial interpretation of microwave edge responses, considered as collective edge magnetoplasmon excitations, measured on arbitrary quantum materials within the SMM theoretical framework proposed by Wang *et al.*[478] in the future, while similar cases also apply for THz nanoscopy considering the experimental freedoms coming from multiphysics coupling, including temperature, magnetic field, etc.

In terms of probing topological insulators, we envision the continuing co-development of THz cryogenic SNOM with tunability on temperature, as well as strong magnetic field, provides a bright future allowing direct experimental observations of transport properties in both antiferromagnetic and ferromagnetic phases at the nanoscale.[482,483] Similar to the situations encountered in SMM quantum material studies, future advancements in cryostat setups,[484] along with integration into broadband nanospectroscopy, will advance our understanding of topological insulators' properties[479,480] and further expand our ability to modulate topological electronic phases through intense THz field excitations.[481,485]

I. Physics-informed AI for s-SNOM quantitative analysis

Considering the complicated physics nature of the s-SNOM tip-sample interactions, it might be unrealistic to put all the s-SNOM experimental details into a model. The questions for quantitative s-SNOM analysis will be—(1) Will artificial intelligence (AI), e.g., machine learning or deep learning algorithms, be helpful for s-SNOM analysis more than publishing a paper to claim the first attempt? (2) How much can it involve and contribute to s-SNOM, especially in the quantitative analysis? Recently, neural networks (NN) as a supervised learning algorithm have been demonstrated by the quantitative analysis of s-SNOM scattering spectra.[183,486,487] However since NN is a data-driven and data-hungry AI framework, a simple translation on s-SNOM scattering spectra hampers the practical utility for quantitative analysis. As a data-driven AI framework, NN suffers from many intrinsic problems as a data-hungry supervised learning algorithm. This is due to the fact that good-quality s-SNOM data with a high signal-to-noise ratio is time-consuming, especially with THz radiation.

No matter how powerful a data-hungry NN is to encode a latent space, the difficulty will be greater for such supervised learning algorithms, compounded by the fact that the s-SNOM probe tip wears after long-term usage, which will change the initial "correct label." Other approaches to data augmentation, such as generative adversarial networks (GAN)[488,489] and other physics-informed generative models, e.g., inspired by the diffusion process[490] or Poisson equation,[491] a recent progressive topic in deep learning, may provide additional insights.

Note that, recently, deep reasoning networks have been demonstrated in materials science for automated crystal-structure phase mapping based on prior scientific knowledge.[492] Since the multiplicative process describing the s-SNOM probe-sample interactions shares a highly similar framework to that of a closed loop feedback control,[493] other hybrid frameworks combining detailed reasoning in tandem with intuitive pattern recognition at more than a qualitative

level[494–496] are expected to aid s-SNOM quantitative analysis. To avoid overfitting data, constructing interpretable neural network architectures (i.e., white-box methods) with knowledge from the first principle[497–499] to capture the complex mapping in s-SNOM scattering process is essential. With more prior interpretable scientific knowledge on the s-SNOM probe-sample interactions, a high-efficiency physics-informed framework targeting s-SNOM complex dielectric extraction[500,501] could be implemented to remove system responses and go beyond the quasi-static limit when only *p*-polarized components are considered.

On the other hand, it should be noted that even the simplest neural network architecture, a multilayer perceptron, has been demonstrated with excellent performances in natural language processing tasks;[502] thus, it is not a bad idea to focus on how to collect promising raw data while obsessing over developing complicated multipronged NN architectures for s-SNOM tasks. In 2023, the astonishing performance of advanced natural language processing by ChatGPT, a large language model (LLM), draws a great attention across a broad range of disciplines to think about AI for science. We envision LLM-assisted prompt engineering as an end-to-end assistant to facilitate the interpretation and analysis for the observed s-SNOM nanoscale responses in the future,[503,504] for example, providing data analysis pipelines to start with or offering physics pictures with basic solid state physics models to interpret spectral responses for educated laymen.

Researchers with interest in the microscopic understanding and nanoscale responses about material properties would benefit from AI-assisted analysis, with the domain knowledge input, to expand the boundary of science. Recently, AI has surprisingly demonstrated human-level automated reasoning on Olympiad-level Euclidean plane geometry mathematical theorems, i.e., AlphaGeometry, approaching the average performance of an International Mathematical Olympiad (IMO) gold medalist.[505] If we were able to translate physics domain knowledge (for example, theorems in complex analysis and electrodynamics) into machine-verifiable formats for AI in the future, how will SNOM practitioners or more broadly, spectroscopists, be re-defined? What is the irreplaceable task for researchers facing the increasingly remarkable capabilities of AI, except to act as prompt engineers with potentially insightful questions?

Finally, an important open question to answer is—how to utilize the power of AI with s-SNOM quantitative analysis after the peak of inflated expectations in the Gartner hype cycle?

VI. CONCLUSIONS

Over the past 40 years, the upper limit of resolving sub-diffraction THz responses has been significantly improved to about tens of nanometers (~ 20 nm), which is remarkably shorter ($< \frac{1}{5000}$) than typical THz wavelengths with the establishment of nowadays THz s-SNOM, surpassing THz a-SNOM. As a THz nanoscopy, THz s-SNOM simultaneously offers both the topography and spatially varying THz light-matter interactions of the interrogated sample at the nanoscale, whereas far-field THz scanners only probe high-spatial-frequency component light-matter interactions and thus lose fine spatial details. More uniquely, THz s-SNOM offers nanoscale spectroscopic features, overcoming far-field THz systems whose THz responses are averaged over several hundred of micrometers.

Additionally, THz s-SNOM stands out in comparison to other material characterization tools including scanning electron microscope (SEM), transmission electron microscopy (TEM), nanoscale secondary ion mass spectrometry (nano-SIMS), and confocal laser scanning

microscopy by harnessing the nondestructive and label-free capabilities at the nanoscale. These characteristics enable THz s-SNOM offering distinctive insights in various application studies, including semiconductors, 2D materials, quantum materials, artificial nanostructures, cells, proteins, peptides, bacteria, and other bio-macromolecules.

To date, THz s-SNOM has been contributing to a breadth of multidisciplinary applications, including characterizing nanoscale conductivity and doping heterogeneity, developing next-generation advanced manufacturing protocols, characterizing electrical properties of peptides, and unveiling exotic nature of collective elementary excitation, e.g., surface polaritons, on 2D materials at THz frequencies.

This review aims to highlight THz s-SNOM as a cutting-edge label-free and nondestructive characterization method for multidisciplinary studies (spanning physics, chemistry, materials science and biology), especially facilitating as a quantitative analysis method to unveil the microscopic origin of light-matter interaction due to sample permittivity change at the nanoscale. In the final section of this review, a few unexplored terrains of THz s-SNOM demanding emergent clarification are summarized, with the road ahead presented in the end.

In summary, THz s-SNOM stands as a luminary amid the fast-rising stars in the realm of the deep sub-wavelength quantitative imaging and spectroscopy well beyond the diffraction limit. We expect THz s-SNOM serving as a standard and robust in-line nanoscale characterization method, like TEM or SEM, but with its nondestructive and label-free uniqueness on material properties in research laboratories and even in high-tech manufacturing industries in the future.

ACKNOWLEDGMENTS

AUTHOR DECLARATIONS
Conflict of Interest

The authors have no conflicts to disclose.

Author Contributions

Xiao Guo: Conceptualization (equal); Data curation (lead); Formal analysis (lead); Investigation (lead); Visualization (lead); Writing – original draft (lead); Writing – review & editing (equal). **Karl Bertling:** Conceptualization (equal); Funding acquisition (supporting); Supervision (supporting); Writing – review & editing (equal). **Bogdan Donose:** Writing – review & editing (equal). **Michael Brünig:** Funding acquisition (supporting); Writing – review & editing (equal). **Adrian Cernescu:** Writing – review & editing (equal). **Alexander Govyadinov:** Writing – review & editing (equal). **Aleksandar D. Rakić:** Conceptualization (equal); Funding acquisition (lead); Supervision (lead); Writing – review & editing (equal).

DATA AVAILABILITY

The data that support the findings of this study are available from the corresponding author upon reasonable request.

REFERENCES

[1] L. Rayleigh, "LVI. On the influence of obstacles arranged in rectangular order upon the properties of a medium," London, Edinburgh Dublin Philos. Mag. **34**, 481–502 (1892).

[2] G. Herzberg, *Molecular Spectra and Molecular Structure* (D. van Nostrand, 1945).

[3] J. D. Watson and F. H. Crick, "Molecular structure of nucleic acids: A structure for deoxyribose nucleic acid," Nature **171**, 737–738 (1953).

[4] S. Torquato, *Random Heterogeneous Materials: Microstructure and Macroscopic Properties* (Springer, 2002).

[5] A. Einstein, "Über die von der molekularkinetischen theorie der wärme geforderte bewegung von in ruhenden flüssigkeiten suspendierten teilchen," Ann. Phys. **322**, 549 (1905).

[6] J. K. Gimzewski and C. Joachim, "Nanoscale science of single molecules using local probes," Science **283**, 1683–1688 (1999).

[7] E. Betzig and J. K. Trautman, "Near-field optics: Microscopy, spectroscopy, and surface modification beyond the diffraction limit," Science **257**, 189–195 (1992).

[8] H. Heinzelmann and D. Pohl, "Scanning near-field optical microscopy," Appl. Phys. A **59**, 89–101 (1994).

[9] B. Hecht, B. Sick, U. P. Wild, V. Deckert, R. Zenobi, O. J. Martin, and D. W. Pohl, "Scanning near-field optical microscopy with aperture probes: Fundamentals and applications," J. Chem. Phys. **112**, 7761–7774 (2000).

[10] F. Zenhausern, M. O'boyle, and H. Wickramasinghe, "Apertureless near-field optical microscope," Appl. Phys. Lett. **65**, 1623–1625 (1994).

[11] F. Keilmann and R. Hillenbrand, "Near-field microscopy by elastic light scattering from a tip," Philos. Trans. R. Soc. A **362**, 787–805 (2004).

[12] F. Keilmann, A. J. Huber, and R. Hillenbrand, "Nanoscale conductivity contrast by scattering-type near-field optical microscopy in the visible, infrared and THz domains," J. Infrared Millimeter, Terahertz Waves **30**, 1255–1268 (2009).

[13] D. V. Kazantsev, E. V. Kuznetsov, S. V. Timofeev, A. V. Shelaev, and E. A. Kazantseva, "Apertureless near-field optical microscopy," Phys.-Usp. **60**, 259–275 (2017).

[14] R. J. Hermann and M. J. Gordon, "Nanoscale optical microscopy and spectroscopy using near-field probes," Annu. Rev. Chem. Biomol. Eng. **9**, 365–387 (2018).

[15] X. Chen, D. Hu, R. Mescall, G. You, D. Basov, Q. Dai, and M. Liu, "Modern scattering-type scanning near-field optical microscopy for advanced material research," Adv. Mater. **31**, 1804774 (2019).

[16] J. Duan, Y. Li, Y. Zhou, Y. Cheng, and J. Chen, "Near-field optics on flatland: From noble metals to van der Waals materials," Adv. Phys.: X **4**, 1593051 (2019).

[17] P. U. Jepsen, D. G. Cooke, and M. Koch, "Terahertz spectroscopy and imaging–modern techniques and applications," Laser Photonic Rev. **5**, 124–166 (2011).

[18] T. Kampfrath, K. Tanaka, and K. A. Nelson, "Resonant and nonresonant control over matter and light by intense terahertz transients," Nat. Photonics **7**, 680–690 (2013).

[19] J. B. Baxter and G. W. Guglietta, "Terahertz spectroscopy," Anal. Chem. **83**, 4342–4368 (2011).

[20] J. A. Spies, J. Neu, U. T. Tayvah, M. D. Capobianco, B. Pattengale, S. Ostresh, and C. A. Schmuttenmaer, "Terahertz spectroscopy of emerging materials," J. Phys. Chem. C **124**, 22335–22346 (2020).

[21] R. A. Lewis, "Physical phenomena in electronic materials in the terahertz region," Proc. IEEE **95**, 1641–1645 (2007).

[22] D. N. Basov, R. D. Averitt, D. Van Der Marel, M. Dressel, and K. Haule, "Electrodynamics of correlated electron materials," Rev. Mod. Phys. **83**, 471 (2011).

[23] J. Lloyd-Hughes and T.-I. Jeon, "A review of the terahertz conductivity of bulk and nano-materials," J. Infrared Millimeter Terahertz Waves **33**, 871–925 (2012).

[24] H. J. Joyce, J. L. Boland, C. L. Davies, S. A. Baig, and M. B. Johnston, "A review of the electrical properties of semiconductor nanowires: Insights gained from terahertz conductivity spectroscopy," Semicond Sci. Technol. **31**, 103003 (2016).

[25]R. Averitt and A. Taylor, "Ultrafast optical and far-infrared quasiparticle dynamics in correlated electron materials," J. Phys.: Condens. Matter **14**, R1357 (2002).

[26]J. D. Caldwell, L. Lindsay, V. Giannini, I. Vurgaftman, T. L. Reinecke, S. A. Maier, and O. J. Glembocki, "Low-loss, infrared and terahertz nanophotonics using surface phonon polaritons," Nanophotonics **4**, 44–68 (2015).

[27]E. Pickwell-MacPherson and V. P. Wallace, "Terahertz pulsed imaging—a potential medical imaging modality?," Photodiagn. Photodyn. Ther. **6**, 128–134 (2009).

[28]G. J. Wilmink and J. E. Grundt, "Invited review article: current state of research on biological effects of terahertz radiation," J. Infrared Millimeter Terahertz Waves **32**, 1074–1122 (2011).

[29]X. Yang, X. Zhao, K. Yang, Y. Liu, Y. Liu, W. Fu, and Y. Luo, "Biomedical applications of terahertz spectroscopy and imaging," Trends Biotechnol. **34**, 810–824 (2016).

[30]O. A. Smolyanskaya, N. V. Chernomyrdin, A. Konovko, K. Zaytsev, I. Ozheredov, O. Cherkasova, M. Nazarov, J.-P. Guillet, S. Kozlov, Y. V. Kistenev, J. Coutaz, P. Mounaix, V. Vaks, J. Son, H. Cheon, V. Wallace, Y. Feldman, I. Popov, A. Yaroslavsky, A. Shkurinov, and V. Tuchin, "Terahertz biophotonics as a tool for studies of dielectric and spectral properties of biological tissues and liquids," Prog. Quantum Electron. **62**, 1–77 (2018).

[31]J.-H. Son, S. J. Oh, and H. Cheon, "Potential clinical applications of terahertz radiation," J. Appl. Phys. **125**, 190901 (2019).

[32]K. Zaytsev, I. Dolganova, N. Chernomyrdin, G. Katyba, A. Gavdush, O. Cherkasova, G. Komandin, M. Shchedrina, A. Khodan, D. Ponomarev et al., "The progress and perspectives of terahertz technology for diagnosis of neoplasms: A review," J. Opt. **22**, 013001 (2020).

[33]A. I. Nikitkina, P. Y. Bikmulina, E. R. Gafarova, N. V. Kosheleva, Y. M. Efremov, E. A. Bezrukov, D. V. Butnaru, I. N. Dolganova, N. V. Chernomyrdin, O. P. Cherkasova, A. A. Gavdush, and P. S. Timashev, "Terahertz radiation and the skin: A review," J. Biomed. Opt. **26**, 1–26 (2021).

[34]A. J. L. Adam, "Review of near-field terahertz measurement methods and their applications," J. Infrared Millimeter Terahertz Waves **32**, 976 (2011).

[35]S. Fan, M. T. Ruggiero, Z. Song, Z. Qian, and V. P. Wallace, "Correlation between saturated fatty acid chain-length and intermolecular forces determined with terahertz spectroscopy," Chem. Commun. **55**, 3670–3673 (2019).

[36]E. Abbe, "VII. on the estimation of aperture in the microscope," J. R. Microsc. Soc. **1**, 388–423 (1881).

[37]M. Born and E. Wolf, *Principles of Optics: Electromagnetic Theory of Propagation, Interference and Diffraction of Light* (Elsevier, 2013).

[38]L. Novotny and B. Hecht, *Principles of Nano-Optics* (Cambridge University Press, 2012).

[39]R. Bachelot and L. Douillard, "Probing the optical near-field," in *Advances in Near-Field Optics* (Springer, 2023), pp. 137–196.

[40]T. Cocker, V. Jelic, R. Hillenbrand, and F. Hegmann, "Nanoscale terahertz scanning probe microscopy," Nat. Photonics **15**, 558–569 (2021).

[41]V. N. Astratov, Y. B. Sahel, Y. C. Eldar, L. Huang, A. Ozcan, N. Zheludev, J. Zhao, Z. Burns, Z. Liu, E. Narimanov et al., "Roadmap on label-free super-resolution imaging," Laser Photonics Rev. **17**, 2200029 (2023).

[42]P. H. Siegel, "Microwaves are everywhere:"SMM: Nano-microwaves,"" IEEE J. Microwave **1**, 838–852 (2021).

[43]M. E. Barber, E. Y. Ma, and Z.-X. Shen, "Microwave impedance microscopy and its application to quantum materials," Nat. Rev. Phys. **4**, 61–74 (2022).

[44]E. H. Synge, "XXXVIII. A suggested method for extending microscopic resolution into the ultra-microscopic region," London, Edinburgh, Dublin Philos. Mag. J. Sci. **6**, 356–362 (1928).

[45]E. Ash and G. Nicholls, "Super-resolution aperture scanning microscope," Nature **237**, 510 (1972).

[46]D. W. Pohl, W. Denk, and M. Lanz, "Optical stethoscopy: Image recording with resolution $\lambda/20$," Appl. Phys. Lett. **44**, 651–653 (1984).

[47]G. Binnig, H. Rohrer, C. Gerber, and E. Weibel, "Surface studies by scanning tunneling microscopy," Phys. Rev. Lett. **49**, 57 (1982).

[48]G. Binnig and H. Rohrer, "Scanning tunneling microscopy," Surf. Sci. **126**, 236–244 (1983).

[49]G. Binnig, C. F. Quate, and C. Gerber, "Atomic force microscope," Phys. Rev. Lett. **56**, 930 (1986).

[50]A. Lewis, M. Isaacson, A. Harootunian, and A. Muray, "Development of a 500 Å spatial resolution light microscope: I. Light is efficiently transmitted through $\lambda/16$ diameter apertures," Ultramicroscopy **13**, 227–231 (1984).

[51]E. Betzig and R. J. Chichester, "Single molecules observed by near-field scanning optical microscopy," Science **262**, 1422–1425 (1993).

[52]A. Piednoir, C. Licoppe, and F. Creuzet, "Imaging and local infrared spectroscopy with a near field optical microscope," Opt. Commun. **129**, 414–422 (1996).

[53]R. Merz, F. Keilmann, R. Haug, and K. Ploog, "Nonequilibrium edge-state transport resolved by far-infrared microscopy," Phys. Rev. Lett. **70**, 651 (1993).

[54]F. Keilmann, "FIR microscopy," Infrared Phys. Technol. **36**, 217–224 (1995).

[55]S. Hunsche, M. Koch, I. Brener, and M. Nuss, "THz near-field imaging," Opt. Commun. **150**, 22–26 (1998).

[56]O. Mitrofanov, I. Brener, M. Wanke, R. Ruel, J. Wynn, A. Bruce, and J. Federici, "Near-field microscope probe for far infrared time domain measurements," Appl. Phys. Lett. **77**, 591–593 (2000).

[57]O. Mitrofanov, I. Brener, R. Harel, J. Wynn, L. Pfeiffer, K. West, and J. Federici, "Terahertz near-field microscopy based on a collection mode detector," Appl. Phys. Lett. **77**, 3496–3498 (2000).

[58]O. Mitrofanov, M. Lee, J. W. P. Hsu, L. N. Pfeiffer, K. W. West, J. D. Wynn, and J. F. Federici, "Terahertz pulse propagation through small apertures," Appl. Phys. Lett. **79**, 907–909 (2001).

[59]O. Mitrofanov, M. Lee, J. W. Hsu, I. Brener, R. Harel, J. F. Federici, J. D. Wynn, L. N. Pfeiffer, and K. W. West, "Collection-mode near-field imaging with 0.5-THz pulses," IEEE J. Sel. Top. Quantum Electron. **7**, 600–607 (2001).

[60]B. Gompf and M. Dressel, "THz-micro-spectroscopy," IEEE J. Sel. Top. Quantum Electron. **14**, 470–475 (2008).

[61]M. Wächter, M. Nagel, and H. Kurz, "Tapered photoconductive terahertz field probe tip with subwavelength spatial resolution," Appl. Phys. Lett. **95**, 041112 (2009).

[62]S. Sawallich, B. Globisch, C. Matheisen, M. Nagel, R. J. Dietz, and T. Göbel, "Photoconductive terahertz near-field detectors for operation with 1550-nm pulsed fiber lasers," IEEE Trans. Terahertz Sci. Technol. **6**, 365–370 (2016).

[63]T. Siday, M. Natrella, J. Wu, H. Liu, and O. Mitrofanov, "Resonant terahertz probes for near-field scattering microscopy," Opt. Express **25**, 27874–27885 (2017).

[64]H. A. Bethe, "Theory of diffraction by small holes," Phys. Rev. **66**, 163 (1944).

[65]Y. Inouye and S. Kawata, "Near-field scanning optical microscope with a metallic probe tip," Opt. Lett. **19**, 159–161 (1994).

[66]R. Bachelot, P. Gleyzes, and A. C. Boccara, "Near field optical microscopy by local perturbation of a diffraction spot," Microsc., Microanal., Microstruct. **5**, 389–397 (1994).

[67]R. Bachelot, P. Gleyzes, and A. Boccara, "Reflection-mode scanning near-field optical microscopy using an apertureless metallic tip," Appl. Opt. **36**, 2160–2170 (1997).

[68]F. Zenhausern, Y. Martin, and H. Wickramasinghe, "Scanning interferometric apertureless microscopy: Optical imaging at 10 angstrom resolution," Science **269**, 1083–1085 (1995).

[69]B. Knoll and F. Keilmann, "Scanning microscopy by mid-infrared near-field scattering," Appl. Phys. A **66**, 477–481 (1998).

[70]B. Knoll and F. Keilmann, "Near-field probing of vibrational absorption for chemical microscopy," Nature **399**, 134 (1999).

[71]S. Amarie, T. Ganz, and F. Keilmann, "Mid-infrared near-field spectroscopy," Opt. Express **17**, 21794–21801 (2009).

[72]F. Huth, M. Schnell, J. Wittborn, N. Ocelic, and R. Hillenbrand, "Infrared-spectroscopic nanoimaging with a thermal source," Nat. Mater. **10**, 352–356 (2011).

[73]M. C. Giordano, L. Viti, O. Mitrofanov, and M. S. Vitiello, "Phase-sensitive terahertz imaging using room-temperature near-field nanodetectors," Optica **5**, 651–657 (2018).

[74]H.-T. Chen, R. Kersting, and G. C. Cho, "Terahertz imaging with nanometer resolution," Appl. Phys. Lett. **83**, 3009–3011 (2003).

[75]A. J. Huber, F. Keilmann, J. Wittborn, J. Aizpurua, and R. Hillenbrand, "Terahertz near-field nanoscopy of mobile carriers in single semiconductor nanodevices," Nano Lett. **8**, 3766–3770 (2008).

24 November 2024 03:57:31

[76]H.-G. von Ribbeck, M. Brehm, D. van der Weide, S. Winnerl, O. Drachenko, M. Helm, and F. Keilmann, "Spectroscopic THz near-field microscope," Opt. Express **16**, 3430–3438 (2008).

[77]F. Kuschewski, H.-G. von Ribbeck, J. Döring, S. Winnerl, L. Eng, and S. Kehr, "Narrow-band near-field nanoscopy in the spectral range from 1.3 to 8.5 THz," Appl. Phys. Lett. **108**, 113102 (2016).

[78]P. Dean, O. Mitrofanov, J. Keeley, I. Kundu, L. Li, E. H. Linfield, and A. G. Davies, "Apertureless near-field terahertz imaging using the self-mixing effect in a quantum cascade laser," Appl. Phys. Lett. **108**, 091113 (2016).

[79]X. Chen, X. Liu, X. Guo, S. Chen, H. Hu, E. Nikulina, X. Ye, Z. Yao, H. A. Bechtel, M. C. Martin *et al.*, "THz near-field imaging of extreme subwavelength metal structures," ACS Photonics **7**, 687–694 (2020).

[80]P. Rubino, J. Keeley, N. Sulollari, A. D. Burnett, A. Valavanis, I. Kundu, M. C. Rosamond, L. Li, E. H. Linfield, A. G. Davies *et al.*, "All-electronic phase-resolved THz microscopy using the self-mixing effect in a semiconductor laser," ACS Photonics **8**, 1001–1006 (2021).

[81]E. A. Pogna, C. Silvestri, L. L. Columbo, M. Brambilla, G. Scamarcio, and M. S. Vitiello, "Terahertz near-field nanoscopy based on detectorless laser feedback interferometry under different feedback regimes," APL Photonics **6**, 061302 (2021).

[82]K. S. Reichel, E. A. A. Pogna, S. Biasco, L. Viti, A. Di Gaspare, H. E. Beere, D. A. Ritchie, and M. S. Vitiello, "Self-mixing interferometry and near-field nanoscopy in quantum cascade random lasers at terahertz frequencies," Nanophotonics **10**, 1495–1503 (2021).

[83]B. Knoll, F. Keilmann, A. Kramer, and R. Guckenberger, "Contrast of microwave near-field microscopy," Appl. Phys. Lett. **70**, 2667–2669 (1997).

[84]G. Dai, G. Geng, X. Zhang, J. Wang, T. Chang, and H.-L. Cui, "W-band near-field microscope," IEEE Access **7**, 48060–48067 (2019).

[85]J. Lee, C. J. Long, H. Yang, X.-D. Xiang, and I. Takeuchi, "Atomic resolution imaging at 2.5 GHz using near-field microwave microscopy," Appl. Phys. Lett. **97**, 183111 (2010).

[86]F. Keilmann, D. Van der Weide, T. Eickelkamp, R. Merz, and D. Stöckle, "Extreme sub-wavelength resolution with a scanning radio-frequency transmission microscope," Opt. Commun. **129**, 15–18 (1996).

[87]A. A. Govyadinov and V. A. Podolskiy, "Metamaterial photonic funnels for subdiffraction light compression and propagation," Phys. Rev. B **73**, 155108 (2006).

[88]T.-J. Huang, T.-H. Tang, L.-Z. Yin, J.-Y. Liu, Y. Tan, and P.-K. Liu, "Experimental demonstration of an ultra-broadband subwavelength resolution probe from microwave to terahertz regime," Opt. Lett. **43**, 3646–3649 (2018).

[89]J. Wessel, "Surface-enhanced optical microscopy," J. Opt. Soc. Am. B **2**, 1538–1541 (1985).

[90]H. K. Wickramasinghe and C. C. Williams, "Apertureless near field optical microscope," U.S. patent 4,947,034 (28 April 1989).

[91]B. Knoll and F. Keilmann, "Infrared conductivity mapping for nanoelectronics," Appl. Phys. Lett. **77**, 3980–3982 (2000).

[92]M. Eisele, T. L. Cocker, M. A. Huber, M. Plankl, L. Viti, D. Ercolani, L. Sorba, M. S. Vitiello, and R. Huber, "Ultrafast multi-terahertz nano-spectroscopy with sub-cycle temporal resolution," Nat. Photonics **8**, 841 (2014).

[93]G. C. Cho, H.-T. Chen, S. Kraatz, N. Karpowicz, and R. Kersting, "Apertureless terahertz near-field microscopy," Semicond. Sci. Technol. **20**, S286 (2005).

[94]F. Buersgens, R. Kersting, and H.-T. Chen, "Terahertz microscopy of charge carriers in semiconductors," Appl. Phys. Lett. **88**, 112115 (2006).

[95]K. Moon, E. Jung, M. Lim, Y. Do, and H. Han, "Terahertz near-field microscope: Analysis and measurements of scattering signals," IEEE Trans. Terahertz Sci. Technol. **1**, 164–168 (2011).

[96]K. Moon, Y. Do, M. Lim, G. Lee, H. Kang, K.-S. Park, and H. Han, "Quantitative coherent scattering spectra in apertureless terahertz pulse near-field microscopes," Appl. Phys. Lett. **101**, 011109 (2012).

[97]K. Moon, H. Park, J. Kim, Y. Do, S. Lee, G. Lee, H. Kang, and H. Han, "Subsurface nanoimaging by broadband terahertz pulse near-field microscopy," Nano Lett. **15**, 549–552 (2015).

[98]P. Klarskov, H. Kim, V. L. Colvin, and D. M. Mittleman, "Nanoscale laser terahertz emission microscopy," ACS Photonics **4**, 2676–2680 (2017).

[99]M. C. Giordano, S. Mastel, C. Liewald, L. L. Columbo, M. Brambilla, L. Viti, A. Politano, K. Zhang, L. Li, A. G. Davies, E. H. Linfield, R. Hillenbrand, F. Keilmann, G. Scamarcio, and M. S. Vitiello, "Phase-resolved terahertz self-detection near-field microscopy," Opt. Express **26**, 18423–18435 (2018).

[100]C. Liewald, S. Mastel, J. Hesler, A. J. Huber, R. Hillenbrand, and F. Keilmann, "All-electronic terahertz nanoscopy," Optica **5**, 159–163 (2018).

[101]Z. Yao, V. Semenenko, J. Zhang, S. Mills, X. Zhao, X. Chen, H. Hu, R. Mescall, T. Ciavatti, S. March, S. R. Bank, T. H. Tao, X. Zhang, V. Perebeinos, Q. Dai, X. Du, and M. Liu, "Photo-induced terahertz near-field dynamics of graphene/InAs heterostructures," Opt. Express **27**, 13611–13623 (2019).

[102]A. Pizzuto, D. M. Mittleman, and P. Klarskov, "Laser THz emission nanoscopy and THz nanoscopy," Opt. Express **28**, 18778–18789 (2020).

[103]E. A. Pogna, M. Asgari, V. Zannier, L. Sorba, L. Viti, and M. S. Vitiello, "Unveiling the detection dynamics of semiconductor nanowire photodetectors by terahertz near-field nanoscopy," Light: Sci. Appl. **9**, 189 (2020).

[104]X. Jin, M. Farina, X. Wang, G. Fabi, X. Cheng, and J. C. Hwang, "Quantitative scanning microwave microscopy of the evolution of a live biological cell in a physiological buffer," IEEE Trans. Microwave Theory Tech. **67**, 5438–5445 (2019).

[105]M. Farina, X. Jin, G. Fabi, E. Pavoni, A. Di Donato, D. Mencarelli, A. Morini, F. Piacenza, R. Al Hadi, Y. Zhao, Y. Ning, T. Pietrangelo, X. Cheng, and J. C. M. Hwang, "Inverted scanning microwave microscope for *in vitro* imaging and characterization of biological cells," Appl. Phys. Lett. **114**, 093703 (2019).

[106]A. Lahrech, R. Bachelot, P. Gleyzes, and A. C. Boccara, "Infrared-reflection-mode near-field microscopy using an apertureless probe with a resolution of $\lambda/600$," Opt. Lett. **21**, 1315–1317 (1996).

[107]N. J. J. van Hoof, S. E. T. ter Huurne, J. G. Rivas, and A. Halpin, "Time-resolved terahertz time-domain near-field microscopy," Opt. Express **26**, 32118–32129 (2018).

[108]N. Van der Valk and P. Planken, "Electro-optic detection of subwavelength terahertz spot sizes in the near field of a metal tip," Appl. Phys. Lett. **81**, 1558–1560 (2002).

[109]V. Pistore, E. A. A. Pogna, L. Viti, L. Li, A. G. Davies, E. H. Linfield, and M. S. Vitiello, "Self-induced phase locking of terahertz frequency combs in a phase-sensitive hyperspectral near-field nanoscope," Adv. Sci. **9**, 2200410 (2022).

[110]F. Qiu, G. You, Z. Tan, W. Wan, C. Wang, X. Liu, X. Chen, R. Liu, H. Tao, Z. Fu *et al.*, "A terahertz near-field nanoscopy revealing edge fringes with a fast and highly sensitive quantum-well photodetector," Iscience **25**, 104637 (2022).

[111]O. Khatib, H. A. Bechtel, M. C. Martin, M. B. Raschke, and G. L. Carr, "Far infrared synchrotron near-field nanoimaging and nanospectroscopy," ACS Photonics **5**, 2773–2779 (2018).

[112]S. Dhillon, M. Vitiello, E. Linfield, A. Davies, M. C. Hoffmann, J. Booske, C. Paoloni, M. Gensch, P. Weightman, G. Williams *et al.*, "The 2017 terahertz science and technology roadmap," J. Phys. D: Appl. Phys. **50**, 043001 (2017).

[113]R. Lewis, "A review of terahertz detectors," J. Phys. D: Appl. Phys. **52**, 433001 (2019).

[114]A. Rakić, T. Taimre, K. Bertling, Y. Lim, P. Dean, A. Valavanis, and D. Indjin, "Sensing and imaging using laser feedback interferometry with quantum cascade lasers," Appl. Phys. Rev. **6**, 021320 (2019).

[115]M. S. Vitiello and A. Tredicucci, "Physics and technology of terahertz quantum cascade lasers," Adv. Phys.: X **6**, 1893809 (2021).

[116]P. Dean, J. Keeley, Y. L. Lim, K. Bertling, T. Taimre, P. Rubino, D. Indjin, and A. Rakić, "Self-mixing in quantum cascade lasers: Theory and applications," in *Mid-Infrared and Terahertz Quantum Cascade Lasers* (Cambridge University Press, 2023), p. 477–508.

[117]A. Pizzuto, E. Castro-Camus, W. Wilson, W. Choi, X. Li, and D. M. Mittleman, "Nonlocal time-resolved terahertz spectroscopy in the near field," ACS Photonics **8**, 2904–2911 (2021).

[118]A. Pizzuto, P. Ma, and D. M. Mittleman, "Near-field terahertz nonlinear optics with blue light," Light: Sci. Appl. **12**, 96 (2023).

[119]J. Cai, M. Dai, S. Chen, P. Chen, J. Wang, H. Xiong, Z. Ren, S. Liu, Z. Liu, C. Wan *et al.*, "Terahertz spin currents resolved with nanometer spatial resolution," Appl. Phys. Rev. **10**, 041414 (2023).

[120]E. A. A. Pogna, L. Viti, A. Politano, M. Brambilla, G. Scamarcio, and M. S. Vitiello, "Mapping propagation of collective modes in Bi_2Se_3 and $Bi_2Te_{2.2}Se_{0.8}$ topological insulators by near-field terahertz nanoscopy," Nat. Commun. **12**, 6672 (2021).

[121]A. Bitzer, A. Ortner, and M. Walther, "Terahertz near-field microscopy with subwavelength spatial resolution based on photoconductive antennas," Appl. Opt. **49**, E1–E6 (2010).

24 November 2024 03:57:31

[122]A. Khalatpour, A. K. Paulsen, C. Deimert, Z. R. Wasilewski, and Q. Hu, "High-power portable terahertz laser systems," Nat. Photonics **15**, 16–20 (2021).

[123]X. Qi, G. Agnew, I. Kundu, T. Taimre, Y. L. Lim, K. Bertling, P. Dean, A. Grier, A. Valavanis, E. H. Linfield *et al.*, "Multi-spectral terahertz sensing: Proposal for a coupled-cavity quantum cascade laser based optical feedback interferometer," Opt. Express **25**, 10153–10165 (2017).

[124]X. Qi, G. Agnew, T. Taimre, S. Han, Y. L. Lim, K. Bertling, A. Demić, P. Dean, D. Indjin, and A. D. Rakić, "Laser feedback interferometry in multi-mode terahertz quantum cascade lasers," Opt. Express **28**, 14246–14262 (2020).

[125]C. Silvestri, X. Qi, T. Taimre, and A. D. Rakić, "Multimode dynamics of terahertz quantum cascade lasers: Spontaneous and actively induced generation of dense and harmonic coherent regimes," Phys. Rev. A **106**, 053526 (2022).

[126]E. Riccardi, V. Pistore, S. Kang, L. Seitner, A. De Vetter, C. Jirauschek, J. Mangeney, L. Li, A. G. Davies, E. H. Linfield *et al.*, "Short pulse generation from a graphene-coupled passively mode-locked terahertz laser," Nat. Photonics **17**, 607–614 (2023).

[127]C. Silvestri, X. Qi, T. Taimre, K. Bertling, and A. D. Rakić, "Frequency combs in quantum cascade lasers: An overview of modeling and experiments," APL Photonics **8**, 020902 (2023).

[128]C. Silvestri, X. Qi, T. Taimre, and A. D. Rakić, "Frequency combs induced by optical feedback and harmonic order tunability in quantum cascade lasers," APL Photonics **8**, 116102 (2023).

[129]C. Silvestri, X. Qi, T. Taimre, and A. D. Rakić, "Harmonic active mode locking in terahertz quantum cascade lasers," Phys. Rev. A **108**, 013501 (2023).

[130]X. Guo, K. Bertling, and A. D. Rakić, "Optical constants from scattering-type scanning near-field optical microscope," Appl. Phys. Lett. **118**, 041103 (2021).

[131]C. Silvestri, L. L. Columbo, and M. Brambilla, "Retrieval of the dielectric properties of a resonant material in the terahertz region via self-detection near field optical microscopy," IEEE J. Sel. Top. Quantum Electron. **29**, 8600211 (2023).

[132]X. Guo, X. He, Z. Degnan, C.-C. Chiu, B. C. Donose, K. Bertling, A. Fedorov, A. D. Rakić, and P. Jacobson, "Terahertz nanospectroscopy of plasmon polaritons for the evaluation of doping in quantum devices," Nanophotonics **12**, 1865–1875 (2023).

[133]F. Wang, H. Nong, T. Fobbe, V. Pistore, S. Houver, S. Markmann, N. Jukam, M. Amanti, C. Sirtori, S. Moumdji *et al.*, "Short terahertz pulse generation from a dispersion compensated modelocked semiconductor laser," Laser Photonics Rev. **11**, 1700013 (2017).

[134]L. Seitner, J. Popp, M. Haider, S. S. Dhillon, M. S. Vitiello, and C. Jirauschek, "Theoretical model of passive mode-locking in terahertz quantum cascade lasers with distributed saturable absorbers," Nanophotonics (published online 2024).

[135]T. Taimre, M. Nikolić, K. Bertling, Y. L. Lim, T. Bosch, and A. D. Rakić, "Laser feedback interferometry: A tutorial on the self-mixing effect for coherent sensing," Adv. Opt. Photonics **7**, 570–631 (2015).

[136]K. Bertling, T. Taimre, G. Agnew, Y. L. Lim, P. Dean, D. Indjin, S. Höfling, R. Weih, M. Kamp, M. von Edlinger *et al.*, "Simple electrical modulation scheme for laser feedback imaging," IEEE Sens. J. **16**, 1937–1942 (2015).

[137]Y. L. Lim, K. Bertling, T. Taimre, T. Gillespie, C. Glenn, A. Robinson, D. Indjin, Y. Han, L. Li, E. H. Linfield *et al.*, "Coherent imaging using laser feedback interferometry with pulsed-mode terahertz quantum cascade lasers," Opt. Express **27**, 10221–10233 (2019).

[138]M. S. Vitiello, "Near-field quantum nanoscopy in the far-infrared enabled by quantum cascade lasers: Opinion," Opt. Mater. Express **13**, 3045–3050 (2023).

[139]D. Mohun, N. Sulollari, M. Salih, L. H. Li, J. E. Cunningham, E. H. Linfield, A. G. Davies, and P. Dean, "Terahertz microscopy using laser feedback interferometry based on a generalised phase-stepping algorithm," Sci. Rep. **14**, 3274 (2024).

[140]L. Wehmeier, M. Liu, S. Park, H. Jang, D. Basov, C. C. Homes, and G. L. Carr, "Ultrabroadband terahertz near-field nanospectroscopy with a HgCdTe detector," ACS Photonics **10**, 4329–4339 (2023).

[141]S.-S. Tuca, G. Badino, G. Gramse, E. Brinciotti, M. Kasper, Y. J. Oh, R. Zhu, C. Rankl, P. Hinterdorfer, and F. Kienberger, "Calibrated complex impedance of CHO cells and E. coli bacteria at GHz frequencies using scanning microwave microscopy," Nanotechnology **27**, 135702 (2016).

[142]M. Farina and J. C. Hwang, "Scanning microwave microscopy for biological applications: Introducing the state of the art and inverted SMM," IEEE Microwave Mag. **21**, 52–59 (2020).

[143]G. Fabi, C. Joseph, E. Pavoni, X. Wang, R. Al Hadi, J. C. Hwang, A. Morini, and M. Farina, "Real-time removal of topographic artifacts in scanning microwave microscopy," IEEE Trans. Microwave Theory Tech. **69**, 2662–2672 (2021).

[144]S. A. Azman, G. Fabi, E. Pavoni, C. Joseph, N. Pini, T. Pietrangelo, L. Pierantoni, A. Morini, D. Mencarelli, A. Di Donato *et al.*, "Inverted scanning microwave microscopy of a vital mitochondrion in liquid," IEEE Microwave Wireless Compon. Lett. **32**, 804–806 (2022).

[145]A. D. Rakić, T. Taimre, K. Bertling, Y. L. Lim, P. Dean, D. Indjin, Z. Ikonić, P. Harrison, A. Valavanis, S. P. Khanna *et al.*, "Swept-frequency feedback interferometry using terahertz frequency QCLs: A method for imaging and materials analysis," Opt. Express **21**, 22194–22205 (2013).

[146]J. Keeley, P. Dean, A. Valavanis, K. Bertling, Y. Lim, R. Alhathlool, T. Taimre, L. Li, D. Indjin, A. Rakić *et al.*, "Three-dimensional terahertz imaging using swept-frequency feedback interferometry with a quantum cascade laser," Opt. Lett. **40**, 994–997 (2015).

[147]N. Ocelic, A. Huber, and R. Hillenbrand, "Pseudoheterodyne detection for background-free near-field spectroscopy," Appl. Phys. Lett. **89**, 101124 (2006).

[148]M. Schnell, P. S. Carney, and R. Hillenbrand, "Synthetic optical holography for rapid nanoimaging," Nat. Commun. **5**, 3499 (2014).

[149]Y. Sasaki and H. Sasaki, "Heterodyne detection for the extraction of the probe-scattering signal in scattering-type scanning near-field optical microscope," Jpn. J. Appl. Phys. **39**, L321 (2000).

[150]R. Hillenbrand and F. Keilmann, "Complex optical constants on a subwavelength scale," Phys. Rev. Lett. **85**, 3029 (2000).

[151]T. Taubner, R. Hillenbrand, and F. Keilmann, "Performance of visible and mid-infrared scattering-type near-field optical microscopes," J. Microsc. **210**, 311–314 (2003).

[152]I. Stefanon, S. Blaize, A. Bruyant, S. Aubert, G. Lerondel, R. Bachelot, and P. Royer, "Heterodyne detection of guided waves using a scattering-type scanning near-field optical microscope," Opt. Express **13**, 5553–5564 (2005).

[153]A. J. Sternbach, J. Hinton, T. Slusar, A. S. McLeod, M. Liu, A. Frenzel, M. Wagner, R. Iraheta, F. Keilmann, A. Leitenstorfer *et al.*, "Artifact free time resolved near-field spectroscopy," Opt. Express **25**, 28589–28611 (2017).

[154]H. Wang, L. Wang, and X. G. Xu, "Scattering-type scanning near-field optical microscopy with low-repetition-rate pulsed light source through phase-domain sampling," Nat. Commun. **7**, 13212 (2016).

[155]S. Palato, P. Schwendke, N. B. Grosse, and J. Stähler, "Pseudoheterodyne near-field imaging at kHz repetition rates via quadrature-assisted discrete demodulation," Appl. Phys. Lett. **120**, 131601 (2022).

[156]J. Neu and C. A. Schmuttenmaer, "Tutorial: An introduction to terahertz time domain spectroscopy (THz-TDS)," J. Appl. Phys. **124**, 231101 (2018).

[157]M. Koch, D. M. Mittleman, J. Ornik, and E. Castro-Camus, "Terahertz time-domain spectroscopy," Nat. Rev. Methods Primers **3**, 49 (2023).

[158]N. A. Aghamiri, F. Huth, A. J. Huber, A. Fali, R. Hillenbrand, and Y. Abate, "Hyperspectral time-domain terahertz nano-imaging," Opt. Express **27**, 24231–24242 (2019).

[159]R. Jing, R. A. Vitalone, S. Xu, C. F. B. Lo, Z. Fei, E. Runburg, Y. Shao, X. Chen, F. Mooshammer, A. S. Mcleod, M. Liu, M. M. Fogler, D. H. Cobden, X. Xu, and D. N. Basov, "Phase-resolved terahertz nanoimaging of WTe$_2$ microcrystals," Phys. Rev. B **107**, 155413 (2023).

[160]G. Dai, Z. Yang, G. Geng, M. Li, T. Chang, D. Wei, C. Du, H.-L. Cui, and H. Wang, "Signal detection techniques for scattering-type scanning near-field optical microscopy," Appl. Spectrosc. Rev. **53**, 806–835 (2018).

[161]J. M. Larson, H. A. Bechtel, and R. Kostecki, "Detection and signal processing for near-field nanoscale Fourier transform infrared spectroscopy," arXiv:2303.10329 (2023).

[162]S. Mastel, M. B. Lundeberg, P. Alonso-González, Y. Gao, K. Watanabe, T. Taniguchi, J. Hone, F. H. L. Koppens, A. Y. Nikitin, and R. Hillenbrand, "Terahertz nanofocusing with cantilevered terahertz-resonant antenna tips," Nano Lett. **17**, 6526–6533 (2017).

[163]X. Zhou, X. Guo, A. Shkurinov, and Y. Zhu, "Concentric-ring-grating-induced strong terahertz near-field enhancement on a micro-tip," J. Opt. **21**, 105005 (2019).

[164]C. Maissen, S. Chen, E. Nikulina, A. Govyadinov, and R. Hillenbrand, "Probes for ultra-sensitive THz nanoscopy," ACS Photonics **6**, 1279–1288 (2019).

24 November 2024 03:57:31

[165]T. Siday, L. L. Hale, R. I. Hermans, and O. Mitrofanov, "Resonance-enhanced terahertz nanoscopy probes," ACS Photonics **7**, 596–601 (2020).

[166]R. Ren, X. Chen, and M. Liu, "High-efficiency scattering probe design for s-polarized near-field microscopy," Appl. Phys. Express **14**, 022002 (2021).

[167]F. Mooshammer, M. Plankl, T. Siday, M. Zizlsperger, F. Sandner, R. Vitalone, R. Jing, M. A. Huber, D. Basov, and R. Huber, "Quantitative terahertz emission nanoscopy with multiresonant near-field probes," Opt. Lett. **46**, 3572–3575 (2021).

[168]Y. Zhang, X. Chen, D. Chen, Z. Yao, S. Xu, P. McArdle, M. M. Qazilbash, and M. Liu, "Partially metal-coated tips for near-field nanospectroscopy," Phys. Rev. Appl. **15**, 014048 (2021).

[169]L. Wehmeier, T. Nörenberg, T. V. de Oliveira, J. M. Klopf, S.-Y. Yang, L. W. Martin, R. Ramesh, L. M. Eng, and S. C. Kehr, "Phonon-induced near-field resonances in multiferroic BiFeO$_3$ thin films at infrared and THz wavelengths," Appl. Phys. Lett. **116**, 071103 (2020).

[170]M. B. Raschke and C. Lienau, "Apertureless near-field optical microscopy: Tip–sample coupling in elastic light scattering," Appl. Phys. Lett. **83**, 5089–5091 (2003).

[171]W. Denk and D. W. Pohl, "Near-field optics: Microscopy with nanometer-size fields," J. Vac. Sci. Technol. B **9**, 510–513 (1991).

[172]L. Novotny, D. W. Pohl, and B. Hecht, "Light confinement in scanning near-field optical microscopy," Ultramicroscopy **61**, 1–9 (1995).

[173]O. J. Martin and C. Girard, "Controlling and tuning strong optical field gradients at a local probe microscope tip apex," Appl. Phys. Lett. **70**, 705–707 (1997).

[174]Y. C. Martin, H. F. Hamann, and H. K. Wickramasinghe, "Strength of the electric field in apertureless near-field optical microscopy," J. Appl. Phys. **89**, 5774–5778 (2001).

[175]N. Calander and M. Willander, "Theory of surface-plasmon resonance optical-field enhancement at prolate spheroids," J. Appl. Phys. **92**, 4878–4884 (2002).

[176]N. Behr and M. B. Raschke, "Optical antenna properties of scanning probe tips: Plasmonic light scattering, tip- sample coupling, and near-field enhancement," J. Phys. Chem. C **112**, 3766–3773 (2008).

[177]P. Aravind and H. Metiu, "The effects of the interaction between resonances in the electromagnetic response of a sphere-plane structure; applications to surface enhanced spectroscopy," Surf. Sci. **124**, 506–528 (1983).

[178]G. W. Ford and W. H. Weber, "Electromagnetic interactions of molecules with metal surfaces," Phys. Rep. **113**, 195–287 (1984).

[179]B. Knoll and F. Keilmann, "Enhanced dielectric contrast in scattering-type scanning near-field optical microscopy," Opt. Commun. **182**, 321–328 (2000).

[180]A. Cvitkovic, N. Ocelic, and R. Hillenbrand, "Analytical model for quantitative prediction of material contrasts in scattering-type near-field optical microscopy," Opt. Express **15**, 8550–8565 (2007).

[181]N. Ocelić, "Quantitative near-field phonon-polariton spectroscopy," Ph.D. thesis (Technische Universität München, 2007).

[182]K. Wang, D. M. Mittleman, N. C. van der Valk, and P. C. Planken, "Antenna effects in terahertz apertureless near-field optical microscopy," Appl. Phys. Lett. **85**, 2715–2717 (2004).

[183]X. Chen, Z. Yao, S. Xu, A. S. McLeod, S. N. Gilbert Corder, Y. Zhao, M. Tsuneto, H. A. Bechtel, M. C. Martin, G. L. Carr, M. M. Fogler, S. G. Stanciu, D. N. Basov, and M. Liu, "Hybrid machine learning for scanning near-field optical spectroscopy," ACS Photonics **8**, 2987–2996 (2021).

[184]S. Amarie and F. Keilmann, "Broadband-infrared assessment of phonon resonance in scattering-type near-field microscopy," Phys. Rev. B **83**, 045404 (2011).

[185]X. Chen, J. Zhang, Z. Yao, H. A. Bechtel, M. C. Martin, G. Carr, and M. Liu, "Ultrabroadband infrared near-field spectroscopy and imaging of local resonators in percolative gold films," J. Opt. Soc. Am. B **36**, 3315–3321 (2019).

[186]L. Jung, J. Pries, T. W. Maß, M. Lewin, D. S. Boyuk, A. T. Mohabir, M. A. Filler, M. Wuttig, and T. Taubner, "Quantification of carrier density gradients along axially-doped silicon nanowires using infrared nanoscopy," ACS Photonics **6**, 1744–1754 (2019).

[187]A. A. Govyadinov, I. Amenabar, F. Huth, P. S. Carney, and R. Hillenbrand, "Quantitative measurement of local infrared absorption and dielectric function with tip-enhanced near-field microscopy," J. Phys. Chem. Lett. **4**, 1526–1531 (2013).

[188]A. A. Govyadinov, S. Mastel, F. Golmar, A. Chuvilin, P. S. Carney, and R. Hillenbrand, "Recovery of permittivity and depth from near-field data as a step toward infrared nanotomography," ACS Nano **8**, 6911–6921 (2014).

[189]A. S. McLeod, P. Kelly, M. Goldflam, Z. Gainsforth, A. J. Westphal, G. Dominguez, M. H. Thiemens, M. M. Fogler, and D. Basov, "Model for quantitative tip-enhanced spectroscopy and the extraction of nanoscale-resolved optical constants," Phys. Rev. B **90**, 085136 (2014).

[190]F. Mooshammer, F. Sandner, M. A. Huber, M. Zizlsperger, H. Weigand, M. Plankl, C. Weyrich, M. Lanius, J. Kampmeier, G. Mussler, D. Grützmacher, J. L. Boland, T. L. Cocker, and R. Huber, "Nanoscale near-field tomography of surface states on (Bi$_{0.5}$Sb$_{0.5}$)$_2$Te$_3$," Nano Lett. **18**, 7515–7523 (2018).

[191]D. E. Tranca, S. G. Stanciu, R. Hristu, B. M. Witgen, and A. Stanciu, "Nanoscale mapping of refractive index by using scattering-type scanning near-field optical microscopy," Nanomed. Nanotechnol. Biol. Med. **14**, 47–50 (2018).

[192]K. Moon, Y. Do, H. Park, J. Kim, H. Kang, G. Lee, J.-H. Lim, J.-W. Kim, and H. Han, "Computed terahertz near-field mapping of molecular resonances of lactose stereo-isomer impurities with sub-attomole sensitivity," Sci. Rep. **9**, 16915 (2019).

[193]S. G. Stanciu, D. E. Tranca, L. Pastorino, S. Boi, Y. M. Song, Y. J. Yoo, S. Ishii, R. Hristu, F. Yang, G. Bussetti, and G. A. Stanciu, "Characterization of nanomaterials by locally determining their complex permittivity with scattering-type scanning near field optical microscopy," ACS Appl. Nano Mater. **3**, 1250–1262 (2020).

[194]F. L. Ruta, A. J. Sternbach, A. B. Dieng, A. S. McLeod, and D. N. Basov, "Quantitative nano-infrared spectroscopy of anisotropic van der Waals materials," Nano Lett. **20**, 7933–7940 (2020).

[195]X. Guo, X. He, Z. Degnan, B. C. Donose, K. Bertling, A. Fedorov, A. D. Rakić, and P. Jacobson, "Near-field terahertz nanoscopy of coplanar microwave resonators," Appl. Phys. Lett. **119**, 091101 (2021).

[196]A. Solemanifar, X. Guo, B. C. Donose, K. Bertling, B. Laycock, and A. D. Rakić, "Probing peptide nanowire conductivity by THz nanoscopy," Nanotechnology **33**, 065503 (2021).

[197]K. Moon, E. Jung, M. Lim, Y. Do, and H. Han, "Quantitative analysis and measurements of near-field interactions in terahertz microscopes," Opt. Express **19**, 11539–11544 (2011).

[198]S. Chui, X. Chen, M. Liu, Z. Lin, and J. Zi, "Scattering of electromagnetic waves from a cone with conformal mapping: Application to scanning near-field optical microscope," Phys. Rev. B **97**, 081406 (2018).

[199]B. Hauer, A. P. Engelhardt, and T. Taubner, "Quasi-analytical model for scattering infrared near-field microscopy on layered systems," Opt. Express **20**, 13173–13188 (2012).

[200]L. M. Zhang, G. O. Andreev, Z. Fei, A. S. McLeod, G. Dominguez, M. Thiemens, A. Castro-Neto, D. Basov, and M. M. Fogler, "Near-field spectroscopy of silicon dioxide thin films," Phys. Rev. B **85**, 075419 (2012).

[201]D. E. Tranca, S. G. Stanciu, R. Hristu, C. Stoichita, S. Tofail, and G. A. Stanciu, "High-resolution quantitative determination of dielectric function by using scattering scanning near-field optical microscopy," Sci. Rep. **5**, 11876 (2015).

[202]B.-Y. Jiang, L. Zhang, A. Castro Neto, D. Basov, and M. Fogler, "Generalized spectral method for near-field optical microscopy," J. Appl. Phys. **119**, 054305 (2016).

[203]Y. Moon, H. Lee, J. Lim, G. Lee, J. Kim, and H. Han, "Reference-free self-calibrating tip-based scattering-type THz near-field microscopy," AIP Adv. **13**, 065211 (2023).

[204]M. Khavronin and D. Svintsov, "Signatures of nonlocal electrical conductivity in near-field microscopy," Phys. Rev. B **107**, 205409 (2023).

[205]P. McArdle, D. Lahneman, A. Biswas, F. Keilmann, and M. Qazilbash, "Near-field infrared nanospectroscopy of surface phonon-polariton resonances," Phys. Rev. Res. **2**, 023272 (2020).

[206]A. D. Rakić, A. B. Djurišić, J. M. Elazar, and M. L. Majewski, "Optical properties of metallic films for vertical-cavity optoelectronic devices," Appl. Opt. **37**, 5271–5283 (1998).

[207]E. D. Palik, *Handbook of Optical Constants of Solids* (Academic Press, 1998), Vol. 3.

[208]A. Fali, S. Gamage, M. Howard, T. G. Folland, N. A. Mahadik, T. Tiwald, K. Bolotin, J. D. Caldwell, and Y. Abate, "Nanoscale spectroscopy of dielectric properties of mica," ACS Photonics **8**, 175–181 (2020).

[209]C. Chen, S. Chen, R. P. Lobo, C. Maciel-Escudero, M. Lewin, T. Taubner, W. Xiong, M. Xu, X. Zhang, X. Miao *et al.*, "Terahertz nanoimaging and nano-spectroscopy of chalcogenide phase-change materials," ACS Photonics **7**, 3499–3506 (2020).

[210]X. Chen and E. Pickwell-MacPherson, "An introduction to terahertz time-domain spectroscopic ellipsometry," APL Photonics **7**, 071101 (2022).

[211]K. Lai, W. Kundhikanjana, H. Peng, Y. Cui, M. Kelly, and Z. Shen, "Tapping mode microwave impedance microscopy," Rev. Sci. Instrum. **80**, 043707 (2009).

[212]H. Huber, M. Moertelmaier, T. Wallis, C. Chiang, M. Hochleitner, A. Imtiaz, Y. Oh, K. Schilcher, M. Dieudonne, J. Smoliner *et al.*, "Calibrated nanoscale capacitance measurements using a scanning microwave microscope," Rev. Sci. Instrum. **81**, 113701 (2010).

[213]M. Farina, D. Mencarelli, A. Di Donato, G. Venanzoni, and A. Morini, "Calibration protocol for broadband near-field microwave microscopy," IEEE Trans. Microwave Theory Tech. **59**, 2769–2776 (2011).

[214]G. Gramse, M. Kasper, L. Fumagalli, G. Gomila, P. Hinterdorfer, and F. Kienberger, "Calibrated complex impedance and permittivity measurements with scanning microwave microscopy," Nanotechnology **25**, 145703 (2014).

[215]E. Brinciotti, G. Gramse, S. Hommel, T. Schweinboeck, A. Altes, M. A. Fenner, J. Smoliner, M. Kasper, G. Badino, S.-S. Tuca, and F. Kienberger, "Probing resistivity and doping concentration of semiconductors at the nanoscale using scanning microwave microscopy," Nanoscale **7**, 14715–14722 (2015).

[216]P. Girard, "Electrostatic force microscopy: Principles and some applications to semiconductors," Nanotechnology **12**, 485 (2001).

[217]C. Gabriel, E. Grant, and I. Young, "Use of time domain spectroscopy for measuring dielectric properties with a coaxial probe," J. Phys. E: Sci. Instrum. **19**, 843 (1986).

[218]S. A. Wartenberg, *RF Measurements of Die and Packages* (Artech House, 2002).

[219]L. Fumagalli, G. Ferrari, M. Sampietro, and G. Gomila, "Dielectric-constant measurement of thin insulating films at low frequency by nanoscale capacitance microscopy," Appl. Phys. Lett. **91**, 243110 (2007).

[220]E. C. Burdette, F. L. Cain, and J. Seals, "In vivo probe measurement technique for determining dielectric properties at VHF through microwave frequencies," IEEE Trans. Microwave Theory Tech. **28**, 414–427 (1980).

[221]X. Chen, Z. Yao, S. G. Stanciu, D. Basov, R. Hillenbrand, and M. Liu, "Rapid simulations of hyperspectral near-field images of three-dimensional heterogeneous surfaces," Opt. Express **29**, 39648–39668 (2021).

[222]L. Mester, A. A. Govyadinov, and R. Hillenbrand, "High-fidelity nano-FTIR spectroscopy by on-pixel normalization of signal harmonics," Nanophotonics **11**, 377–390 (2021).

[223]X.-C. Zhang and J. Xu, *Introduction to THz Wave Photonics* (Springer, 2010), Vol. 29.

[224]R. A. Lewis, *Terahertz Physics* (Cambridge University Press, 2012).

[225]M. Naftaly, *Terahertz Metrology* (Artech House, 2015).

[226]A. Leitenstorfer, A. S. Moskalenko, T. Kampfrath, J. Kono, E. Castro-Camus, K. Peng, N. Qureshi, D. Turchinovich, K. Tanaka, A. Markelz, M. Havenith, C. Hough, H. J. Joyce, W. J. Padilla, B. Zhou, K.-Y. Kim, X.-C. Zhang, P. U. Jepsen, S. Dhillon, M. Vitiello, E. Linfield, A. G. Davies, M. C. Hoffmann, R. Lewis, M. Tonouchi, P. Klarskov, T. S. Seifert, Y. A. Gerasimenko, D. Mihailovic, R. Huber, J. L. Boland, O. Mitrofanov, P. Dean, B. N. Ellison, P. G. Huggard, S. P. Rea, C. Walker, D. T. Leisawitz, J. R. Gao, C. Li, Q. Chen, G. Valušis, V. P. Wallace, E. Pickwell-MacPherson, X. Shang, J. Hesler, N. Ridler, C. C. Renaud, I. Kallfass, T. Nagatsuma, J. A. Zeitler, D. Arnone, M. B. Johnston, and J. Cunningham, "The 2023 terahertz science and technology roadmap," J. Phys. D: Appl. Phys. **56**, 223001 (2023).

[227]R. Lewis, "Semiconductor terahertz physics," Ann. Phys. **535**, 2200393 (2023).

[228]D. Cooke, A. MacDonald, A. Hryciw, J. Wang, Q. Li, A. Meldrum, and F. Hegmann, "Transient terahertz conductivity in photoexcited silicon nanocrystal films," Phys. Rev. B **73**, 193311 (2006).

[229]M. Walther, D. Cooke, C. Sherstan, M. Hajar, M. Freeman, and F. Hegmann, "Terahertz conductivity of thin gold films at the metal-insulator percolation transition," Phys. Rev. B **76**, 125408 (2007).

[230]T. Zhao, P. Xie, H. Wan, T. Ding, M. Liu, J. Xie, E. Li, X. Chen, T. Wang, Q. Zhang *et al.*, "Ultrathin MXene assemblies approach the intrinsic absorption limit in the 0.5–10 THz band," Nat. Photonics **17**, 622 (2023).

[231]J. Allen, T. Sanders, J. Horvat, R. Lewis, and K. Rule, "Determination of vibrational modes of l-alanine single crystals by a combination of terahertz spectroscopy measurements and density functional calculations," Phys. Rev. Lett. **130**, 226901 (2023).

[232]R. Ulbricht, E. Hendry, J. Shan, T. F. Heinz, and M. Bonn, "Carrier dynamics in semiconductors studied with time-resolved terahertz spectroscopy," Rev. Mod. Phys. **83**, 543 (2011).

[233]S. Fan, Y. He, B. S. Ung, and E. Pickwell-MacPherson, "The growth of biomedical terahertz research," J. Phys. D: Appl. Phys. **47**, 374009 (2014).

[234]J. Sibik and J. A. Zeitler, "Direct measurement of molecular mobility and crystallisation of amorphous pharmaceuticals using terahertz spectroscopy," Adv. Drug Delivery Rev. **100**, 147–157 (2016).

[235]P. Bawuah and J. A. Zeitler, "Advances in terahertz time-domain spectroscopy of pharmaceutical solids: A review," Trends Anal. Chem. **139**, 116272 (2021).

[236]P. A. Banks, E. M. Kleist, and M. T. Ruggiero, "Investigating the function and design of molecular materials through terahertz vibrational spectroscopy," Nat. Rev. Chem. **7**, 480–495 (2023).

[237]Y. Shao, Y. Wang, D. Zhu, X. Xiong, Z. Tian, A. V. Balakin, A. P. Shkurinov, D. Xu, Y. Wu, Y. Peng, and Y. Zhu, "Measuring heavy metal ions in water using nature existed microalgae as medium based on terahertz technology," J. Hazard. Mater. **435**, 129028 (2022).

[238]A. Ren, A. Zahid, D. Fan, X. Yang, M. A. Imran, A. Alomainy, and Q. H. Abbasi, "State-of-the-art in terahertz sensing for food and water security—a comprehensive review," Trends Food Sci. Technol. **85**, 241–251 (2019).

[239]C. L. Koch-Dandolo, T. Filtenborg, K. Fukunaga, J. Skou-Hansen, and P. U. Jepsen, "Reflection terahertz time-domain imaging for analysis of an 18th century neoclassical easel painting," Appl. Opt. **54**, 5123–5129 (2015).

[240]K. Krügener, M. Schwerdtfeger, S. F. Busch, A. Soltani, E. Castro-Camus, M. Koch, and W. Viöl, "Terahertz meets sculptural and architectural art: Evaluation and conservation of stone objects with T-ray technology," Sci. Rep. **5**, 14842 (2015).

[241]J. Dong, A. Locquet, M. Melis, and D. Citrin, "Global mapping of stratigraphy of an old-master painting using sparsity-based terahertz reflectometry," Sci. Rep. **7**, 15098 (2017).

[242]F. E. Lambert, J. Ornik, N.-A. Staats, A. Jäckel, G. G. Hernandez-Cardoso, J. Taiber, E.-M. Stübling, R. Budolph, O. Mack, H. Portsteffen *et al.*, "Layer separation mapping and consolidation evaluation of a fifteenth century panel painting using terahertz time-domain imaging," Sci. Rep. **12**, 21038 (2022).

[243]J. Zhang, X. Chen, S. Mills, T. Ciavatti, Z. Yao, R. Mescall, H. Hu, V. Semenenko, Z. Fei, H. Li *et al.*, "Terahertz nanoimaging of graphene," ACS Photonics **5**, 2645–2651 (2018).

[244]I. Lavor, L. Cavalcante, A. Chaves, F. Peeters, and B. Van Duppen, "Probing the structure and composition of van der Waals heterostructures using the nonlocality of Dirac plasmons in the terahertz regime," 2D Mater. **8**, 015014 (2020).

[245]M. M. Wiecha, R. Kapoor, and H. G. Roskos, "Terahertz scattering-type near-field microscopy quantitatively determines the conductivity and charge carrier density of optically doped and impurity-doped silicon," APL Photonics **6**, 126108 (2021).

[246]A. Bitzer, H. Merbold, A. Thoman, T. Feurer, H. Helm, and M. Walther, "Terahertz near-field imaging of electric and magnetic resonances of a planar metamaterial," Opt. Express **17**, 3826–3834 (2009).

[247]R. Jacob, S. Winnerl, M. Fehrenbacher, J. Bhattacharyya, H. Schneider, M. T. Wenzel, H.-G. von Ribbeck, L. M. Eng, P. Atkinson, O. G. Schmidt, and M. Helm, "Intersublevel spectroscopy on single InAs-quantum dots by terahertz near-field microscopy," Nano Lett. **12**, 4336–4340 (2012).

[248]R. Degl'Innocenti, R. Wallis, B. Wei, L. Xiao, S. J. Kindness, O. Mitrofanov, P. Braeuninger-Weimer, S. Hofmann, H. E. Beere, and D. A. Ritchie, "Terahertz nanoscopy of plasmonic resonances with a quantum cascade laser," ACS Photonics **4**, 2150–2157 (2017).

[249]G. Acuna, S. Heucke, F. Kuchler, H.-T. Chen, A. Taylor, and R. Kersting, "Surface plasmons in terahertz metamaterials," Opt. Express **16**, 18745–18751 (2008).

[250]O. Mitrofanov, I. Khromova, T. Siday, R. J. Thompson, A. N. Ponomarev, I. Brener, and J. L. Reno, "Near-field spectroscopy and imaging of subwavelength plasmonic terahertz resonators," IEEE Trans. Terahertz Sci. Technol. **6**, 382–388 (2016).

[251]R. Jing, Y. Shao, Z. Fei, C. F. B. Lo, R. A. Vitalone, F. L. Ruta, J. Staunton, W. J.-C. Zheng, A. S. Mcleod, Z. Sun *et al.*, "Terahertz response of monolayer and few-layer WTe_2 at the nanoscale," Nat. Commun. **12**, 5594 (2021).

[252]S. Chen, P. L. Leng, A. Konečná, E. Modin, M. Gutierrez-Amigo, E. Vicentini, B. Martín-García, M. Barra-Burillo, I. Niehues, C. M. Escudero, X. Y. Xie, L. E. Hueso, E. Artacho, J. Aizpurua, I. Errea, M. G. Vergniory, A. Chuvilin, F. X. Xiu, and R. Hillenbrand, "Real-space observation of ultraconfined in-plane anisotropic acoustic terahertz plasmon polaritons," Nat. Mater. **22**, 860–866 (2023).

[253]F. H. Feres, R. A. Mayer, L. Wehmeier, F. C. Maia, E. Viana, A. Malachias, H. A. Bechtel, J. M. Klopf, L. M. Eng, S. C. Kehr *et al.*, "Sub-diffractional cavity modes of terahertz hyperbolic phonon polaritons in tin oxide," Nat. Commun. **12**, 1995 (2021).

[254]F. H. Feres, I. D. Barcelos, A. R. Cadore, L. Wehmeier, T. Nörenberg, R. A. Mayer, R. O. Freitas, L. M. Eng, S. C. Kehr, and F. C. B. Maia, "Graphene nano-optics in the terahertz gap," Nano Lett. **23**, 3913–3920 (2023).

[255]M. Plankl, P. F. Junior, F. Mooshammer, T. Siday, M. Zizlsperger, F. Sandner, F. Schiegl, S. Maier, M. A. Huber, M. Gmitra, J. Fabian, J. L. Boland, T. L. Cocker, and R. Huber, "Subcycle contact-free nanoscopy of ultrafast interlayer transport in atomically thin heterostructures," Nat. Photonics **15**, 594–600 (2021).

[256]A. J. Sternbach, R. A. Vitalone, S. Shabani, J. Zhang, T. P. Darlington, S. L. Moore, S. H. Chae, E. Seewald, X. Xu, C. R. Dean *et al.*, "Quenched excitons in WSe_2/α-$RuCl_3$ heterostructures revealed by multimessenger nanoscopy," Nano Lett. **23**, 5070–5075 (2023).

[257]R. H. Kim, C. Huang, Y. Luan, L.-L. Wang, Z. Liu, J.-M. Park, L. Luo, P. M. Lozano, G. Gu, D. Turan *et al.*, "Terahertz nano-imaging of electronic strip heterogeneity in a Dirac semimetal," ACS Photonics **8**, 1873–1880 (2021).

[258]H. Zhan, V. Astley, M. Hvasta, J. A. Deibel, D. M. Mittleman, and Y.-S. Lim, "The metal-insulator transition in VO_2 studied using terahertz apertureless near-field microscopy," Appl. Phys. Lett. **91**, 162110 (2007).

[259]H. T. Stinson, A. Sternbach, O. Najera, R. Jing, A. S. Mcleod, T. V. Slusar, A. Mueller, L. Anderegg, H. T. Kim, M. Rozenberg, and D. N. Basov, "Imaging the nanoscale phase separation in vanadium dioxide thin films at terahertz frequencies," Nat. Commun. **9**, 3604 (2018).

[260]J. Barnett, L. Wehmeier, A. Heßler, M. Lewin, J. Pries, M. Wuttig, J. M. Klopf, S. C. Kehr, L. M. Eng, and T. Taubner, "Far-infrared near-field optical imaging and kelvin probe force microscopy of laser-crystallized and-amorphized phase change material $Ge_3Sb_2Te_6$," Nano Lett. **21**, 9012–9020 (2021).

[261]A. Soltani, F. Kuschewski, M. Bonmann, A. Generalov, A. Vorobiev, F. Ludwig, M. M. Wiecha, D. Čibiraitė, F. Walla, S. Winnerl *et al.*, "Direct nanoscopic observation of plasma waves in the channel of a graphene field-effect transistor," Light: Sci. Appl. **9**, 97 (2020).

[262]V. Pushkarev, H. Němec, V. C. Paingad, J. Maňák, V. Jurka, V. Novák, T. Ostatnický, and P. Kužel, "Charge transport in single-crystalline GaAs nanobars: Impact of band bending revealed by terahertz spectroscopy," Adv. Funct. Mater. **32**, 2107403 (2022).

[263]R. H. Kim, Z. Liu, C. Huang, J.-M. Park, S. J. Haeuser, Z. Song, Y. Yan, Y. Yao, L. Luo, and J. Wang, "Terahertz nanoimaging of perovskite solar cell materials," ACS Photonics **9**, 3550–3556 (2022).

[264]J. Hou, P. Chen, A. Shukla, A. Krajnc, T. Wang, X. Li, R. Doasa, L. H. Tizei, B. Chan, D. N. Johnstone *et al.*, "Liquid-phase sintering of lead halide perovskites and metal-organic framework glasses," Science **374**, 621–625 (2021).

[265]A. M. Jakob, S. G. Robson, V. Schmitt, V. Mourik, M. Posselt, D. Spemann, B. C. Johnson, H. R. Firgau, E. Mayes, J. C. McCallum *et al.*, "Deterministic shallow dopant implantation in silicon with detection confidence upper-bound to 99.85% by ion–solid interactions," Adv. Mater. **34**, 2103235 (2022).

[266]L. Thomas, T. Hannotte, C. N. Santos, B. Walter, M. Lavancier, S. Eliet, M. Faucher, J.-F. Lampin, and R. Peretti, "Imaging of THz photonic modes by scattering scanning near-field optical microscopy," ACS Appl. Mater. Interfaces **14**, 32608–32617 (2022).

[267]C. Wu, C. Wang, G. You, and J. Cao, "Terahertz nanoscopy of metal and gallium implanted silicon," ACS Adv. Opt. Mater. **1**, 843–851 (2023).

[268]S. Ge, D. Zhang, Z. Peng, and J. Meng, "Rough surface effect in terahertz near-field microscopy: 3D simulation analysis," Appl. Opt. **62**, 6333–6342 (2023).

[269]T. L. Cocker, D. Baillie, M. Buruma, L. V. Titova, R. D. Sydora, F. Marsiglio, and F. A. Hegmann, "Microscopic origin of the Drude–Smith model," Phys. Rev. B **96**, 205439 (2017).

[270]N. Smith, "Drude theory and the optical properties of liquid mercury," Phys. Lett. A **26**, 126–127 (1968).

[271]N. Smith, "Classical generalization of the Drude formula for the optical conductivity," Phys. Rev. B **64**, 155106 (2001).

[272]H.-K. Nienhuys and V. Sundström, "Influence of plasmons on terahertz conductivity measurements," Appl. Phys. Lett. **87**, 012101 (2005).

[273]M. T. Quick, N. Owschimikow, and A. W. Achtstein, "Terahertz charge carrier mobility in 1D and 2D semiconductor nanoparticles," J. Phys. Chem. Lett. **12**, 7688–7695 (2021).

[274]M. T. Quick, S. Ayari, N. Owschimikow, S. Jaziri, and A. W. Achtstein, "Quantum nature of THz conductivity: Excitons, charges, and trions in 2D semiconductor nanoplatelets and implications for THz imaging and solar hydrogen generation," ACS Appl. Nano Mater. **5**, 8306–8313 (2022).

[275]M. T. Quick, S. Ayari, N. Owschimikow, S. Jaziri, and A. W. Achtstein, "THz mobility and polarizability: Impact of transformation and dephasing on the spectral response of excitons in a 2d semiconductor," Phys. Chem. Chem. Phys. **25**, 3354–3360 (2023).

[276]M. T. Quick, Q. Wach, N. Owschimikow, and A. W. Achtstein, "THz response of charge carriers in nanoparticles: Microscopic master equations reveal an unexplored equilibration current and nonlinear mobility regimes," Adv. Photonics Res. **4**, 2200243 (2023).

[277]X. Guo, Z. Degnan, J. A. Steele, E. Solano, B. C. Donose, K. Bertling, A. Fedorov, A. D. Rakić, and P. Jacobson, "Near-field localization of the boson peak on tantalum films for superconducting quantum devices," J. Phys. Chem. Lett. **14**, 4892–4900 (2023).

[278]S. B. Hancock, D. P. Landau, N. A. Aghamiri, and Y. Abate, "Langevin dynamics/Monte Carlo simulations method for calculating nanoscale dielectric functions of materials," Phys. Rev. Mater. **6**, 076001 (2022).

[279]Y. Yu, C. Yang, M. Baggioli, A. E. Phillips, A. Zaccone, L. Zhang, R. Kajimoto, M. Nakamura, D. Yu, and L. Hong, "The ω^3 scaling of the vibrational density of states in quasi-2D nanoconfined solids," Nat. Commun. **13**, 3649 (2022).

[280]S. Liu, P. Zhang, W. Liu, S. Gong, R. Zhong, Y. Zhang, and M. Hu, "Surface polariton Cherenkov light radiation source," Phys. Rev. Lett. **109**, 153902 (2012).

[281]D. N. Basov, A. Asenjo-Garcia, P. J. Schuck, X. Zhu, and A. Rubio, "Polariton panorama," Nanophotonics **10**, 549–577 (2020).

[282]T. V. A. G. de Oliveira, T. Nörenberg, G. Álvarez-Pérez, L. Wehmeier, J. Taboada-Gutiérrez, M. Obst, F. Hempel, E. J. Lee, J. M. Klopf, I. Errea, A. Y. Nikitin, S. C. Kehr, P. Alonso-Gonzalez, and L. M. Eng, "Nanoscale-confined terahertz polaritons in a van der Waals crystal," Adv. Mater. **33**, 2005777 (2021).

[283]S. Chen, A. Bylinkin, Z. Wang, M. Schnell, G. Chandan, P. Li, A. Y. Nikitin, S. Law, and R. Hillenbrand, "Real-space nanoimaging of THz polaritons in the topological insulator Bi_2Se_3," Nat. Commun. **13**, 1374 (2022).

[284]S. Schäffer, C. O. Ogolla, Y. Loth, T. Haeger, C. Kreusel, M. Runkel, T. Riedl, B. Butz, A. K. Wigger, and P. H. Bolívar, "Imaging the terahertz nanoscale conductivity of polycrystalline $CsPbBr_3$ perovskite thin films," Nano Lett. **23**, 2074–2080 (2023).

[285]T. Nörenberg, G. Álvarez Pérez, M. Obst, L. Wehmeier, F. Hempel, J. M. Klopf, A. Y. Nikitin, S. C. Kehr, L. M. Eng, P. Alonso-González, and T. V. A. G. de Oliveira, "Germanium monosulfide as a natural platform for highly anisotropic THz polaritons," ACS Nano **16**, 20174–20185 (2022).

[286]D. Barcons Ruiz, N. C. Hesp, H. H. Sheinfux, C. R. Marimón, A. Maissen, A. Principi, R. Asgari, T. Taniguchi, K. Watanabe, M. Polini *et al.*, "Experimental signatures of the transition from acoustic plasmon to electronic sound in graphene," Sci. Adv. **9**, eadi0415 (2023).

[287]P. Alonso-González, A. Y. Nikitin, Y. Gao, A. Woessner, M. B. Lundeberg, A. Principi, N. Forcellini, W. Yan, S. Vélez, A. J. Huber *et al.*, "Acoustic terahertz graphene plasmons revealed by photocurrent nanoscopy," Nat. Nanotechnol. **12**, 31–35 (2017).

[288]U. Buchenau, M. Prager, N. Nücker, A. Dianoux, N. Ahmad, and W. Phillips, "Low-frequency modes in vitreous silica," Phys. Rev. B **34**, 5665 (1986).

[289]V. K. Malinovsky and A. P. Sokolov, "The nature of boson peak in Raman scattering in glasses," Solid State Commun. **57**, 757–761 (1986).

24 November 2024 03:57:31

[290]M. Kabeya, T. Mori, Y. Fujii, A. Koreeda, B. W. Lee, J.-H. Ko, and S. Kojima, "Boson peak dynamics of glassy glucose studied by integrated terahertz-band spectroscopy," Phys. Rev. B **94**, 224204 (2016).

[291]R. H. Kim, J. M. Park, S. Haeuser, C. Huang, D. Cheng, T. Koschny, J. Oh, C. Kopas, H. Cansizoglu, K. Yadavalli et al., "Visualizing heterogeneous dipole fields by terahertz light coupling in individual nano-junctions," Commun. Phys. **6**, 147 (2023).

[292]F. Hu and Z. Fei, "Recent progress on exciton polaritons in layered transition-metal dichalcogenides," Adv. Opt. Mater. **8**, 1901003 (2020).

[293]M. Obst, T. Nörenberg, G. Álvarez-Pérez, T. V. de Oliveira, J. Taboada-Gutiérrez, F. H. Feres, F. G. Kaps, O. Hatem, A. Luferau, A. Y. Nikitin et al., "Terahertz twistoptics–engineering canalized phonon polaritons," ACS Nano **17**, 19313–19322 (2023).

[294]J. Duan, G. Álvarez-Pérez, C. Lanza, K. Voronin, A. Tresguerres-Mata, N. Capote-Robayna, J. Álvarez-Cuervo, A. Tarazaga Martín-Luengo, J. Martín-Sánchez, V. Volkov et al., "Multiple and spectrally robust photonic magic angles in reconfigurable α-MoO₃ trilayers," Nat. Mater. **22**, 867–872 (2023).

[295]E. Galiffi, G. Carini, X. Ni, G. Álvarez-Pérez, S. Yves, E. M. Renzi, R. Nolen, S. Wasserroth, M. Wolf, P. Alonso-Gonzalez et al., "Extreme light confinement and control in low-symmetry phonon-polaritonic crystals," Nat. Rev. Mater. **9**, 9–28 (2024).

[296]A. K. Geim and I. V. Grigorieva, "Van der Waals heterostructures," Nature **499**, 419–425 (2013).

[297]R. Xiang, T. Inoue, Y. Zheng, A. Kumamoto, Y. Qian, Y. Sato, M. Liu, D. Tang, D. Gokhale, J. Guo et al., "One-dimensional van der Waals heterostructures," Science **367**, 537–542 (2020).

[298]C. Li, J. Jang, T. Badloe, T. Yang, J. Kim, J. Kim, M. Nguyen, S. A. Maier, J. Rho, H. Ren, and I. Aharonovich, "Arbitrarily structured quantum emission with a multifunctional metalens," eLight **3**, 19 (2023).

[299]Y. Wu, J. Duan, W. Ma, Q. Ou, P. Li, P. Alonso-González, J. D. Caldwell, and Q. Bao, "Manipulating polaritons at the extreme scale in van der Waals materials," Nat. Rev. Phys. **4**, 578–594 (2022).

[300]J. Lv, Y. Wu, J. Liu, Y. Gong, G. Si, G. Hu, Q. Zhang, Y. Zhang, J.-X. Tang, M. S. Fuhrer, H. Chen, S. A. Maier, Q. Cheng-Wei, and O. Qingdong, "Hyperbolic polariton crystals with configurable low-symmetry Bloch modes," Nat. Commun. **14**, 3894 (2023).

[301]U. Zschieschang, U. Waizmann, J. Weis, J. W. Borchert, and H. Klauk, "Nanoscale flexible organic thin-film transistors," Sci. Adv. **8**, eabm9845 (2022).

[302]M. Kober-Czerny, S. G. Motti, P. Holzhey, B. Wenger, J. Lim, L. M. Herz, and H. J. Snaith, "Excellent long-range charge-carrier mobility in 2D perovskites," Adv. Funct. Mater. **32**, 2203064 (2022).

[303]Y. Zhou, L. M. Herz, A. K. Jen, and M. Saliba, "Advances and challenges in understanding the microscopic structure–property–performance relationship in perovskite solar cells," Nat. Energy **7**, 794–807 (2022).

[304]L. R. Buizza, H. C. Sansom, A. D. Wright, A. M. Ulatowski, M. B. Johnston, H. J. Snaith, and L. M. Herz, "Interplay of structure, charge-carrier localization and dynamics in copper-silver-bismuth-halide semiconductors," Adv. Funct. Mater. **32**, 2108392 (2022).

[305]M. Frenzel, M. Cherasse, J. M. Urban, F. Wang, B. Xiang, L. Nest, L. Huber, L. Perfetti, M. Wolf, T. Kampfrath et al., "Nonlinear terahertz control of the lead halide perovskite lattice," Sci. Adv. **9**, eadg3856 (2023).

[306]Y. Luo, M. R. Abidian, J.-H. Ahn, D. Akinwande, A. M. Andrews, M. Antonietti, Z. Bao, M. Berggren, C. A. Berkey, C. J. Bettinger et al., "Technology roadmap for flexible sensors," ACS Nano **17**, 5211–5295 (2023).

[307]A. Vázquez-Guardado, Y. Yang, and J. A. Rogers, "Challenges and opportunities in flexible, stretchable and morphable bio-interfaced technologies," Natl. Sci. Rev. **9**, nwac016 (2022).

[308]Y. Jiang, S. Ji, J. Sun, J. Huang, Y. Li, G. Zou, T. Salim, C. Wang, W. Li, H. Jin et al., "A universal interface for plug-and-play assembly of stretchable devices," Nature **614**, 456–462 (2023).

[309]W. Wang, Y. Jiang, D. Zhong, Z. Zhang, S. Choudhury, J.-C. Lai, H. Gong, S. Niu, X. Yan, Y. Zheng et al., "Neuromorphic sensorimotor loop embodied by monolithically integrated, low-voltage, soft e-skin," Science **380**, 735–742 (2023).

[310]T. Cheng, J. Shao, and Z. L. Wang, "Triboelectric nanogenerators," Nat. Rev. Methods Primers **3**, 39 (2023).

[311]C. Heo, T. Ha, C. You, T. Huynh, H. Lim, J. Kim, M. R. Kesama, J. Lee, T.-T. Kim, and Y. H. Lee, "Identifying fibrillization state of aβ protein via near-field THz conductance measurement," ACS Nano **14**, 6548–6558 (2020).

[312]Z. Yang, D. Tang, J. Hu, M. Tang, M. Zhang, H.-L. Cui, L. Wang, C. Chang, C. Fan, J. Li, and H. Wang, "Near-field nanoscopic terahertz imaging of single proteins," Small **17**, 2005814 (2021).

[313]Z. Li, S. Yan, Z. Zang, G. Geng, Z. Yang, J. Li, L. Wang, C. Yao, H.-L. Cui, C. Chang, and H. Wang, "Single cell imaging with near-field terahertz scanning microscopy," Cell Proliferation **53**, e12788 (2020).

[314]X. Qi, K. Bertling, M. S. Stark, T. Taimre, Y.-C. Kao, Y. L. Lim, S. Han, B. O'Brien, A. Collins, M. Walsh, J. Torniainen, T. Gillespie, B. C. Donose, P. Dean, L. H. Li, E. H. Linfield, A. G. Davies, D. Indjin, H. P. Soyer, and A. D. Rakić, "Terahertz imaging of human skin pathologies using laser feedback interferometry with quantum cascade lasers," Biomed. Opt. Express **14**, 1393–1410 (2023).

[315]G. Geng, G. Dai, D. Li, S. Zhou, Z. Li, Z. Yang, Y. Xu, J. Han, T. Chang, H.-L. Cui, and H. Wang, "Imaging brain tissue slices with terahertz near-field microscopy," Biotechnol. Prog. **35**, e2741 (2019).

[316]S. Schäffer, A. K. Wigger, and P. H. Bolívar, "Substrate-enhanced THz nanoscopic recognition of single bacteria," in *2019 44th International Conference on Infrared, Millimeter, and Terahertz Waves (IRMMW-THz)* (IEEE, 2019), pp. 1–2.

[317]A. Tselev, J. Velmurugan, A. V. Ievlev, S. V. Kalinin, and A. Kolmakov, "Seeing through walls at the nanoscale: Microwave microscopy of enclosed objects and processes in liquids," ACS Nano **10**, 3562–3570 (2016).

[318]S. Gu, T. Lin, and T. Lasri, "Dielectric properties characterization of saline solutions by near-field microwave microscopy," Meas. Sci. Technol. **28**, 014014 (2016).

[319]D. A. Ohlberg, D. Tami, A. C. Gadelha, E. G. Neto, F. C. Santana, D. Miranda, W. Avelino, K. Watanabe, T. Taniguchi, L. C. Campos et al., "The limits of near field immersion microwave microscopy evaluated by imaging bilayer graphene moiré patterns," Nat. Commun. **12**, 2980 (2021).

[320]M. Farina, C. Joseph, S. A. Azman, A. Morini, L. Pierantoni, D. Mencarelli, A. di Donato, T. Pietrangelo, and R. Al Hadi, "Analytical expressions for spreading resistance in lossy media and their application to the calibration of scanning microwave microscopy," RSC Adv. **13**, 21277–21282 (2023).

[321]E. Seabron, S. MacLaren, X. Xie, S. V. Rotkin, J. A. Rogers, and W. L. Wilson, "Scanning probe microwave reflectivity of aligned single-walled carbon nanotubes: Imaging of electronic structure and quantum behavior at the nanoscale," ACS Nano **10**, 360–368 (2016).

[322]F. Guan, X. Guo, S. Zhang, K. Zeng, Y. Hu, C. Wu, S. Zhou, Y. Xiang, X. Yang, Q. Dai, and S. Zhang, "Compensating losses in polariton propagation with synthesized complex frequency excitation," Nat. Mater. **23**, 506–511 (2024).

[323]F. Guan, X. Guo, K. Zeng, S. Zhang, Z. Nie, S. Ma, Q. Dai, J. Pendry, X. Zhang, and S. Zhang, "Overcoming losses in superlenses with synthetic waves of complex frequency," Science **381**, 766–771 (2023).

[324]A. Tuniz and B. T. Kuhlmey, "Subwavelength terahertz imaging via virtual superlensing in the radiating near field," Nat. Commun. **14**, 6393 (2023).

[325]J.-S. Park, S. W. D. Lim, A. Amirzhan, H. Kang, K. Karrfalt, D. Kim, J. Leger, A. Urbas, M. Ossiander, Z. Li, and F. Capasso, "All-glass 100 mm diameter visible metalens for imaging the Cosmos," ACS Nano **18**, 3187–3189 (2024).

[326]M. Beddoe, T. Gölz, M. Barkey, E. Bau, M. Godejohann, S. A. Maier, F. Keilmann, M. Moldovan, D. Prodan, N. Ilie et al., "Probing the micro-and nanoscopic properties of dental materials using infrared spectroscopy: A proof-of-principle study," Acta Biomater. **168**, 309–322 (2023).

[327]R. Wilcken, J. Nishida, J. F. Triana, A. John-Herpin, H. Altug, S. Sharma, F. Herrera, and M. B. Raschke, "Antenna-coupled infrared nanospectroscopy of intramolecular vibrational interaction," Proc. Natl. Acad. Sci. U. S. A. **120**, e2220852120 (2023).

[328]H. Cheon, J. H. Paik, M. Choi, H.-J. Yang, and J.-H. Son, "Detection and manipulation of methylation in blood cancer DNA using terahertz radiation," Sci. Rep. **9**, 6413–6413 (2019).

[329]Y. H. Tao, S. I. Hodgetts, A. R. Harvey, and V. P. Wallace, "Reproducibility of terahertz peaks in a frozen aqueous solution of 5-methylcytidine," J. Infrared Millimeter Terahertz Waves **42**, 588–606 (2021).

[330]M. Brehm, T. Taubner, R. Hillenbrand, and F. Keilmann, "Infrared spectroscopic mapping of single nanoparticles and viruses at nanoscale resolution," Nano Lett. **6**, 1307–1310 (2006).

[331]S. Berweger, D. M. Nguyen, E. A. Muller, H. A. Bechtel, T. T. Perkins, and M. B. Raschke, "Nano-chemical infrared imaging of membrane proteins in lipid bilayers," J. Am. Chem. Soc. **135**, 18292–18295 (2013).

[332]I. Amenabar, S. Poly, W. Nuansing, E. H. Hubrich, A. A. Govyadinov, F. Huth, R. Krutokhvostov, L. Zhang, M. Knez, J. Heberle et al., "Structural analysis and mapping of individual protein complexes by infrared nanospectroscopy," Nat. Commun. **4**, 2890 (2013).

[333]B. T. O'Callahan, K. T. Crampton, I. V. Novikova, T. Jian, C.-L. Chen, J. E. Evans, M. B. Raschke, P. Z. El-Khoury, and A. S. Lea, "Imaging nanoscale heterogeneity in ultrathin biomimetic and biological crystals," J. Phys. Chem. C **122**, 24891–24895 (2018).

[334]B. T. O'Callahan, M. Hentschel, M. B. Raschke, P. Z. El-Khoury, and A. S. Lea, "Ultrasensitive tip-and antenna-enhanced infrared nanoscopy of protein complexes," J. Phys. Chem. C **123**, 17505–17509 (2019).

[335]O. Khatib, J. D. Wood, A. S. McLeod, M. D. Goldflam, M. Wagner, G. L. Damhorst, J. C. Koepke, G. P. Doidge, A. Rangarajan, R. Bashir et al., "Graphene-based platform for infrared near-field nanospectroscopy of water and biological materials in an aqueous environment," ACS Nano **9**, 7968–7975 (2015).

[336]K. J. Kaltenecker, T. Gölz, E. Bau, and F. Keilmann, "Infrared-spectroscopic, dynamic near-field microscopy of living cells and nanoparticles in water," Sci. Rep. **11**, 21860 (2021).

[337]B. T. O'Callahan, K.-D. Park, I. V. Novikova, T. Jian, C.-L. Chen, E. A. Muller, P. Z. El-Khoury, M. B. Raschke, and A. S. Lea, "In liquid infrared scattering scanning near-field optical microscopy for chemical and biological nanoimaging," Nano Lett. **20**, 4497–4504 (2020).

[338]E. Pfitzner and J. Heberle, "Infrared scattering-type scanning near-field optical microscopy of biomembranes in water," J. Phys. Chem. Lett. **11**, 8183–8188 (2020).

[339]D. Virmani, A. Bylinkin, I. Dolado, E. Janzen, J. H. Edgar, and R. Hillenbrand, "Amplitude-and phase-resolved infrared nanoimaging and nanospectroscopy of polaritons in a liquid environment," Nano Lett. **21**, 1360–1367 (2021).

[340]X. Zhao, D. Li, Y.-H. Lu, B. Rad, C. Yan, H. A. Bechtel, P. D. Ashby, and M. B. Salmeron, "In vitro investigation of protein assembly by combined microscopy and infrared spectroscopy at the nanometer scale," Proc. Natl. Acad. Sci. U. S. A. **119**, e2200019119 (2022).

[341]Z. Wang, M. Zheng, H. Duan, S. Hu, and Z. Yuan, "Re-configuring mainstream anammox," Chem. Eng. J. **445**, 136817 (2022).

[342]H. Duan, S. Watts, M. Zheng, Z. Wang, J. Zhao, H. Li, P. Liu, J. Dwyer, P. McPhee, M. Rattier et al., "Achieving robust mainstream nitrite shunt at pilot-scale with integrated sidestream sludge treatment and step-feed," Water Res. **223**, 119034 (2022).

[343]X. Zhang, Z. Yuan, and S. Hu, "Anaerobic oxidation of methane mediated by microbial extracellular respiration," Environ. Microbiol. Rep. **13**, 790–804 (2021).

[344]X. Zhang, G. H. Joyce, A. O. Leu, J. Zhao, H. Rabiee, B. Virdis, G. W. Tyson, Z. Yuan, S. J. McIlroy, and S. Hu, "Multi-heme cytochrome-mediated extracellular electron transfer by the anaerobic methanotroph 'Candidatus methanoperedens nitroreducens'," Nat. Commun. **14**, 6118 (2023).

[345]Z. Wang, T. Liu, H. Duan, Y. Song, X. Lu, S. Hu, Z. Yuan, D. Batstone, and M. Zheng, "Post-treatment options for anaerobically digested sludge: Current status and future prospect," Water Res. **205**, 117665 (2021).

[346]G. C. Wong, J. D. Antani, P. P. Lele, J. Chen, B. Nan, M. J. Kühn, A. Persat, J.-L. Bru, N. M. Høyland-Kroghsbo, A. Siryaporn et al., "Roadmap on emerging concepts in the physical biology of bacterial biofilms: From surface sensing to community formation," Phys. Biol. **18**, 051501 (2021).

[347]Z. Wang, M. Zheng, H. Duan, Z. Yuan, and S. Hu, "A 20-year journey of partial nitritation and anammox (PN/A): From sidestream toward mainstream," Environ. Sci. Technol. **56**, 7522–7531 (2022).

[348]J. Li, W. Ahmed, S. Metcalfe, W. J. Smith, P. M. Choi, G. Jackson, X. Cen, M. Zheng, S. L. Simpson, K. V. Thomas et al., "Impact of sewer biofilms on fate of SARS-CoV-2 RNA and wastewater surveillance," Nat. Water **1**, 272–280 (2023).

[349]F. Wang, Y. Gu, J. P. O'Brien, M. Y. Sophia, S. E. Yalcin, V. Srikanth, C. Shen, D. Vu, N. L. Ing, A. I. Hochbaum et al., "Structure of microbial nanowires reveals stacked hemes that transport electrons over micrometers," Cell **177**, 361–369 (2019).

[350]S. E. Yalcin, J. P. O'Brien, Y. Gu, K. Reiss, M. Y. Sophia, R. Jain, V. Srikanth, P. J. Dahl, W. Huynh, D. Vu et al., "Electric field stimulates production of highly conductive microbial OmcZ nanowires," Nat. Chem. Biol. **16**, 1136–1142 (2020).

[351]D. R. Lovley and D. E. Holmes, "Electromicrobiology: The ecophysiology of phylogenetically diverse electroactive microorganisms," Nat. Rev. Microbiol. **20**, 5–19 (2021).

[352]D. Liang, X. Liu, T. L. Woodard, D. E. Holmes, J. A. Smith, K. P. Nevin, Y. Feng, and D. R. Lovley, "Extracellular electron exchange capabilities of Desulfovibrio ferrophilus and Desulfopila corrodens," Environ. Sci. Technol. **55**, 16195–16203 (2021).

[353]Y. Gu, M. J. Guberman-Pfeffer, V. Srikanth, C. Shen, F. Giska, K. Gupta, Y. Londer, F. A. Samatey, V. S. Batista, and N. S. Malvankar, "Structure of geobacter cytochrome OmcZ identifies mechanism of nanowire assembly and conductivity," Nat. Microbiol. **8**, 284–298 (2023).

[354]F. Wang, L. Craig, X. Liu, C. Rensing, and E. H. Egelman, "Models are useful until high-resolution structures are available," Trends Microbiol. **31**, 550–551 (2023).

[355]F. Wang, L. Craig, X. Liu, C. Rensing, and E. H. Egelman, "Microbial nanowires: Type IV pili or cytochrome filaments?," Trends Microbiol. **31**, 384–392 (2023).

[356]Y. Cao, Y. E, P. Huang, and X.-C. Zhang, "Broadband terahertz wave emission from liquid metal," Appl. Phys. Lett. **117**, 041107 (2020).

[357]Y. E, L. Zhang, A. Tsypkin, S. Kozlov, C. Zhang, and X.-C. Zhang, "Progress, challenges, and opportunities of terahertz emission from liquids," J. Opt. Soc. Am. B **39**, A43–A51 (2022).

[358]Y. Tan, H. Zhao, W.-M. Wang, R. Zhang, Y.-J. Zhao, C.-L. Zhang, X.-C. Zhang, and L.-L. Zhang, "Water-based coherent detection of broadband terahertz pulses," Phys. Rev. Lett. **128**, 093902 (2022).

[359]M.-H. Zhang, W. Xiao, W.-M. Wang, R. Zhang, C.-L. Zhang, X.-C. Zhang, and L.-L. Zhang, "Highly sensitive detection of broadband terahertz waves using aqueous salt solutions," Opt. Express **30**, 39142–39151 (2022).

[360]P. S. Carney, B. Deutsch, A. A. Govyadinov, and R. Hillenbrand, "Phase in nanooptics," ACS Nano **6**, 8–12 (2012).

[361]F. Mohn, L. Gross, N. Moll, and G. Meyer, "Imaging the charge distribution within a single molecule," Nat. Nanotechnol. **7**, 227–231 (2012).

[362]A. Farokh Payam and A. Passian, "Imaging beyond the surface region: Probing hidden materials via atomic force microscopy," Sci. Adv. **9**, eadg8292 (2023).

[363]K. P. Gaikovich and P. K. Gaikovich, "Inverse problem of near-field scattering in multilayer media," Inverse Prob. **26**, 125013 (2010).

[364]A. G. Markelz and D. M. Mittleman, "Perspective on terahertz applications in bioscience and biotechnology," ACS Photonics **9**, 1117–1126 (2022).

[365]T. Taubner, F. Keilmann, and R. Hillenbrand, "Nanoscale-resolved subsurface imaging by scattering-type near-field optical microscopy," Opt. Express **13**, 8893–8899 (2005).

[366]C.-F. Wang, B. Kafle, T. E. Tesema, H. Kookhaee, and T. G. Habteyes, "Molecular sensitivity of near-field vibrational infrared imaging," J. Phys. Chem. C **124**, 21018–21026 (2020).

[367]W. Zhang and Y. Chen, "Visibility of subsurface nanostructures in scattering-type scanning near-field optical microscopy imaging," Opt. Express **28**, 6696–6707 (2020).

[368]Y. Wang, Z. Xia, H. Wu, S. Li, T. Wang, and B. Sun, "Unrevealing charge carrier selective layer in silicon heterojunction solar cells via multifunctional atomic force probes," Sol. RRL **3**, 1900312 (2019).

[369]L. Mester, A. A. Govyadinov, S. Chen, M. Goikoetxea, and R. Hillenbrand, "Subsurface chemical nanoidentification by nano-FTIR spectroscopy," Nat. Commun. **11**, 3359 (2020).

[370]H. He, Z. Chen, Y.-T. Lin, S. H. Hahn, J. Yu, A. C. van Duin, T. D. Gokus, S. V. Rotkin, and S. H. Kim, "Subsurface structural change of silica upon nanoscale physical contact: Chemical plasticity beyond topographic elasticity," Acta Mater. **208**, 116694 (2021).

[371]X. Zhang, A. J. Du, P. Lee, D. D. Sun, and J. O. Leckie, "TiO$_2$ nanowire membrane for concurrent filtration and photocatalytic oxidation of humic acid in water," J. Membr. Sci. **313**, 44–51 (2008).

[372]Z. Wang, X. Yan, Q. Hou, Y. Liu, X. Zeng, Y. Kang, W. Zhao, X. Li, S. Yuan, R. Qiu et al., "Scalable high yield exfoliation for monolayer nanosheets," Nat. Commun. **14**, 236 (2023).

[373]R. Xu, Y. Kang, W. Zhang, B. Pan, and X. Zhang, "Two-dimensional MXene membranes with biomimetic sub-nanochannels for enhanced cation sieving," Nat. Commun. **14**, 4907 (2023).

[374]M. Van Exter and D. Grischkowsky, "Optical and electronic properties of doped silicon from 0.1 to 2 THz," Appl. Phys. Lett. **56**, 1694–1696 (1990).

[375]T.-I. Jeon and D. Grischkowsky, "Nature of conduction in doped silicon," Phys. Rev. Lett. **78**, 1106 (1997).

[376]S. Nashima, O. Morikawa, K. Takata, and M. Hangyo, "Measurement of optical properties of highly doped silicon by terahertz time domain reflection spectroscopy," Appl. Phys. Lett. **79**, 3923–3925 (2001).

[377]T. Nagashima and M. Hangyo, "Measurement of complex optical constants of a highly doped Si wafer using terahertz ellipsometry," Appl. Phys. Lett. **79**, 3917–3919 (2001).

[378]K. Willis, S. Hagness, and I. Knezevic, "Terahertz conductivity of doped silicon calculated using the ensemble Monte Carlo/finite-difference time-domain simulation technique," Appl. Phys. Lett. **96**, 062106 (2010).

[379]N. Katzenellenbogen and D. Grischkowsky, "Electrical characterization to 4 THz of n-and p-type GaAs using THz time-domain spectroscopy," Appl. Phys. Lett. **61**, 840–842 (1992).

[380]P. Huggard, J. Cluff, G. Moore, C. Shaw, S. Andrews, S. Keiding, E. Linfield, and D. Ritchie, "Drude conductivity of highly doped GaAs at terahertz frequencies," J. Appl. Phys. **87**, 2382–2385 (2000).

[381]E. Tournié, L. Monge Bartolome, M. Rio Calvo, Z. Loghmari, D. A. Díaz-Thomas, R. Teissier, A. N. Baranov, L. Cerutti, and J.-B. Rodriguez, "Mid-infrared III–V semiconductor lasers epitaxially grown on Si substrates," Light: Sci. Appl. **11**, 165 (2022).

[382]B. Macco and W. Kessels, "Atomic layer deposition of conductive and semiconductive oxides," Appl. Phys. Rev. **9**, 041313 (2022).

[383]A. Bylinkin, F. Calavalle, M. Barra-Burillo, R. V. Kirtaev, E. Nikulina, E. Modin, E. Janzen, J. H. Edgar, F. Casanova, L. E. Hueso et al., "Dual-band coupling of phonon and surface plasmon polaritons with vibrational and electronic excitations in molecules," Nano Lett. **23**, 3985–3993 (2023).

[384]I. Dolado, C. Maciel-Escudero, E. Nikulina, E. Modin, F. Calavalle, A. Bylinkin, F. J. Alfaro-Mozaz, J. Li, J. H. Edgar, F. Casanova, S. Velex, L. E. Hueso, R. Esteban, J. Aizpurua, and R. Hillenbrand, "Remote near-field spectroscopy of vibrational strong coupling between organic molecules and phononic nanoresonators," Nat. Commun. **13**, 6850 (2022).

[385]M. Dapolito, X. Chen, C. Li, M. Tsuneto, S. Zhang, X. Du, M. Liu, and A. Gozar, "Scattering-type scanning near-field optical microscopy with Akiyama piezo-probes," Appl. Phys. Lett. **120**, 013104 (2022).

[386]J. Belhassen, S. Glass, E. Teblum, G. A. Stanciu, D. E. Tranca, Z. Zalevsky, S. G. Stanciu, and A. Karsenty, "Toward augmenting tip-enhanced nanoscopy with optically resolved scanning probe tips," Adv. Photonics Nexus **2**, 026002 (2023).

[387]H. B. Casimir and D. Polder, "The influence of retardation on the London-van der Waals forces," Phys. Rev. **73**, 360 (1948).

[388]J. Kondo, "Resistance minimum in dilute magnetic alloys," Prog. Theor. Phys. **32**, 37–49 (1964).

[389]B. D. Josephson, "The discovery of tunnelling supercurrents," Rev. Mod. Phys. **46**, 251 (1974).

[390]H. Ishii, H. Kataura, H. Shiozawa, H. Yoshioka, H. Otsubo, Y. Takayama, T. Miyahara, S. Suzuki, Y. Achiba, M. Nakatake et al., "Direct observation of Tomonaga–Luttinger-liquid state in carbon nanotubes at low temperatures," Nature **426**, 540–544 (2003).

[391]M. W. Zwierlein, J. R. Abo-Shaeer, A. Schirotzek, C. H. Schunck, and W. Ketterle, "Vortices and superfluidity in a strongly interacting Fermi gas," Nature **435**, 1047–1051 (2005).

[392]H. U. Yang, E. Hebestreit, E. E. Josberger, and M. B. Raschke, "A cryogenic scattering-type scanning near-field optical microscope," Rev. Sci. Instrum. **84**, 023701 (2013).

[393]D. Lang, J. Döring, T. Nörenberg, Á. Butykai, I. Kézsmárki, H. Schneider, S. Winnerl, M. Helm, S. C. Kehr, and L. M. Eng, "Infrared nanoscopy down to liquid helium temperatures," Rev. Sci. Instrum. **89**, 033702 (2018).

[394]A. McLeod, E. Van Heumen, J. Ramirez, S. Wang, T. Saerbeck, S. Guenon, M. Goldflam, L. Anderegg, P. Kelly, A. Mueller, M. K. Liu, I. K. Schuller, and D. N. Basov, "Nanotextured phase coexistence in the correlated insulator V_2O_3," Nat. Phys. **13**, 80–86 (2017).

[395]G. Ni, A. McLeod, Z. Sun, L. Wang, L. Xiong, K. Post, S. Sunku, B.-Y. Jiang, J. Hone, C. R. Dean, M. M. Fogler, and D. N. Basov, "Fundamental limits to graphene plasmonics," Nature **557**, 530–533 (2018).

[396]W. Luo, M. Boselli, J.-M. Poumirol, I. Ardizzone, J. Teyssier, D. van Der Marel, S. Gariglio, J.-M. Triscone, and A. B. Kuzmenko, "High sensitivity variable-temperature infrared nanoscopy of conducting oxide interfaces," Nat. Commun. **10**, 2774 (2019).

[397]S. Taraskin, S. Simdyankin, S. Elliott, J. Neilson, and T. Lo, "Universal features of terahertz absorption in disordered materials," Phys. Rev. Lett. **97**, 055504 (2006).

[398]D. Cortie, M. Cyster, T. Ablott, C. Richardson, J. Smith, G. Iles, X. Wang, D. Mitchell, R. Mole, N. de Souza et al., "Boson peak in ultrathin alumina layers investigated with neutron spectroscopy," Phys. Rev. Res. **2**, 023320 (2020).

[399]T. Mori, Y. Jiang, Y. Fujii, S. Kitani, H. Mizuno, A. Koreeda, L. Motoji, H. Tokoro, K. Shiraki, Y. Yamamoto, and S. Kojima, "Detection of boson peak and fractal dynamics of disordered systems using terahertz spectroscopy," Phys. Rev. E **102**, 022502 (2020).

[400]M. Tømterud, S. D. Eder, C. Büchner, M. Heyde, H.-J. Freund, I. Simonsen, J. R. Manson, and B. Holst, "Observation of the boson peak in a two-dimensional material," Nat. Phys. **19**, 1910–1915 (2023).

[401]A. Zaccone, *Theory of Disordered Solids: From Atomistic Dynamics to Mechanical, Vibrational, and Thermal Properties* (Springer Nature, 2023), Vol. 1015.

[402]M. Baggioli and A. Zaccone, "Universal origin of boson peak vibrational anomalies in ordered crystals and in amorphous materials," Phys. Rev. Lett. **122**, 145501 (2019).

[403]C. Jiang, M. Baggioli, and J. F. Douglas, "A quantitative theoretical model of the boson peak based on stringlet excitations," arXiv:2307.12839 (2023).

[404]Y.-C. Hu and H. Tanaka, "Origin of the boson peak in amorphous solids," Nat. Phys. **18**, 669–677 (2022).

[405]R. Kim, J.-M. Park, S. Haeuser, L. Luo, and J. Wang, "A sub-2 Kelvin cryogenic magneto-terahertz scattering-type scanning near-field optical microscope (cm-THz-sSNOM)," Rev. Sci. Instrum. **94**, 043702 (2023).

[406]M. Dapolito, M. Tsuneto, W. Zheng, L. Wehmeier, S. Xu, X. Chen, J. Sun, Z. Du, Y. Shao, R. Jing et al., "Infrared nano-imaging of Dirac magnetoexcitons in graphene," Nat. Nanotechnol. **18**, 1409–1415 (2023).

[407]K. Von Klitzing, "The quantized Hall effect," Rev. Mod. Phys. **58**, 519 (1986).

[408]D. C. Tsui, "Nobel lecture: Interplay of disorder and interaction in two-dimensional electron gas in intense magnetic fields," Rev. Mod. Phys. **71**, 891 (1999).

[409]X. L. Wang, "Proposal for a new class of materials: Spin gapless semiconductors," Phys. Rev. Lett. **100**, 156404 (2008).

[410]S. Krinner, N. Lacroix, A. Remm, A. Di Paolo, E. Genois, C. Leroux, C. Hellings, S. Lazar, F. Swiadek, J. Herrmann et al., "Realizing repeated quantum error correction in a distance-three surface code," Nature **605**, 669–674 (2022).

[411]S. Storz, J. Schär, A. Kulikov, P. Magnard, P. Kurpiers, J. Lütolf, T. Walter, A. Copetudo, K. Reuer, A. Akin et al., "Loophole-free Bell inequality violation with superconducting circuits," Nature **617**, 265–270 (2023).

[412]M. B. Johnston and H. J. Joyce, "Polarization anisotropy in nanowires: Fundamental concepts and progress towards terahertz-band polarization devices," Prog. Quantum Electron. **85**, 100417 (2022).

[413]S. K. Lamoreaux, "The Casimir force: Background, experiments, and applications," Rep. Prog. Phys. **68**, 201 (2004).

[414]G. Klimchitskaya, U. Mohideen, and V. Mostepanenko, "The Casimir force between real materials: Experiment and theory," Rev. Mod. Phys. **81**, 1827 (2009).

[415]B. Wit, G. Gramse, and S. Müllegger, "Calibrated microwave reflectance in low-temperature scanning tunneling microscopy," arXiv:2304.08331 (2023).

[416]Y. Zhou, A. Waelchli, M. Boselli, I. Crassee, A. Bercher, W. Luo, J. Duan, J. van Mechelen, D. van der Marel, J. Teyssier et al., "Thermal and electrostatic tuning of surface phonon-polaritons in $LaAlO_3/SrTiO_3$ heterostructures," Nat. Commun. **14**, 7686 (2023).

[417]S. Xu, Y. Li, R. A. Vitalone, R. Jing, A. J. Sternbach, S. Zhang, J. Ingham, M. Delor, J. McIver, M. Yankowitz et al., "Electronic interactions in Dirac fluids visualized by nano-terahertz spacetime mapping," arXiv:2311.11502 (2023).

[418]I. O. Nedoliuk, S. Hu, A. K. Geim, and A. B. Kuzmenko, "Colossal infrared and terahertz magneto-optical activity in a two-dimensional Dirac material," Nat. Nanotechnol. **14**, 756–761 (2019).

24 November 2024 03:57:31

[419]L. Wehmeier, S. Xu, R. A. Mayer, B. Vermilyea, M. Tsuneto, M. Dapolito, R. Pu, Z. Du, X. Chen, W. Zheng et al., "Nano-imaging of Landau-phonon polaritons in Dirac heterostructures," arXiv:2312.14093 (2023).

[420]I. Rajapaksa, K. Uenal, and H. K. Wickramasinghe, "Image force microscopy of molecular resonance: A microscope principle," Appl. Phys. Lett. **97**, 073121 (2010).

[421]Z. Apalla, A. Lallas, E. Sotiriou, E. Lazaridou, and D. Ioannides, "Epidemiological trends in skin cancer," Dermatol. Pract. Concept. **7**, 1 (2017).

[422]R. L. Barnhill, J. A. Fine, G. C. Roush, and M. Berwick, "Predicting five-year outcome for patients with cutaneous melanoma in a population-based study," Cancer **78**, 427–432 (1996).

[423]M. Arumi-Uria, N. S. McNutt, and B. Finnerty, "Grading of atypia in nevi: Correlation with melanoma risk," Mod. Pathol. **16**, 764 (2003).

[424]X. Chen, H. Lindley-Hatcher, R. I. Stantchev, J. Wang, K. Li, A. Hernandez Serrano, Z. D. Taylor, E. Castro-Camus, and E. Pickwell-MacPherson, "Terahertz (THz) biophotonics technology: Instrumentation, techniques, and biomedical applications," Chem. Phys. Rev. **3**, 011311 (2022).

[425]F. Wahaia, I. Kasalynas, D. Seliuta, G. Molis, A. Urbanowicz, C. D. C. Silva, F. Carneiro, G. Valusis, and P. L. Granja, "Study of paraffin-embedded colon cancer tissue using terahertz spectroscopy," J. Mol. Struct. **1079**, 448–453 (2015).

[426]Y. C. Sim, J. Y. Park, K.-M. Ahn, C. Park, and J.-H. Son, "Terahertz imaging of excised oral cancer at frozen temperature," Biomed. Opt. Express **4**, 1413–1421 (2013).

[427]S. Yang, L. Ding, S. Wang, C. Du, L. Feng, H. Qiu, C. Zhang, J. Wu, K. Fan, B. Jin et al., "Studying oral tissue via real-time high-resolution terahertz spectroscopic imaging," Phys. Rev. Appl. **19**, 034033 (2023).

[428]S. J. Oh, S.-H. Kim, Y. B. Ji, K. Jeong, Y. Park, J. Yang, D. W. Park, S. K. Noh, S.-G. Kang, Y.-M. Huh et al., "Study of freshly excised brain tissues using terahertz imaging," Biomed. Opt. Express **5**, 2837–2842 (2014).

[429]A. J. Fitzgerald, V. P. Wallace, M. Jimenez-Linan, L. Bobrow, R. J. Pye, A. D. Purushotham, and D. D. Arnone, "Terahertz pulsed imaging of human breast tumors," Radiology **239**, 533–540 (2006).

[430]S. Sy, S. Huang, Y.-X. J. Wang, J. Yu, A. T. Ahuja, Y.-T. Zhang, and E. Pickwell-MacPherson, "Terahertz spectroscopy of liver cirrhosis: Investigating the origin of contrast," Phys. Med. Biol. **55**, 7587 (2010).

[431]K. Ross and R. Gordon, "Water in malignant tissue, measured by cell refractometry and nuclear magnetic resonance," J. Microsc. **128**, 7–21 (1982).

[432]R. M. Woodward, V. P. Wallace, R. J. Pye, B. E. Cole, D. D. Arnone, E. H. Linfield, and M. Pepper, "Terahertz pulse imaging of ex vivo basal cell carcinoma," J. Invest. Dermatol. **120**, 72–78 (2003).

[433]E. Pickwell, B. Cole, A. Fitzgerald, V. Wallace, and M. Pepper, "Simulation of terahertz pulse propagation in biological systems," Appl. Phys. Lett. **84**, 2190–2192 (2004).

[434]V. P. Wallace, A. J. Fitzgerald, E. Pickwell, R. J. Pye, P. F. Taday, N. Flanagan, and T. Ha, "Terahertz pulsed spectroscopy of human basal cell carcinoma," Appl. Spectrosc. **60**, 1127–1133 (2006).

[435]E. P. J. Parrott, Y. Sun, and E. Pickwell-MacPherson, "Terahertz spectroscopy: Its future role in medical diagnoses," J. Mol. Struct. **1006**, 66–76 (2011).

[436]L. Xie, Y. Yao, and Y. Ying, "The application of terahertz spectroscopy to protein detection: A review," Appl. Spectrosc. Rev. **49**, 448–461 (2014).

[437]K. I. Zaytsev, K. G. Kudrin, V. E. Karasik, I. V. Reshetov, and S. O. Yurchenko, "In vivo terahertz spectroscopy of pigmentary skin nevi: Pilot study of non-invasive early diagnosis of dysplasia," Appl. Phys. Lett. **106**, 053702 (2015).

[438]X. G. Peralta, D. Lipscomb, G. J. Wilmink, and I. Echchgadda, "Terahertz spectroscopy of human skin tissue models with different melanin content," Biomed. Opt. Express **10**, 2942–2955 (2019).

[439]A. Kucheryavenko, I. Dolganova, A. Zhokhov, V. Masalov, G. Musina, V. Tuchin, N. Chernomyrdin, A. Gavdush, D. Il'enkova, S. Garnov, and K. Zaytsev, "Terahertz-wave scattering in tissues: Examining the limits of the applicability of effective-medium theory," Phys. Rev. Appl. **20**, 054050 (2023).

[440]K. Kanevche, D. J. Burr, D. J. Nürnberg, P. K. Hass, A. Elsaesser, and J. Heberle, "Infrared nanoscopy and tomography of intracellular structures," Commun. Biol. **4**, 1341 (2021).

[441]C. Meineke, M. Prager, J. Hayes, Q. Wen, L. Z. Kastner, D. Schuh, K. Fritsch, O. Pronin, M. Stein, F. Schäfer et al., "Scalable high-repetition-rate sub-half-cycle terahertz pulses from spatially indirect interband transitions," Light: Sci. Appl. **11**, 151 (2022).

[442]A. Di Gaspare, V. Pistore, E. Riccardi, E. A. Pogna, H. E. Beere, D. A. Ritchie, L. Li, A. G. Davies, E. H. Linfield, A. C. Ferrari, and M. S. Vitiello, "Self-induced mode-locking in electrically pumped far-infrared random lasers," Adv. Sci. **10**, 2206824 (2023).

[443]S. Mansourzadeh, T. Vogel, A. Omar, M. Shalaby, M. Cinchetti, and C. J. Saraceno, "Broadband, high power THz source at 540 kHz using organic crystal BNA," APL Photonics **8**, 011301 (2023).

[444]X. Wu, D. Kong, S. Hao, Y. Zeng, X. Yu, B. Zhang, M. Dai, S. Liu, J. Wang, Z. Ren et al., "Generation of 13.9-mJ terahertz radiation from lithium niobate materials," Adv. Mater. **35**, 2208947 (2023).

[445]Y. Liang, Z. Liu, Q. Tian, T. Li, X. Lin, L. Yan, Y. Du, R. Li, J. Shi, C. Cheng et al., "Widely tunable electron bunch trains for the generation of high-power narrowband 1–10 THz radiation," Nat. Photonics **17**, 259–263 (2023).

[446]X. Zhang, M. Hu, Z. Zhang, Y. Wang, T. Zhang, X. Xu, T. Zhao, Z. Wu, R. Zhong, D. Liu et al., "High-efficiency threshold-less Cherenkov radiation generation by a graphene hyperbolic grating in the terahertz band," Carbon **183**, 225–231 (2021).

[447]J. L. Boland, D. A. Damry, C. Q. Xia, P. Schönherr, D. Prabhakaran, L. M. Herz, T. Hesjedal, and M. B. Johnston, "Narrowband, angle-tunable, helicity-dependent terahertz emission from nanowires of the topological Dirac semi-metal Cd3As2," ACS Photonics **10**, 1473–1484 (2023).

[448]O. Cherkasova, D. Serdyukov, A. Ratushnyak, E. Nemova, E. Kozlov, Y. V. Shidlovskii, K. Zaytsev, and V. Tuchin, "Effects of terahertz radiation on living cells: A review," Opt. Spectrosc. **128**, 855–866 (2020).

[449]Z. Yan, L.-G. Zhu, K. Meng, W. Huang, and Q. Shi, "THz medical imaging: from in vitro to in vivo," Trends Biotechnol. **40**, 816–830 (2022).

[450]L. Olivieri, L. Peters, V. Cecconi, A. Cutrona, M. Rowley, J. S. Totero Gongora, A. Pasquazi, and M. Peccianti, "Terahertz nonlinear ghost imaging via plane decomposition: Toward near-field micro-volumetry," ACS Photonics **10**, 1726–1734 (2023).

[451]A. Pizzuto, X. Chen, H. Hu, Q. Dai, M. Liu, and D. M. Mittleman, "Anomalous contrast in broadband THz near-field imaging of gold microstructures," Opt. Express **29**, 15190–15198 (2021).

[452]Y. Moon, H. Lee, J. Jung, and H. Han, "Direct visualization of carbon black aggregates in nitrile butadiene rubber by THz near-field microscope," Sci. Rep. **13**, 7846 (2023).

[453]P. Kubaščík, A. Farkaš, K. Olejník, T. Troha, M. Hўvl, F. Krizek, D. C. Joshi, T. Ostatnický, J. Jechumtál, E. Schmoranzerová et al., "Terahertz probing of anisotropic conductivity and morphology of CuMnAs epitaxial thin films," arXiv:2303.15268 (2023).

[454]K. S. Kumar, G. L. Prajapati, R. Dagar, M. Vagadia, D. S. Rana, and M. Tonouchi, "Terahertz electrodynamics in transition metal oxides," Adv. Opt. Mater. **8**, 1900958 (2020).

[455]M. Kotiuga, Z. Zhang, J. Li, F. Rodolakis, H. Zhou, R. Sutarto, F. He, Q. Wang, Y. Sun, Y. Wang et al., "Carrier localization in perovskite nickelates from oxygen vacancies," Proc. Natl. Acad. Sci. U. S. A. **116**, 21992–21997 (2019).

[456]F. Gunkel, D. V. Christensen, Y. Chen, and N. Pryds, "Oxygen vacancies: The (in) visible friend of oxide electronics," Appl. Phys. Lett. **116**, 120505 (2020).

[457]M. Wenskat, M. Čižek, M. O. Liedke, M. Butterling, M. Stiehl, G. D. L. Semione, C. Backes, C. Bate, O. Melikhova, E. Hirschmann et al., "Vacancy dynamics in niobium and its native oxides and their potential implications for quantum computing and superconducting accelerators," Phys. Rev. B **106**, 094516 (2022).

[458]D. Wang, J.-Q. Xu, H.-J. Zhang, and Q.-H. Wang, "Anisotropic scattering caused by apical oxygen vacancies in thin films of overdoped high-temperature cuprate superconductors," Phys. Rev. Lett. **128**, 137001 (2022).

[459]Y. E. Suyolcu, G. Christiani, P. T. Gemperline, S. R. Provence, A. Bussmann-Holder, R. B. Comes, P. A. van Aken, and G. Logvenov, "Engineering ordered arrangements of oxygen vacancies at the surface of superconducting La2CuO4 thin films," J. Vac. Sci. Technol. **40**, 013214 (2022).

[460]Y. Wang, J. Venezuela, and M. Dargusch, "Biodegradable shape memory alloys: Progress and prospects," Biomaterials **279**, 121215 (2021).

[461]J. E. Moore, "The birth of topological insulators," Nature **464**, 194–198 (2010).

[462]A. Gao, Y.-F. Liu, C. Hu, J.-X. Qiu, C. Tzschaschel, B. Ghosh, S.-C. Ho, D. Bérubé, R. Chen, H. Sun *et al.*, "Layer Hall effect in a 2D topological axion antiferromagnet," Nature **595**, 521–525 (2021).

[463]Y. Wang, L. Yang, X.-L. Shi, X. Shi, L. Chen, M. S. Dargusch, J. Zou, and Z.-G. Chen, "Flexible thermoelectric materials and generators: Challenges and innovations," Adv. Mater. **31**, 1807916 (2019).

[464]Y. Wang, M. Hong, W.-D. Liu, X.-L. Shi, S.-D. Xu, Q. Sun, H. Gao, S. Lu, J. Zou, and Z.-G. Chen, "$Bi_{0.5}Sb_{1.5}Te_3$/PEDOT: PSS-based flexible thermoelectric film and device," Chem. Eng. J. **397**, 125360 (2020).

[465]E. T. Papaioannou and R. Beigang, "THz spintronic emitters: A review on achievements and future challenges," Nanophotonics **10**, 1243–1257 (2021).

[466]Y. Tokura, M. Kawasaki, and N. Nagaosa, "Emergent functions of quantum materials," Nat. Phys. **13**, 1056–1068 (2017).

[467]Y. Tokura, K. Yasuda, and A. Tsukazaki, "Magnetic topological insulators," Nat. Rev. Phys. **1**, 126–143 (2019).

[468]O. Breunig and Y. Ando, "Opportunities in topological insulator devices," Nat. Rev. Phys. **4**, 184–193 (2022).

[469]Y. Wang, M. Hong, J. Venezuela, T. Liu, and M. Dargusch, "Expedient secondary functions of flexible piezoelectrics for biomedical energy harvesting," Bioact. Mater. **22**, 291–311 (2023).

[470]Y. Wang, W.-D. Liu, H. Gao, L.-J. Wang, M. Li, X.-L. Shi, M. Hong, H. Wang, J. Zou, and Z.-G. Chen, "High porosity in nanostructured n-type Bi_2Te_3 obtaining ultralow lattice thermal conductivity," ACS Appl. Mater. Interfaces **11**, 31237–31244 (2019).

[471]Z.-H. Zheng, X.-L. Shi, D.-W. Ao, W.-D. Liu, M. Li, L.-Z. Kou, Y.-X. Chen, F. Li, M. Wei, G.-X. Liang *et al.*, "Harvesting waste heat with flexible Bi_2Te_3 thermoelectric thin film," Nat. Sustainability **6**, 180–191 (2023).

[472]Y. Lu, L. L. Hale, A. M. Zaman, S. J. Addamane, I. Brener, O. Mitrofanov, and R. Degl'Innocenti, "Near-field spectroscopy of individual asymmetric split-ring terahertz resonators," ACS Photonics **10**, 2832–2838 (2023).

[473]L. L. Hale, Z. Wang, C. T. Harris, I. Brener, S. Law, and O. Mitrofanov, "Near-field spectroscopy of Dirac plasmons in Bi_2Se_3 ribbon arrays," APL Photonics **8**, 051304 (2023).

[474]K. Lai, W. Kundhikanjana, M. A. Kelly, Z.-X. Shen, J. Shabani, and M. Shayegan, "Imaging of Coulomb-driven quantum Hall edge states," Phys. Rev. Lett. **107**, 176809 (2011).

[475]Y.-T. Cui, B. Wen, E. Y. Ma, G. Diankov, Z. Han, F. Amet, T. Taniguchi, K. Watanabe, D. Goldhaber-Gordon, C. R. Dean, and Z.-X. Shen, "Unconventional correlation between quantum Hall transport quantization and bulk state filling in gated graphene devices," Phys. Rev. Lett. **117**, 186601 (2016).

[476]B. Cheng, P. L. Kramer, Z.-X. Shen, and M. C. Hoffmann, "Terahertz-driven local dipolar correlation in a quantum paraelectric," Phys. Rev. Lett. **130**, 126902 (2023).

[477]Y. Huang, J. D. Querales-Flores, S. W. Teitelbaum, J. Cao, T. Henighan, H. Liu, M. Jiang, G. De la Peña, V. Krapivin, J. Haber *et al.*, "Ultrafast measurements of mode-specific deformation potentials of Bi_2Te_3 and Bi_2Se_3," Phys. Rev. X **13**, 041050 (2023).

[478]T. Wang, C. Wu, M. Mogi, M. Kawamura, Y. Tokura, Z.-X. Shen, Y.-Z. You, and M. T. Allen, "Probing the edge states of Chern insulators using microwave impedance microscopy," Phys. Rev. B **108**, 235432 (2023).

[479]V. Pistore, L. Viti, C. Schiattarella, Z. Wang, S. Law, O. Mitrofanov, and M. S. Vitiello, "Holographic nano-imaging of terahertz Dirac plasmon polaritons topological insulator antenna resonators," Small (published online 2023).

[480]V. Pistore, L. Viti, C. Schiattarella, E. Riccardi, C. S. Knox, A. Yagmur, J. J. Burton, S. Sasaki, A. G. Davies, E. H. Linfield *et al.*, "Terahertz plasmon polaritons in large area Bi_2Se_3 topological insulators," Adv. Opt. Mater. **12**, 2301673 (2023).

[481]H. Handa, Y. Okamura, R. Yoshimi, A. Tsukazaki, K. S. Takahashi, Y. Tokura, and Y. Takahashi, "Terahertz field driven giant nonlinear phonon response in ferroelectric semiconductor In-doped (Sn, Pb)Te," Phys. Rev. B **109**, L081102 (2024).

[482]W.-B. Dai, H. Li, D.-H. Xu, C.-Z. Chen, and X. Xie, "Quantum anomalous layer Hall effect in the topological magnet $MnBi_2Te_4$," Phys. Rev. B **106**, 245425 (2022).

[483]S. Li, T. Liu, C. Liu, Y. Wang, H.-Z. Lu, and X. C. Xie, "Progress on antiferromagnetic topological insulator $MnBi_2Te_4$," Natl. Sci. Rev. **11**, nwac296 (2023).

[484]M. E. Barber, Y. Li, J. Gibson, J. Yu, Z. Jiang, Y. Hu, Z. Ji, N. Nandi, J. C. Hoke, L. B.-V. Horn *et al.*, "Characterization of two fast-turnaround dry dilution refrigerators for scanning probe microscopy," arXiv:2401.04373 (2024).

[485]L. Luo, X. Yang, X. Liu, Z. Liu, C. Vaswani, D. Cheng, M. Mootz, X. Zhao, Y. Yao, C.-Z. Wang *et al.*, "Ultrafast manipulation of topologically enhanced surface transport driven by mid-infrared and terahertz pulses in Bi_2Se_3," Nat. Commun. **10**, 607 (2019).

[486]X. Chen, S. Xu, S. Shabani, Y. Zhao, M. Fu, A. J. Millis, M. M. Fogler, A. N. Pasupathy, M. Liu, and D. N. Basov, "Machine learning for optical scanning probe nanoscopy," Adv. Mater. **35**, 2109171 (2022).

[487]Y. Zhao, X. Chen, Z. Yao, M. K. Liu, and M. M. Fogler, "Deep-learning-aided extraction of optical constants in scanning near-field optical microscopy," J. Appl. Phys. **133**, 133105 (2023).

[488]J.-Y. Zhu, T. Park, P. Isola, and A. A. Efros, "Unpaired image-to-image translation using cycle-consistent adversarial networks," in *Proceedings of the IEEE International Conference on Computer Vision* (IEEE, 2017), pp. 2223–2232.

[489]I. Goodfellow, J. Pouget-Abadie, M. Mirza, B. Xu, D. Warde-Farley, S. Ozair, A. Courville, and Y. Bengio, "Generative adversarial networks," Commun. ACM **63**, 139–144 (2020).

[490]L. Yang, Z. Zhang, Y. Song, S. Hong, R. Xu, Y. Zhao, Y. Shao, W. Zhang, B. Cui, and M.-H. Yang, "Diffusion models: A comprehensive survey of methods and applications," arXiv:2209.00796 (2022).

[491]Y. Xu, Z. Liu, M. Tegmark, and T. Jaakkola, "Poisson flow generative models," arXiv:2209.11178 (2022).

[492]D. Chen, Y. Bai, S. Ament, W. Zhao, D. Guevarra, L. Zhou, B. Selman, R. B. van Dover, J. M. Gregoire, and C. P. Gomes, "Automating crystal-structure phase mapping by combining deep learning with constraint reasoning," Nat. Mach. Intell. **3**, 812–822 (2021).

[493]J. Degrave, F. Felici, J. Buchli, M. Neunert, B. Tracey, F. Carpanese, T. Ewalds, R. Hafner, A. Abdolmaleki, D. de Las Casas, C. Donner, L. Fritz, C. Galperti, A. Huber, J. Keeling, M. Tsimpoukelli, J. Kay, A. Merle, J.-M. Moret, S. Noury, F. Pesamosca, D. Pfau, S. Olivier, C. Sommariva, S. Coda, B. Duval, A. Fasoli, P. Kohli, K. Kavukcuoglu, D. Hassabis, and M. Riedmiller, "Magnetic control of tokamak plasmas through deep reinforcement learning," Nature **602**, 414–419 (2022).

[494]Z. Li, N. Kovachki, K. Azizzadenesheli, B. Liu, K. Bhattacharya, A. Stuart, and A. Anandkumar, "Fourier neural operator for parametric partial differential equations," in International Conference on Learning Representations (2021).

[495]J. Yu, L. Lu, X. Meng, and G. E. Karniadakis, "Gradient-enhanced physics-informed neural networks for forward and inverse PDE problems," Comput. Methods Appl. Mech. Eng. **393**, 114823 (2022).

[496]S. Cuomo, V. S. Di Cola, F. Giampaolo, G. Rozza, M. Raissi, and F. Piccialli, "Scientific machine learning through physics–informed neural networks: Where we are and what's next," J. Sci. Comput. **92**, 88 (2022).

[497]K. H. R. Chan, Y. Yu, C. You, H. Qi, J. Wright, and Y. Ma, "Deep networks from the principle of rate reduction," arXiv:2010.14765 (2020).

[498]E. Weinan, "The dawning of a new era in applied mathematics," Not. Am. Math. Soc. **68**, 565–571 (2021).

[499]T. G. Grossmann, U. J. Komorowska, J. Latz, and C.-B. Schönlieb, "Can physics-informed neural networks beat the finite element method?," arXiv:2302.04107 (2023).

[500]M. Ko, U. K. Panchal, H. Andrade-Loarca, and A. Mendez-Vazquez, "CoShNet: A hybrid complex valued neural network using shearlets," arXiv:2208.06882 (2022).

[501]T. O'Leary-Roseberry, U. Villa, P. Chen, and O. Ghattas, "Derivative-informed projected neural networks for high-dimensional parametric maps governed by PDEs," Comput. Methods Appl. Mech. Eng. **388**, 114199 (2022).

[502]H. Liu, Z. Dai, D. So, and Q. V. Le, "Pay attention to MLPs," Adv. Neural Inf. Process. Syst. **34**, 9204–9215 (2021).

[503]W. Liang, G. A. Tadesse, D. Ho, L. Fei-Fei, M. Zaharia, C. Zhang, and J. Zou, "Advances, challenges and opportunities in creating data for trustworthy AI," Nat. Mach. Intell. **4**, 669–677 (2022).

[504]C. Stokel-Walker and R. Van Noorden, "What ChatGPT and generative AI mean for science," Nature **614**, 214–216 (2023).

[505]T. H. Trinh, Y. Wu, Q. V. Le, H. He, and T. Luong, "Solving olympiad geometry without human demonstrations," Nature **625**, 476–482 (2024).